Control of blood pressure, breathing, and acute stress via the rostral ventrolateral medulla

Benjamin Brown Holloway

Columbia, Tennessee

B.S., University of Tennessee, 2009

A Dissertation presented to the Graduate Faculty

of the University of Virginia in Candidacy for the Degree of

Doctor of Philosophy

Department of Neuroscience

University of Virginia

August 1, 2019

Table of Contents

Chapter 4: Summary and implications of results

Abstract

Rationale

The rostral ventrolateral medulla oblongata (RVLM) is an important region in the brainstem for the neural control of the sympathetic tone and blood pressure. The neurons within the RVLM necessary for these functions remain unidentified, though one population—the catecholaminergic C1 neurons—has been proposed. C1 neurons are activated by lowering blood pressure, they are inhibited by stimulation of the baroreflex, they directly innervate sympathetic preganglionic neurons, and, when artificially stimulated, C1 cells increase sympathetic nerve activity and raise blood pressure. Despite these promising data, recent studies indicate that C1 cells are not required for generating sympathetic tone and maintaining resting blood pressure in conscious animals. As both sympathetic nerve activity and resting blood pressure are thought to be dependent on input from neurons within the RVLM, I explored in my first study whether a second, non-catecholaminergic RVLM group could play a role in generating sympathetic nerve activity and maintaining resting blood pressure.

C1 neurons are no longer thought to be necessary for resting blood pressure maintenance, therefore a different view of C1 in cardiovascular control has developed. Previous studies have indicated that C1 neurons may play an important role in coping with acute stress. C1 neurons are activated during physiological and psychological stress, and inhibition of C1 during physiological stress—but not during quiescence—lowers blood pressure. Further, stimulation of C1 increases sympathetic nerve activity and stimulates release of catecholamines in peripheral circulation, a trademark of the acute stress response (also known as the ‘fight-or-flight’ response). Peripheral catecholamine

release promotes survival during acute stress by increasing cardiac output, decreasing blood flow to the digestive system, and increasing blood flow to skeletal muscle. Equally important to coping with an acute stress is the release of catecholamines within the brain, which promotes arousal and increases vigilance. Neuroanatomical data suggests that C1 neurons may innervate central catecholaminergic neurons and activate catecholamine release in the brain, potentially orchestrating a system-wide catecholaminergic response during acute stress. Therefore, in my second study I explored whether C1 neurons directly innervate catecholaminergic neurons in the central nervous system, and what the nature of this innervation could be.

Besides cardiovascular control, the RVLM also plays an important role in the neural control of breathing. Specifically, chemosensitive neurons in the retrotrapezoid nucleus (RTN) regulate blood pH by adjusting breathing in a carbon dioxide-dependent manner. Some data indicate that RTN may also be important to the neural regulation of breathing in general, i.e. independent of the chemosensitive response. The circuits and mechanisms by which RTN control breathing are poorly understood, and while RTN neurons are demonstrably glutamatergic, they also express markers for several signaling molecules that could participate in neurotransmission. Therefore, in my third project I investigated whether glutamate release from RTN was required in regulation of breathing via the RTN.

Methods

In each study, I used the light-gated channelrhodopsin actuator to stimulate a specific group of neurons which were targeted with the Cre-lox system and transgenic mice or viral promoters. Across my three projects, I optogenetically stimulated putatively excitatory neurons of the RVLM, C1 neurons specifically, and a combination of RTN and C1 neurons. I targeted transgene expression to putatively excitatory RVLM by injecting AAV which encodes for the CaMKIIα promoter—which has been claimed to lead to selective expression in excitatory neurons. To specifically target C1 neurons, I used the dopamine-*β*-hydroxylase $Cre^{+/0}$ mouse strain (DβH-Cre), which results in Cre expression in only C1 neurons within the RVLM. To target RTN and C1 neurons, I used a lentivirus driven by the artificial promoter PRSx8—which specifically targets C1 and RTN neurons when injected locally into the RVLM.

To measure the consequences of optogenetic stimulation of the RVLM, I recorded aortic pressure in conscious, freely behaving mice by inserting a catheter through the left carotid artery which was attached to a telemetric blood pressure probe. I measured C1-stimulation evoked postsynaptic activity of catecholaminergic neurons by performing whole cell patch clamp recordings in brain slices from reporter mice where catecholaminergic neurons expressed a red florescent protein, and C1 neurons expressed channelrhodopsin-YFP via AAV injection. To measure breathing frequency and volume during stimulation of C1/RTN, I placed mice in a whole body plethysmography chamber —a device which measures changes in airflow, from which breathing data can be extracted.

Results

In DβH-Cre mice, local injection of Cre-dependent caspase AAV resulted in a thorough and specific lesion of C1 neurons. Optogenetic stimulation of the RVLM in conscious DβH-Cre mice robustly increased blood pressure, in both C1-lesioned and C1 intact mice. Under anesthesia, activation of only the spinal axons increased blood pressure, again independent of C1 lesion. In WT mice, injection of retrograde Cre AAV into the spinal cord and injection of Cre-dependent channelrhodopsin AAV into the RVLM resulting in expression of the opsin in bulbospinal neurons—including C1 neurons. Stimulation of these bulbospinal non-C1 and C1 neurons increased blood pressure in conscious mice, while stimulation of C1 specifically in DβH-Cre did not increase blood pressure.

In brain slices, optogenetic stimulation of C1 axons and terminals reliably evoked excitatory postsynaptic currents (EPSCs) and increased firing rates of voltage- and current-clamped catecholaminergic neurons, respectively. Evoked EPSCs were blocked after application of the fast-Na^+ channel blocker tetrodotoxin (TTX), which prevents generation of action potentials and action potential-dependent synaptic release. After application of both TTX and 4-aminopyridine (4-AP), optogenetic stimulation was again capable of evoking ESPCs. Finally, application of the glutamatergic blockers cyanquixaline (CNQX) and R-2-amino-5-phosphonopentanoate (AP5) prevented evoked ESPCs by optogenetic stimulation of C1 terminals.

DβH-$Cre^{+/0}$_$Vglut2^{flox/0}$ mice bred with $Vglut2^{flox/flox}$ mice generated a conditional knockout cross strain of DβH-$Cre^{+/0}$_$Vglut2^{flox/flox}$ mice (henceforth, DβH-cKO mice). DβH-cKO mice could not produce detectable Vglut2 protein in DβH neurons via

immunohistochemistry, while immunoreactive-Vglut2 protein was detected in both adjacent neurons, as well as in DβH neurons from non-DβH-cKO mice. Selective optogenetic stimulation of C1 in DβH-Cre mice increased breathing, while stimulation of C1 in DβH-cKO did not increase breathing. We then injected PRSx8-channelrhodopsin lentivirus into the RVLM of DβH-Cre and DβH-cKO mice, which resulted in expression of the opsin in both C1 and RTN neurons. Optogenetic stimulation of either mouse group robustly increased breathing, much greater than stimulation of C1 alone. Finally, we injected PRSx8-Cre lentivirus and Cre-dependent channelrhodopsin AAV into the RVLM of either WT or Vglut2$^{flox/flox}$ mice. This resulted in the expression of the opsin in both C1 and RTN, and neurons expressing the opsin in Vglut$^{flox/flox}$ mice lacked detectable Vglut2 protein while those from WT mice had detectable Vglut2 protein. Optogenetic stimulation of C1 and RTN in WT mice robustly increased breathing, while stimulation from Vglut2$^{flox/flox}$ mice produced no change in breathing.

Conclusions

Non-C1 spinally projecting neurons are capable of regulating blood pressure

Optogenetic stimulation of neurons within the RVLM before and after virtually complete lesion of C1 causes a robust increase in blood pressure in conscious mice, demonstrating that non-catecholaminergic RVLM is capable of regulating blood pressure. However, this increase in blood pressure could be due to any number of pathways from RVLM. Under anesthesia, optogenetic stimulation of only the axons in the spinal cord from neurons in the RVLM again increased blood pressure regardless of C1 lesion,

demonstrating that selective stimulation only the spinally projecting non-catecholaminergic neurons is sufficient to increase blood pressure, at least under anesthesia. Finally, we stimulated spinally projecting RVLM neurons—both C1 and non-C1—in conscious mice. This again resulted in an increase in blood pressure. We then compared the result of C1 stimulation alone versus stimulation of both C1 and non-C1 bulbospinal neurons. Stimulation of C1 alone did not increase blood pressure, while stimulation of both populations increased blood pressure. Therefore, we conclude that non-catecholaminergic spinally projecting neurons are capable of regulating blood pressure in conscious mice.

C1 monosynaptically activates central catecholaminergic neurons by releasing glutamate

I recorded neuronal activity from central catecholaminergic neurons which were either identified as catecholaminergic via post-hoc IHC or by florescence in DβH-Cre mice crossed with a reporter strain. Once I identified neurons that displayed neuronal activity due to optogenetic stimulation of C1 axons, I tested whether or not this activity was monosynaptic by using TTX. As TTX blocks action potential generation, all polysynaptic activity is abated, and any remaining evoked activity after its application must result from monosynaptic connections. While TTX blocked optogenetically evoked EPSCs in catecholaminergic neurons from C1, application of TTX + 4-AP was sufficient to recover the response while still preventing action potential generation and polysynaptic activity. The addition of 4-AP blocks K^+ repolarization, which allows for the optogenetic stimulation of the channelrhodopsin protein to generate enough depolarization to activate voltage-dependent Ca^{++} channels and therefore induce release of synaptic vesicles. This

monosynaptic activation resulted in evoked EPSCs, which were then shown to have been the result of glutamate as blockade of glutamatergic receptors eliminated the evoked EPSCs from optogenetic stimulation of C1 terminals. Therefore, we conclude that C1 monosynaptically activates central catecholaminergic neurons by releasing glutamate.

RTN neurons require Vglut2 to drive breathing

We have previously shown that optogenetic stimulation of C1 neurons in mice in which C1 neurons lack Vglut2 (DβH-Cre$^{+/-}$_Vglut2$^{flox/flox}$) does not increase breathing. We wished to know if the increase in breathing due to stimulation of RTN was also dependent on Vglut2, however there is currently no way to specifically target RTN neurons. The artificial PRSx8 promoter specifically targets C1 and RTN neurons when injected locally into the RVLM. Optogenetic stimulation of RTN and C1 after injection of the PRSx8 lentivirus robustly increased breathing in control mice, but also in mice where C1 neurons lack Vglut2 and cannot influence breathing, demonstrating that RTN stimulation is driving breathing in these mice. Then, in WT mice, we stimulated RTN and C1 using a cocktail of PRSx8-Cre lentivirus and Cre-dependent channelrhodopsin, and optogenetic stimulation again produced a large increase in breathing. We injected the same viral cocktail to label RTN and C1 in Vglut2$^{flox/flox}$ mice, which prevents expression of Vglut2 in both C1 and RTN neurons. Optogenetic stimulation in this case produced very little activation of breathing despite many C1 and RTN neurons expressing the channelrhopsin protein. This demonstrates that the increase in breathing due to optogenetic stimulation of RTN requires Vglut2 and is likely dependent on glutamate release.

Acknowledgements

My career as a scientist would not be possible without the help and friendship of numerous individuals throughout my life, and to each of them I am grateful. I would like to thank my family: my three brothers: Bo, Will, and Sam, my sister Carrie, and my mother and father for their continued support and friendship throughout graduate school. I would also like to thank a few people that were specifically critical for this dissertation work, beginning with my advisor Dr. Patrice Guyenet. I would like to thank Patrice for teaching me to never be complacent with my conclusions—"you can never be paranoid enough"—and for encouraging me to remain open-minded and unwavering in the pursuit of truth—"you argue like a Frenchman". Next, I would like to thank Dr. Ruth Stornetta, for her friendship, and for her expert work in histology and microscopy which have played such a prominent role in my research. I would also like to thank a few of the former and current members and collaborators of the Guyenet lab who made my research not only possible but also a lot of fun: Dr. Chikara Abe, Dr. Seth DePuy, Dr. Yingtang Shi, Dr. Doug Bayliss, Daniel Stornetta, Kenneth "Theeg" Viar Jr., Dr. Tyler Basting, Dr. Peter Burke, Dr. George Souza, Dr. Ian Wenker, Dr. Steve Abbott, and Dr. Roy Kanbar. I would also like to thank Dr. Michelle Bland and Lisa Grimes, both of whom were instrumental in improving the clarity and quality of my writing. I would like to thank the many undergraduate students who helped with this work, and to thank Brian Cullaty, the University of Virginia Center for Undergraduate Excellence, and Grace Styklunas for providing me the opportunity to carry out an undergraduate-graduate research project through the Double Hoo Fellowship. I would like to thank the Biomedical Sciences Graduate Program, the Neuroscience Graduate Program, and the American Heart

Association for providing support for this work. I would also like to thank the late Bob and Mary Wagner for their generous support of basic science research at the University of Virginia School of Medicine through the Robert R. Wagner Fellowship Fund. I would like to thank my committee head, Dr. Scott Zeitlin, and my committee members Dr. Mark Beenhakkar, Dr. Bettina Winckler, Dr. Brant Isakson, and Dr. Doug Bayliss for their time and guidance throughout my graduate research. Finally, I would to thank the many unnamed but indispensable individuals who contributed to my progression as a scientist and growth as a researcher. To each of you I am obliged, and it is to you that I dedicate this work.

Chapter 1: Introduction

1.1 Overview

During my dissertation research I have investigated how the rostral ventrolateral medulla (RVLM) regulates blood pressure and breathing. Much of this work has been divided across three populations of neurons within the RVLM: non-C1 neurons, C1 neurons, and retrotrapezoid nucleus neurons. In the following section of Chapter 1, I will review the background and significance of this dissertation research, I will briefly discuss the important anatomy for these two systems, and I will introduce a few essential concepts in the neural regulation of the cardiovascular system. In Chapter 2, I will discuss my work investigating the roles of non-C1 and C1 neurons in regulating blood pressure and regulating catecholamine levels. In Chapter 3, I will discuss the neural control of breathing, and present my research on the retrotrapezoid nucleus neurons. In the final chapter of my dissertation, I will review the major findings of this dissertation work and discuss its impact on our current understanding of the RVLM and its role in blood pressure regulation and acute stress.

1.2 Cardiovascular disease and hypertension

Prevalence, mortality and cost of cardiovascular disease

Cardiovascular diseases are a group of diseases involving the heart or the vasculature, is the leading cause of death both globally and in the United States. According to the World Health Organization, in 2012 cardiovascular disease accounted for 17.5 million deaths— 31% of all deaths worldwide—and over 800,000 deaths in the

US, again roughly 31% of total deaths [1]. In 2012, greater than 1 in 3 Americans had at least one type of cardiovascular disease and the total financial loss of cardiovascular disease in the US was estimated to be over $396 billion [1]. In 2030, it is predicted that 43.9% of the US population will have some form of cardiovascular disease, raising the financial burden of cardiovascular disease to an estimated $918 billion [1]. Key risk factors for cardiovascular disease outlined by the NIH are high blood pressure, high blood cholesterol, diabetes, smoking, obesity, inactivity, genetic predisposition, preeclampsia, poor diet, and age.

Prevalence, mortality and cost of hypertension

Hypertension has recently been redefined as having systolic BP ≥130mmHg or diastolic BP ≥80mmHg. This new definition lowers systolic and diastolic limits from the 2003 limits of 140 and 90mmHg. A previous study by the World Heart Federation using the 2003 limits found that over 970 million people globally have hypertension, and the prevalence is estimated to increase to 1.56 billion in 2025. In the US, ~80 million adults —nearly 1in 3—has hypertension, and by 2030 the prevalence is estimated to increase to 41% of the US adult population (Figure 1) [1]. In the US, the new guidelines will increase the prevalence of hypertension to 46% of the adult population, though this new population will now be classified as stage 1 hypertension, and individuals falling under the previous guidelines will fall under the stage 2 hypertension category (Figure 2). Hypertension is classified as primary (essential) or secondary hypertension. Primary hypertension is idiopathic and accounts for 95% of hypertensive cases. The remaining 5%

of hypertensive individuals have secondary hypertension—hypertension that is caused by an identifiable medical condition such as kidney or endocrine disorders[2].

Controlling hypertension

Hypertension—one of the key risk factors for cardiovascular disease—is the single most important risk factor for stroke. Roughly 800,000 Americans have a stroke each year, and nearly 140,000 of those are fatal. Importantly, lowering blood pressure in hypertensive individuals decreases the risk of having a stroke or developing cardiovascular disease, and medication is typically effective in lowering blood pressure. However, some individuals have resistant hypertension and do not respond to treatment (~11% of US adults with hypertension) [3-6]. Hypertensive individuals are often unaware that they have high blood pressure, as the condition rarely causes any noticeable or unpleasant effects. This also likely contributes to the low adherence to treatment, as antihypertensive medication often does cause negative side effects, in contrast to the disease itself. A recent study found that a significant portion of patients who had applied for renal nerve denervation and were classified as having resistant hypertension were not actually resistant to treatment but instead had poor medication adherence [6]. Regardless of the cause, the number of hypertensive individuals that go untreated is significant. In 2012, the Nation Health and Nutrition Examination Survey showed that over 17% of US adults with hypertension were unaware that they had hypertension, and nearly 25% were not taking medication to lower their BP (Figure 2) [7].

Can hypertension be 'self-protective'?

Nearly 95% of hypertensive causes have no known cause. It is clear that elevated arterial pressure increases the risk of cardiovascular disease and stroke, however, lowering arterial pressure in certain hypertensive individuals may also carry health risks. Some researchers have proposed that high blood pressure may actually play a beneficial role in alleviating low cerebral perfusion in particular individuals. It has long been known that decreased cerebral perfusion can affect arterial pressure, such as in the Cushing reflex. In 1901, William Harvey Cushing demonstrated that when intracranial pressure (ICP) was elevated to a level that approaches or exceeds arterial pressure—i.e. when cerebral compression attenuates cerebral perfusion—arterial pressure is in turn elevated to overcome ICP and restore cerebral perfusion [8]. Cerebral perfusion is determined by cerebral resistance and cerebral perfusion pressure—the difference in mean arterial pressure and ICP. Results from Cushing's study suggested that there is a mechanism in the medulla for sensing some cardiovascular aspect indicative of cerebral perfusion which can drastically elevate arterial pressure—in Cushing's experiments up to 250 mmHg for over 10 minutes.

Cushing Mechanism and the Selfish Brain Theory

While the potency of this reflex was immediately recognized, the mechanism underlying the Cushing reflex has historically been dismissed in terms of effecting arterial pressure outside of grave brain ischemia. This notion has recently been challenged, and in 2009, Paton et al. proposed that previous studies underestimated the sensitivity of the Cushing response, and that the observed reflex is actually "a terminal pathological event of a physiological mechanism that is an overlooked but key regulator

of blood pressure". Paton dubbed the mechanism Cushing's mechanism to differentiate it from the originally described Cushing reflex [9]. This concept falls under the greater Selfish Brain Theory originally developed by Achim Peters in the context of energy allocation. The theory states that the brain prioritizes its own needs, sometimes at the expense of secondary organs.

In the context of hypertension, this means that if cerebral perfusion was attenuated, the brain would secure its own perfusion by elevating arterial pressure, overcoming the normal mechanisms that act to lower elevated pressure. There is mounting evidence that cerebral blood flow may be maintained at the expense systemic arterial pressure at common pathophysiological levels—i.e. poor cerebral perfusion may generate and maintain blood pressure levels commonly seen in hypertension, not just play a role in extreme cerebral ischemia. Spontaneously-hypertensive-rats display decreased basilar and vertebral artery diameters with thicker vessel walls versus Wistar-Kyoto rats, and thus likely decreased cerebral blood flow at the same arterial pressure [9]. In man, hypertensive patients have narrower vertebral arteries, and higher systemic arterial pressure is most strongly correlated with increasing vertebral artery resistance compared to resistance of other arteries [10]. In a recent study published in Circulation Research, Warnert et al. found a positive correlation with cerebrovascular variants— vertebral artery hypoplasia and incomplete circle of Willis—and increased cerebral resistance, increased lacunar infarcts, and reduced cerebral blood flow (Figure 4) [11]. Importantly, patients with hypertension do not display vertebral arterial narrowing, suggesting that the small diameter vessels may be causative of the hypertension and not a consequence of the disease. If hypertension is caused by elevated cerebral resistance, it is predicted that

lowering arterial pressure would exacerbate the underlying cerebral hypoperfusion [11]. And, more importantly, if instead of treating the hypertension, cerebral blood flow was improved in these individuals, then arterial pressure would drop to normal levels. Whether hypertension is sometimes caused by an impaired cerebral perfusion at healthy system arterial pressures remain unknown, but these concerns do highlight the importance in understanding hypertensive etiology in each individual to provide the most appropriate and safe treatments.

Conclusions

In summary, hypertension and cardiovascular disease have high prevalence which is estimated to increase over the next decade. Due to the predicted high financial burden and mortality rate, there is a critical need to curb the growing prevalence of cardiovascular disease and hypertension. Medication is generally effective in lowering BP, however the inconspicuous nature of hypertension—dubbed “the silent killer”—combined with difficulties in accurate diagnoses and the low rate of medication adherence likely means that better preventative methods are required to significantly decrease the incidence of hypertension. In certain individuals, lowering arterial pressure through medication may unmask underlying problems which blood pressure was actually elevated to counteract. Unfortunately, without better understanding the exact determinants of arterial pressure, the potential to predict the unintended consequences of hypertensive treatment as well as the potential to develop precise and effective means to prevent the progression of hypertension and cardiovascular disease are greatly limited.

1.3 Regulation of the cardiovascular system

Autonomic and cardiovascular systems

The cardiovascular system maintains an optimal external environment for tissues and cells by providing nutrients and removing waste through blood flow. Blood flow is a result of perfusion pressure—the pressure difference along the length of the vessel—against the resistance of the vessel. The heart generates arterial pressure by forcefully ejecting blood into the aorta, which must flow against the combined resistance of the entire circulatory system—systemic vascular resistance. Circulation is divided into two components, that between the heart and lungs—the pulmonary system—and the systemic circulatory system between heart and body. Arterial circulation is a high pressure system, and the walls of the arteries are thick and surrounded by smooth muscles cells which causes a high rate of blood flow. In contrast, the venous system is highly compliant and pressure in this system tends to expand the vessel creating a reservoir of blood. Due to this high compliance, the majority of blood resides in the venous portion (~64%) of systemic circulation (Figure 5) [12].

Physics of the cardiovascular system

The regulation of blood flow occurs primary by dilating or constricting blood vessels, and very small changes in radius can greatly alter blood flow, as shown by Poiseuille's Law:. Blood vessels are constricted or dilated by smooth muscle cells that surround the vessel endothelia. Local regulation of blood flow largely occurs by intrinsic

mechanisms, collectively known as autoregulation, which attempt to maintain adequate blood flow for complete tissue oxygenation despite changes in perfusion pressure (Figure 6) [13]. Under certain conditions autoregulation alone may be insufficient to maintain adequate blood flow, and cardiac output—the amount of blood pumped into the aorta per minute—must increase in order to maintain complete oxygenation of tissues. Under even more demanding conditions, systemic metabolic demands may *exceed* maximal cardiac output, in which case blood must be shunted from non-essential vascular beds to preserve perfusion of the brain and retain consciousness.

Autonomic regulation of the cardiovascular system.

The relationship between the cardiovascular and autonomic nervous systems is complex, but it can loosely be summarized as collection sensorimotor circuits involved with the detection and control of cardiovascular homeostasis. The autonomic portion can be broken into three major groups: motor, sensory, and central. The motor end of the autonomic nervous system—especially the sympathetic component—is capable of rapidly and vigorously controlling blood flow throughout the body. The sensory end of the autonomic nervous system interprets the state of the cardiovascular system and reports this information to the central component of the autonomic nervous system, which ultimately determines how the efferent autonomic motor system responds.

The autonomic motor system consists of the sympathetic and parasympathetic arms. The physiological determinants of blood pressure—heart rate, stroke volume, and vascular resistance—are all directly regulated by the sympathetic nervous system, which

innervates the heart and vasculature (Figures 7 and 8). The sympathetic nervous system consists of cholinergic preganglionic neurons which are located in the spinal cord and ganglionic neurons in the sympathetic chain ganglia or prevertebral ganglia. Sympathetic postganglionic fibers are almost exclusively noradrenergic—the most well-known exceptions being the cholinergic sympathetic postganglionic fibers that innervate the sweat glands and the direct preganglionic innervation adrenergic chromaffin cells in the adrenal medulla—but they often contain other synaptically active chemicals such as neuropeptide Y, ATP, dopamine, gonadotropin-releasing hormone, and substance P. Sympathetic activation increases heart rate by increasing the rate of sinoatrial node discharge, atrioventricular discharge and conduction velocity, and it increases heart stroke volume by directly sensitizing cardiomyocytes which increases heart contractility. The effects of sympathetic activation on the heart—cardiac acceleration and hyper-contractility—are caused by activation β_1 receptors (G_s) throughout the cardiac tissue. In the vasculature, sympathetic activation increases system vascular resistance and stroke volume primarily by activating α_1 receptors (G_q) on arterial and venous vascular smooth muscle. The activated smooth muscle cells constrict the blood vessels, thereby increasing the resistance of the vessel. On the arterial side of circulation, altering smooth muscle tone changes vessel resistance and can redirect perfusion, such as systemic constriction to preserve blood for the brain and skeletal muscles during exercise or vessel dilation to perfuse the gastrointestinal system during digestion. On the venous side of circulation, activation of smooth muscle will cause constriction of veins, which squeezes the pooled venous blood into circulation and thus increase venous return, stroke volume, and cardiac

output. Sympathetic activation can robustly increase cardiac output as well as arterial pressure.

The parasympathetic arm of the autonomic nervous system consists of cholinergic preganglionic and cholinergic ganglionic neurons. Unlike the preganglionic sympathetic innervation of the pre- and paravertebral ganglia, the parasympathetic preganglionic neurons travel far from the soma in the spinal cord and synapse onto ganglia near the effector organ. The primary cardiovascular effect of parasympathetic stimulation is decreased heart rate and decreased contractility of the heart, both through activation of M_2 muscarinic receptors in cardiac tissue.

Autonomic cardiovascular reflexes

The three components of the autonomic nervous system are linked to form reflex circuits which typically function to maintain cardiovascular homeostasis, though these circuits can be modulated by the central commands to produce different cardiovascular states. One important example of such a circuit is the baroreflex pathway. In this reflex, cardiovascular information is transduced into synaptic activity by baroreceptor neurons—sensory neurons from the petrosal and nodose ganglia that have mechanosensitive endings which innervate the outer layer (also known as the tunica externa or adventitia) of particular segments of vessels, bilaterally in the carotid sinuses and in the aortic arch. These sinoaortic baroreceptors indirectly sense arterial pressure by detecting vascular movement generated by dilation and contraction during diastole and systole, which

ultimately provide a negative feedback onto the sympathetic nervous system—however much of the pathway is still speculative (Figure 8) [14].

Is the baroreflex capable of regulating long term blood pressure?

The baroreflex has long been recognized as a critical mechanism in short term (second to minutes) regulation of arterial pressure, and recent studies indicate that it may also play an important role in setting arterial pressure in the long term (days to weeks)—though this concept has had a turbulent history and it remains controversial today. It is important to establish what mechanisms are involved in the long term regulation of blood pressure, as these mechanisms are the most likely to be responsible for the generation and maintenance of hypertension. Therefore, the next section will discuss critical studies that provide the evidence against and in favor of the baroreflex as a long term mediator of arterial pressure.

Since the work of Allen Cowley and Arthur Guyton in 1973, the two periods of arterial regulation, short term—across seconds to a few minutes—and long term—periods exceeding 12-24h, have been explained as two separate regulatory mechanisms with little crosstalk, as exemplified in Allen Cowley's review of the subject: "the feedback control systems that provide rapid stabilization of arterial pressure are fundamentally different from those that determine the long-term level of arterial pressure" [15]. If this is the case, then the baroreflex, which is critical in the short term, cannot be expected to play a role in long term arterial pressure regulation. Cowley and Guyton's contention was in stark contrast to many studies in the early and middle 20th

century that showed denervation of the sinoaortic baroreceptors (i.e. complete denervation) was sufficient to produce chronic hypertension [16-18]. However, Cowley noted that technical flaws in these early studies may have resulted in misleading data with respect to 24h mean arterial pressure. In order to measure arterial pressure, animals were given an arterial puncture. Stress or excitement can substantially raise arterial pressure in the short term, and these experiments relied on several intermittent arterial punctures as approximations for long term blood pressure averages. Therefore, several short term fluctuations in pressure due to the excitement or stress during the arterial puncture could grossly misrepresent the actual 24h mean arterial pressure. This was likely the case, as when Cowley performed sinoaortic deneravation experiments on dogs instrumented with chronic arterial catheters, he discovered that short term fluctuations in blood pressure where increased yet there was no change in the 24hour mean arterial pressure versus dogs with intact baroreceptors (Figure 9) [19]. Cowley summarized his argument against a role in long term arterial pressure regulation via the baroreflex in three points: baroreceptor gain is insufficient to account for long term blood pressure regularity, baroreceptors reset when sustained changes in blood pressure are maintained, and when the baroreceptors are denervated, no change is observed in the 24h mean arterial pressure [15]. These points formed the basis of the dogma of the baroreflex: mechanisms which generate long term blood pressure regulation are separate from the baroreceptor reflex, which is concerned with buffering rapid alterations in blood pressure in the short term.

A few recent studies have challenged the Guyton-Cowley dogma. Terry Thrasher has pointed out that Cowley's original claims either lack the critical experiments needed to confirm them, and recent experiments suggest that Cowley's arguments may rely on

what appear to be experimental artifacts [20, 21]. For example, several studies have demonstrated baroreceptor resetting during acute experimental procedures. However, long term mechanisms of baroreceptor resetting are extrapolated from acute experiments which are cannot address the temporal component of baroreceptor resetting or its relevance to conscious animals, a concept made evident by Allen Cowley's own study with respect to short term approximations for 24h mean arterial pressure [22, 23]. Further, work by Thomas Lohmeier indicates that the baroreflex is actually constitutively active in at least some cases of hypertension and may play a compensatory mechanism, which is incompatible with the baroreceptor resetting theory [22, 23].

Cowley's conclusions are largely based on sinoaortic denervation studies, yet recent studies from Thomas Lohmeier and from Thrasher indicate the consequences of sinoaortic denervation on the nervous system are not equivalent to sinoaortic inhibition. Intact baroreceptors do seem to contribute to long term blood pressure through sympathetic inhibition [20, 24]. Work from Lohmeier's laboratory utilized a split-bladder technique to investigate the contribution of the baroreflex and the renal sympathetic nerve on fluid volume regulation by the kidney, in either angiotensin II induced or norepinephrine induced hypertension models [22, 23, 25]. In these experiments the bladder is hemi-sectioned and one kidney is denervated, under the assumption that differences in the volume of fluid excreted between the kidneys is a consequence of the renal sympathetic nerve. Under control conditions, both kidneys excreted equal volumes of fluid. After infusion of angiotensin II and during the progression of hypertension, fluid retention was observed from both kidneys, though the innervated kidney excreted more volume than the denervated kidney. This suggests that inhibition of renal sympathetic

activity through the baroreflex is chronically active in an attempt to mitigate the high blood pressure induced in the angiotensin II model. However, this result does not prove that the baroreceptor is responsible for the difference in volume between each kidney. Further, it is unclear why a kidney devoid of sympathetic input would excrete less than a kidney with reduced sympathetic input. One interpretation is that denervated kidneys display an increased sensitivity to circulating catecholamines such that during the progression of hypertension the consequences of systemic sympathetic activation actually have a greater efficacy on a kidney devoid of direct sympathetic innervation. Indeed, basal sympathetic efficacy could account for the differences in fluid volume, and—as suggested by Cowley—the sympathetic tone can alter long term arterial pressure by either direct or circulating signals simply adjusts the set point of not the baroreflex but the actual long term baroreceptor organ, the kidneys. Thus, these results are not yet incompatible with Cowley's concepts on long term pressure regulation. However, researchers in Lohmeier's laboratory performed one additional experiment. After hemi-sectioning the bladder and unilateral renal sympathetic denervation, the sinoaortic baroreceptors were then denervated. After recovery from the baro-denervation surgery, animals were again exposed to angiotensin II. Interestingly, without baroreceptor input, fluid volume excreted by the innervated kidney was now lower than that of the denervated kidney (Figure 10). Thus, the compensatory increase in excretion from the innervated compared to the denervated kidney in angiotensin II hypertension is dependent on an intact baroreflex, and is likely not the consequence of renal pressure-sensitive process.

That decreasing the activity of a nerve produces a stronger inhibition than complete denervation is alarming, and it may indicate a misinterpretation of the baroreflex due to the complex consequences of nerve cut. This is also supported by Thrasher's 2002 study, where he demonstrated that after denervation of baroreceptors from the aortic arch and from one of the carotid arteries, he could generate chronic neurogenic hypertension by ligating the innervated carotid artery but not the denervated carotid artery [20]. After ligation, sinus pressure on the innervated, ligated artery is maintained at the expense of mean arterial pressure (Figure 11). Thrasher interpreted his results as evidence that the baroreceptors do not reset, are chronically activated, and result in an uncompensated, sustained increase in systemic blood pressure in order to maintain sinus pressure. In the final experiment, Thrasher removed the ligation from the innervated artery and blood pressure values returned to baseline. This data implies that not only is baroreflex malfunction capable of generating and maintaining hypertension, but restoring the baroreflex to normal function is sufficient to alleviate the neurogenic hypertension. This long term elevated arterial pressure due to decreased baroreflex activity is in stark contrast to bilateral sinoaortic denervation, in which mean arterial pressure returns to normal only a few days after the surgery. These provocative studies may be the first indications that nerve cutting causes consequences beyond complete inhibition of the neural activity and caution should be taken when drawing conclusions from the results of such studies.

Conclusions

In summary, studies in the early 20th century suggested that denervation of the sinoaortic baroreceptors was sufficient to generate and maintain hypertension. However, Cowley and Guyton demonstrated that the resulting "hypertension" subsides within a few days after the denervation surgery, and while short term fluctuations are exaggerated in barodenervated animals, 24h mean arterial pressure was maintained. Therefore, they conclude that the baroreceptors are important to short term blood pressure regulation but do not contribute to long term regulation. Recent studies by Lohmeier and Thrasher have indicated that Cowley's denervation studies produced consequences beyond simple inhibition of the baroreflex, and that baroreceptors are important to long term blood pressure. These studies also indicate that decreasing baroreceptor activity is sufficient to generate and maintain systemic hypertension, while increasing baroreflex activity is sufficient to alleviate hypertension.

Works Cited

1. Writing Group, M., et al., *Heart Disease and Stroke Statistics-2016 Update: A Report From the American Heart Association.* Circulation, 2016. **133**(4): p. e38-60.
2. Carretero, O.A. and S. Oparil, *Essential hypertension. Part I: definition and etiology.* Circulation, 2000. **101**(3): p. 329-35.
3. Persell, S.D., *Prevalence of resistant hypertension in the United States, 2003-2008.* Hypertension, 2011. **57**(6): p. 1076-80.
4. Roberie, D.R. and W.J. Elliott, *What is the prevalence of resistant hypertension in the United States?* Curr Opin Cardiol, 2012. **27**(4): p. 386-91.
5. Joyner, M.J. and J.K. Limberg, *Blood Pressure: Return of the Sympathetics?* Curr Hypertens Rep, 2016. **18**(1): p. 7.
6. Patel, P., et al., *Screening for non-adherence to antihypertensive treatment as a part of the diagnostic pathway to renal denervation.* J Hum Hypertens, 2016. **30**(6): p. 368-73.
7. Nwankwo, T., et al., *Hypertension among adults in the United States: National Health and Nutrition Examination Survey, 2011-2012.* NCHS Data Brief, 2013(133): p. 1-8.
8. Cushing, H.W., *Concerning a definitive regulatory mechanism of the vaso-motor centre which controls blood pressure during cerebral compression. Bull Johns Hopk Hosp*, 1901. **12**: p. 290-292.

9. Paton, J.F., C.J. Dickinson, and G. Mitchell, *Harvey Cushing and the regulation of blood pressure in giraffe, rat and man: introducing 'Cushing's mechanism'.* Exp Physiol, 2009. **94**(1): p. 11-7.

10. Dickinson, C.J. and A.D. Thomason, *Vertebral and internal carotid arteries in relation to hypertension and cerebrovascular disease.* Lancet, 1959. **2**(7090): p. 46-8.

11. Warnert, E.A., et al., *Is High Blood Pressure Self-Protection for the Brain?* Circ Res, 2016. **119**(12): p. e140-e151.

12. Hall, J., *Guyton and Hall Textbook of Medical Physiology.* 2016.

13. Klanunde, R., *Cardiovascular Physiology Concepts.* 2011.

14. Wehrwein, E.A. and M.J. Joyner, *Regulation of blood pressure by the arterial baroreflex and autonomic nervous system.* Handb Clin Neurol, 2013. **117**: p. 89-102.

15. Cowley, A.W., Jr., *Long-term control of arterial blood pressure.* Physiol Rev., 1992. **72**(1): p. 231-300.

16. Thomas, C.B., *Experimental hypertension from section of moderator nerves: Relationship of acute pressor response to development and cause of chronichypertension.* Johns Hopkins Hosp Bull, 1954. **74**: p. 335-377.

17. Ferrario, C.M., J.W. McCubbin, and I.H. Page, *Hemodynamic characteristics of chronic experimental neurogenic hypertension in unanesthetized dogs.* Circ Res, 1969. **24**(6): p. 911-22.

18. Nowak, S.J.G., *Chronic hypertension produced by carotid sinus and aortic-depressor nerve section.* Ann Surg 1940. **111**: p. 102-111.

19. Cowley, A.W., Jr., J.F. Liard, and A.C. Guyton, *Role of baroreceptor reflex in daily control of arterial blood pressure and other variables in dogs.* Circ Res, 1973. **32**(5): p. 564-76.

20. Thrasher, T.N., *Unloading arterial baroreceptors causes neurogenic hypertension.* American Journal of Physiology: Regulatory, Integrative and Comparative Physiology, 2002. **282**(4): p. R1044-R1053.

21. Thrasher, T.N., *Baroreceptors, baroreceptor unloading, and the long-term control of blood pressure.* Am.J.Physiol.Regul.Integr.Comp.Physiol., 2005. **288**(4): p. R819-R827.

22. Lohmeier, T.E. and R. Iliescu, *The baroreflex as a long-term controller of arterial pressure.* Physiology (Bethesda), 2015. **30**(2): p. 148-58.

23. Lohmeier, T.E., et al., *Global- and renal-specific sympathoinhibition in aldosterone hypertension.* Hypertension, 2015. **65**(6): p. 1223-30.

24. Lohmeier, T.E., *The sympathetic nervous system and long-term blood pressure regulation.* American Journal of Hypertension, 2001. **14**(6 PT 2): p. 147S-154S.

25. Lohmeier, T.E., et al., *Sustained influence of the renal nerves to attenuate sodium retention in angiotensin hypertension.* American Journal of Physiology: Regulatory, Integrative and Comparative Physiology, 2001. **281**(2): p. R434-R443.

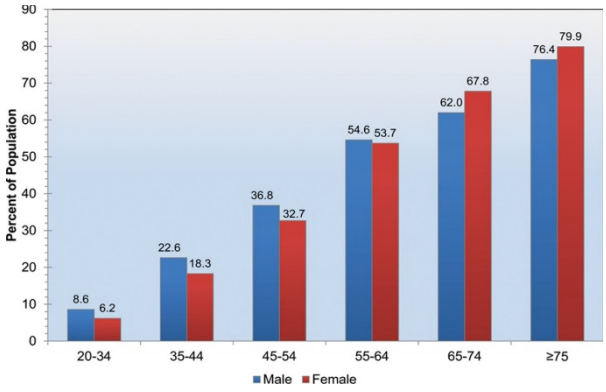
Percent of Population
90
80
70
60
50
40
30
20
10
0
8.6
6.2
22.6
18.3
36.8
32.7
54.6
53.7
62.0
67.8
76.4
79.9
20-34
35-44
45-54
55-64
65-74
≥75
Male
Female

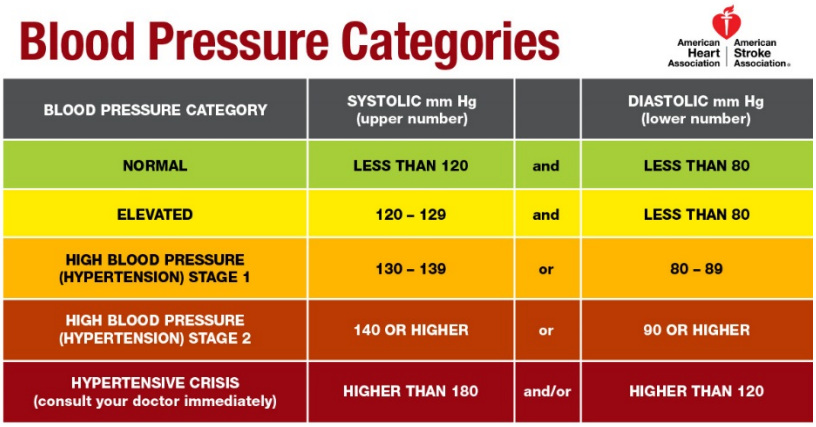

Figure 1: Prevalence of high blood pressure in adults ≥20 years of age by age and sex

Hypertension is defined as systolic blood pressure ≥140 mm Hg or diastolic blood pressure ≥90 mm Hg, if the subject said "yes" to taking antihypertensive medication, or if the subject was told on 2 occasions that he or she had hypertension.

National Center for Health Statistics and National Heart, Lung, and Blood Institute. National Health and Nutrition Examination Survey: 2007–2012

Figure 2: New 2017 guidelines for defining hypertension

Pre-hypertensive has been eliminated and Stage 1, Stage 2, and Crisis categories have been created.

American Heart Association

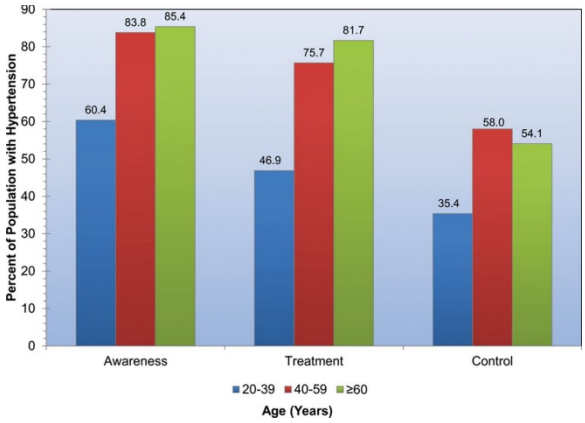
Percent of Population with Hypertension
90
80
70
60
50
40
30
20
10
0
60.4
83.8
85.4
46.9
75.7
81.7
35.4
58.0
54.1
Awareness
Treatment
Control
20-39
40-59
≥60
Age (Years)

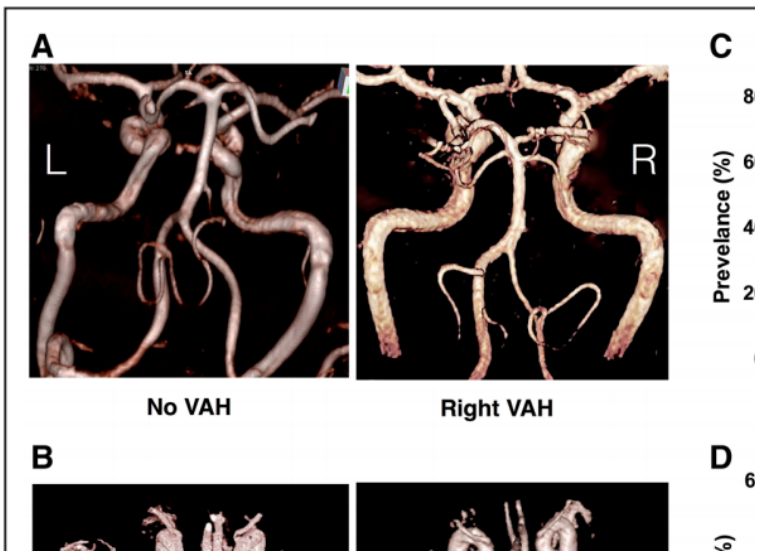

Figure 3: Extent of awareness, treatment, and control of high blood pressure by age

Hypertension (2003 not 2017) is defined as systolic blood pressure ≥140 mm Hg or diastolic blood pressure ≥90 mm Hg, or if the subject said "yes" to taking antihypertensive medication.

National Center for Health Statistics and National Heart, Lung, and Blood Institute. National Health and Nutrition Examination Survey: 2007–2012

Figure 4: Congenital cerebrovascular variants of the posterior cerebral circulation are more prevalent in people with hypertension compared with normotensive controls

A and B, Examples of vertebral artery hypoplasia (VAH; right image) and an incomplete posterior circle of Willis (iCoW; no posterior communicating arteries; pCoA; right image). C, Retrospective study (n=133), prevalence of VAH and iCoW is higher in patients with hypertension compared with the prevalence in controls. There were no differences in age (51±2 vs 51±2 years, P=0.93), sex (males; 56% vs 50%, P=0.50), systolic blood pressure (169±3 vs 170.1±3 mmHg, P=0.87), or diastolic blood pressure (97±2 vs 96±5 mmHg, P=0.72) between hypertensive patients with VAH and those without this anatomic variant. D, Case– control study (n=136), prevalence of VAH and VAH with an incomplete posterior CoW in hypertensives and normotensive controls. The retrospective study is compared with data previously described by Park et al.15 **P=0.006 (binary logistic regression), ****P

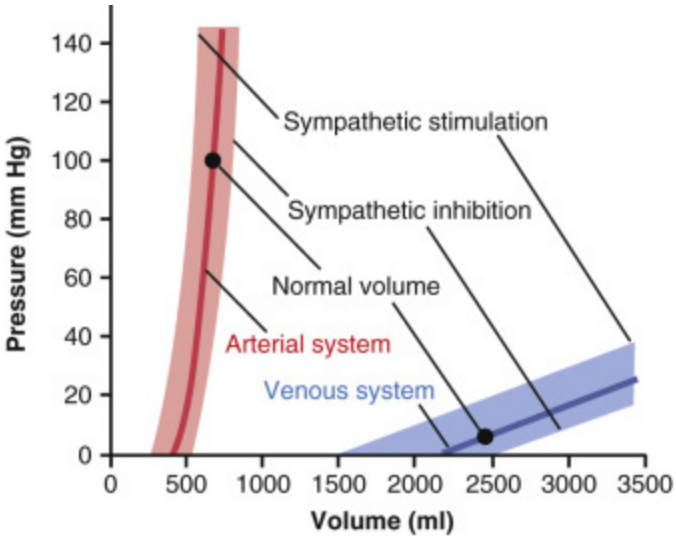
Pressure (mm Hg)
140
120
100
80
60
40
20
0
0
500
1000
1500
2000
2500
3000
3500
Volume (ml)
Sympathetic stimulation
Sympathetic inhibition
Normal volume
Arterial system
Venous system

Figure 5: Volume-pressure relationships in venous and arterial systems

Volume-pressure curves illustrate the effect that pressure has on blood volume in stiff arteries versus compliant veins.

Guyton and Hall Textbook of Medical Physiology

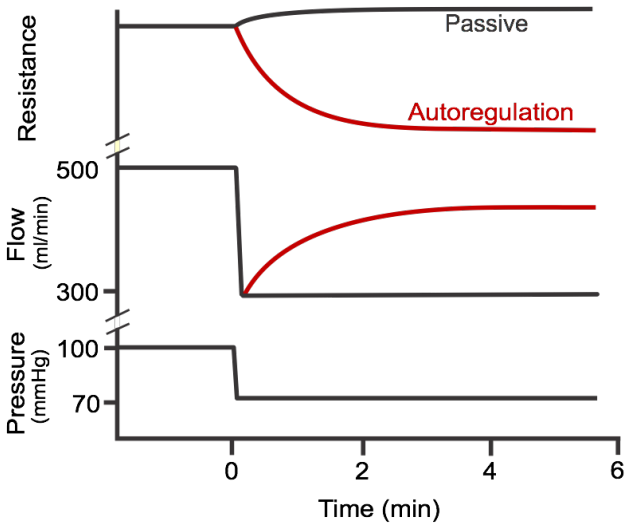
Resistance
Passive
Autoregulation
Flow (ml/min)
500
300
Pressure (mmHg)
100
70
0
2
4
6
Time (min)

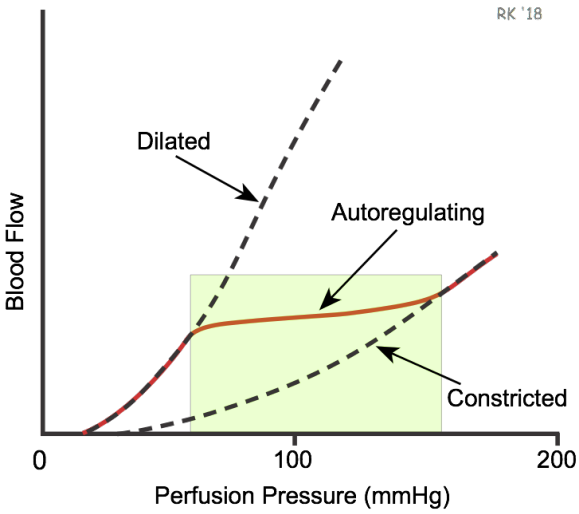
RK '18
Blood Flow
Dilated
Autoregulating
Constricted
0
100
200
Perfusion Pressure (mmHg)

Figure : Blood flow by autoregulation as a function of perfusion pressure

A drop in perfusion pressure causes a passive vessel to compress (resistance increases) and limits flow. However, if a vessel is autoregulatory (red), smooth muscle relaxes which causes dilation and maintains blood flow despite the change in perfusion pressure.

Cardiovascular Physiology Concepts

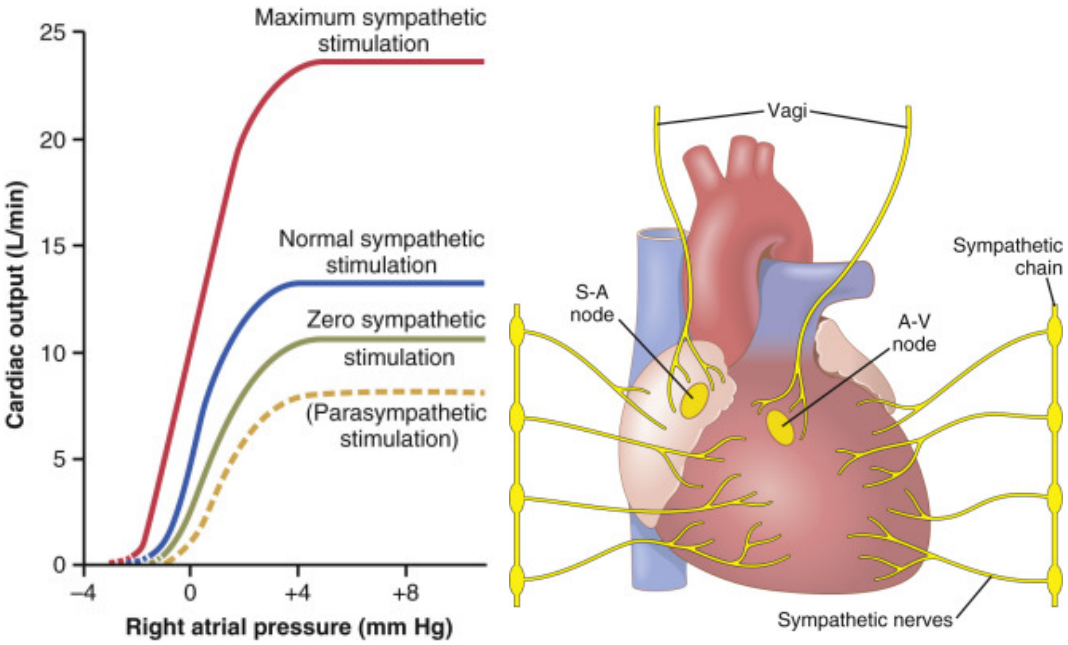
Maximum sympathetic stimulation
Normal sympathetic stimulation
Zero sympathetic stimulation
(Parasympathetic stimulation)
Cardiac output (L/min)
25
20
15
10
5
0
–4
0
+4
+8
Right atrial pressure (mm Hg)
Vagi
Sympathetic chain
S-A node
A-V node
Sympathetic nerves

Figure 7: Autonomic innervation of the heart.

Left: Activation of sympathetic postganglionic fibers causes noradrenaline release in cardiac tissue, which binds to β_1 adrenergic receptors on cardiomyocytes and pacemaker cells. **Right:** Sympathetic activity can robustly increase cardiac output, shown here as a function of right atrial pressure.

Guyton and Hall Textbook of Medical Physiology

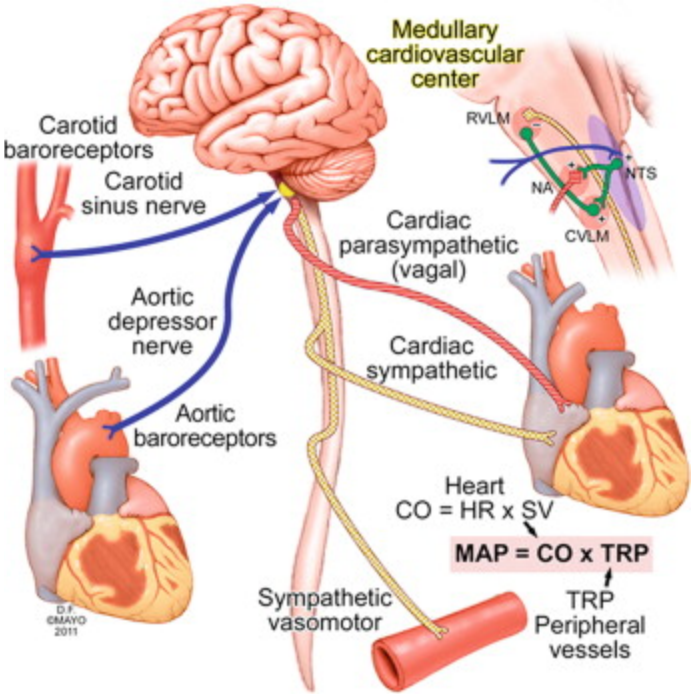
Medullary cardiovascular center
RVLM
NA
NTS
CVLM
Carotid baroreceptors
Carotid sinus nerve
Cardiac parasympathetic (vagal)
Aortic depressor nerve
Cardiac sympathetic
Aortic baroreceptors
Heart
CO = HR x SV
MAP = CO x TRP
TRP
Peripheral vessels
Sympathetic vasomotor
D.F. ©MAYO 2011

Figure 8: Parasympathetic and sympathetic pathways of the baroreflex

The baroreflex pathway includes the sinoaortic baroreceptor sensory afferents (blue) which project onto the medullary cardiovascular center of the brainstem (top right) and ultimately inhibit sympathetic activity to the heart and vessels (yellow) and activate parasympathetic cardiac efferents all of which decrease heart rate (HR), stroke volume (SV) and total peripheral resistance (TRP) and thus mean arterial pressure (MAP).

Wehrwein and Joyner 2013

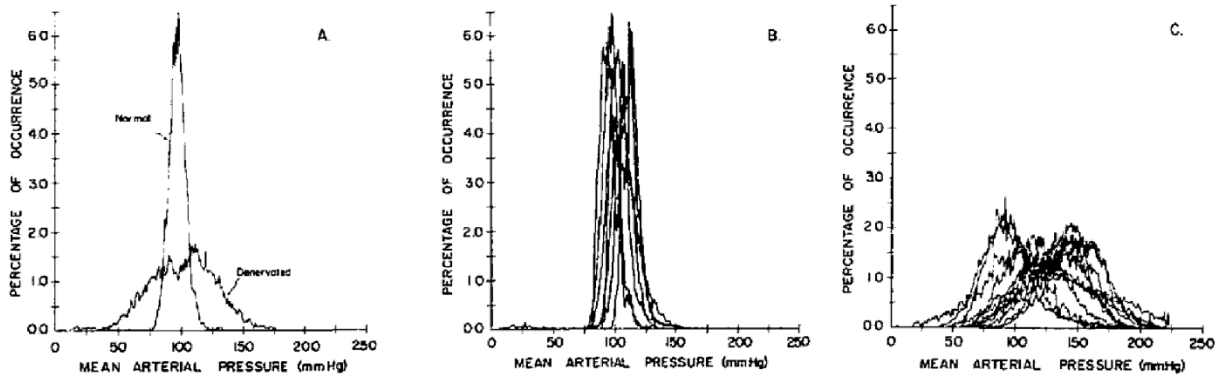
A.
B.
C.
PERCENTAGE OF OCCURRENCE
MEAN ARTERIAL PRESSURE (mmHg)
Normal
Denervated
0
10
20
30
40
50
60
50
100
150
200
250

Figure 9: Frequency distribution curves of 24-hour continuous recordings of mean arterial blood pressure in normal and sinoaortic denervated dogs

A: Individual dog before and after denervation, B: Composite overlay of 10 normal dogs. C: Composite overlay of 12 denervated dogs. This figure demonstrates a fundamental role of the baroreflex in mediating fine control of blood pressure in the short term and suggests that mean arterial pressure can be maintained in the long term despite ablation of the baroreceptors.

Cowley 1973

48

A

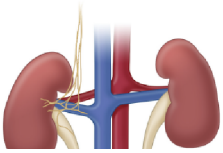

Figure 10: Daily sodium/fluid excretion from innervated and denervated kidneys

Daily sodium/fluid excretion from innervated and denervated kidneys under **(A) control conditions**, during **(B) ANG II hypertension**, and during **(C) ANG II hypertension after sinoaortic denervation (SAD)**. Sodium intake was constant, and daily sodium balance was achieved under all conditions. During ANG II hypertension, there was a relatively greater rate of sodium excretion from innervated than denervated kidneys before but not after SAD, consistent with sustained baroreflex-mediated inhibition of renal sympathetic nerve activity. In the absence of the baroreflex (C), the lower rate of sodium excretion from innervated vs. denervated kidneys may reflect central actions of ANG II to increase renal sympathetic nerve activity.

Lohmeier 2015

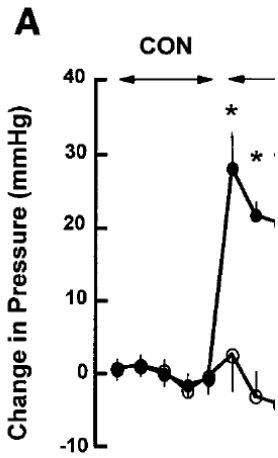
A
CON
Change in Pressure (mmHg)
40
30
20
10
0
-10
*
*

Figure 11: Unloading the intact carotid baroreceptor increases carotid sinus pressure at the expense of systemic arterial pressure

(A) During ligation of the innervated carotid artery (EXP), the carotid sinus pressure (open circles) is maintained at the expense of mean arterial pressure (closed circles)

Thrasher 2002

Chapter 2: Regulation of blood pressure and catecholamines via the RVLM

2.1 Blood pressure regulation via the RVLM

History of the RVLM

Experiments in the early 1850s demonstrated that sympathetic nerves were required to maintain vasomotor tone in vascular beds [1, 2]. Soon after, it was shown that this sympathetic activity was reliant on the central nervous system [3]. Further studies in the 1870s discovered that coronal sectioning in a rostro-caudal direction along the neuraxis had little effect on systemic blood pressure until the medulla was severed—at which point blood pressure (blood pressure) plummeted to levels observed only after complete transection of all supraspinal input. This enormous drop in blood pressure was again elicited if the ventral portion of this medullary region was sectioned [4, 5]. Thus, within a few decades from the initial study discovering that sympathetic nerves provide vasomotor tone, it was already clear that the ventral medulla was critically involved in maintenance of blood pressure—at least under anesthetized conditions.

Despite this rapid advancement in locating the origin of sympathetic vasomotor tone, the decades that followed these early observations did little to further isolate the critical area within the ventral medulla. Much of the research during this period revolved around electrical stimulation—which activates a combination of cell bodies, dendrites, and axons of passage—or electrophysiological identification of barosensitive regions via stimulation of the carotid sinus nerve—which activates many non-barosensitive circuits. This work deviated the focus of neuronal blood pressure regulation research from the ventral medulla, and during this period much of the early work localizing the ventral

medulla was largely overlooked. Then, in the 1960s and 1970s, roughly a century after Dittmar's original localization experiments, the ventral medulla was rediscovered as a critical region for blood pressure regulation and sympathetic outflow. Through 1974-1976, Silver, Feldberg, and Guertzenstein discovered that blood pressure could be decreased by topically applying drugs to the RVLM of anesthetized cat or increased by electrical stimulation (Figure 12) [6, 7]. Christopher Ross then stimulated or inhibited the RVLM of anesthetized rats, which also produced large increases or enormous drops in blood pressure, and importantly, Ross charted the precise location in the VLM that elicited the blood pressure response [8].

Ross et al. began by mapping blood pressure responses to low-level electrical stimulation along the ventral surface of the medulla. Some rats were then transected at the cervical spinal cord, and given the same electrical stimuli in the region which generated the greatest rise in blood pressure when stimulated. After transection, electrical stimulation of the RVLM failed to generate significant changes in blood pressure, and the small changes that were elicited by stimulation were blocked by vasopressin antagonist (Figure 13, left panel). This demonstrated that in rats, the vast majority of the elicited rise in blood pressure by electrical stimulation of the RVLM was dependent on the integrity supraspinal input to the spinal cord (i.e. neuronal input from the brain to the spinal cord) and only a minute pressor effect was evoked by activating hormonal circuits. In other rats, chemicals were microinjected at the locations that generated the greatest rise in blood pressure. Injections of glutamate substantially increased blood pressure while bilateral injections of GABA recapitulated the drop in pressure observed after spinal transection (Figure 13, middle and right panels). Importantly, when glutamate was

injected 1mm rostral, caudal, or medial to the RVLM, the robust increase in blood pressure was not evoked. Therefore, by microinjecting GABA and glutamate into the rat RVLM, Ross et al demonstrated that (1.) *cell bodies* of the neurons important to blood pressure regulation are located in the medulla, overcoming the uncertainty in data from electrical RVLM stimulation which activates fibers of passage, (2.) neurons isolated to the rostral portion of the VLM make up the population critical to blood pressure regulation in rodent as injections 1mm away from the RVLM did not elicit the same effect, and (3.) neurons in the RVLM constitute the *entire* supra-spinal blood pressure regulatory output—at least under these anesthetized conditions. This seminal paper on blood pressure regulation then begged the following question: which neurons and pathways in the RVLM are the critical ones for blood pressure regulation?

Importantly, supra-spinal input had been shown to be critical for blood pressure maintenance, and the previously mentioned Ross study demonstrated this input was also critical for the RVLM-stimulation evoked rise in blood pressure. Therefore, the simplest pathway to explain both of these results would be a direct projection from the RVLM into the spinal cord. Several anatomical studies have identified spinally projecting pathways from the RVLM, including a dense projection from this region onto the intermediolateral cell column of the spinal cord—the location of the sympathetic preganglionic neurons [9-15]. These results indicate that at least some of the critical blood pressure regulatory neurons within the RVLM could be pre-sympathetic—they directly innervate sympathetic preganglionic neurons. Together, these critical works established the importance of the RVLM in the regulation of blood pressure, and suggested that a direct pre-sympathetic

RVLM population could be the critical central neurons for the neural maintenance of blood pressure.

Presympathetic RVLM neurons

The foremost candidate population in the RVLM responsible for generation of sympathetic tone and maintenance of blood pressure is the pre-sympathetic group. These neurons could determine sympathetic activity and blood pressure by directly controlling sympathetic preganglionic neurons within the spinal cord. In the RVLM, a few clusters of neurons have been identified as spinally-projecting—i.e. bulbospinal, and several studies have identified direct projections from the RVLM onto sympathetic preganglionic neurons (*see [16] for review*). Many of these presympathetic neurons are demonstrably catecholaminergic—i.e. C1—though some portion of presympathetic RVLM neurons seem to lack detectable levels of catecholaminergic machinery via immunohistochemical labeling—sometimes referred to as 'non C1'†. Of the two presympathetic groups, C1 neurons are by far the better studied. C1 neurons are barosensitive and selective stimulation of C1 increases sympathetic nerve activity and increases blood pressure [16, 17]. C1 has been shown to excite postsynaptic neurons in the brain by releasing glutamate, and they likely excite preganglionic sympathetic neurons by this mechanism as C1 terminals in the intermediolateral cell column both contain Vglut2—a packaging protein necessary for vesicle loading of glutamate—and form excitatory synapses. Importantly, inhibition of C1 neurons lowers blood pressure—at least under certain anesthetized conditions. Interestingly selective lesioning of C1 did not affect resting blood pressure and optogenetic inhibition in conscious rats marginally lowered blood

pressure, despite having profound effects on blood pressure when the inhibition was performed under various stresses in the same rats [18]. These data indicate that C1 neurons may not play a role in setting resting blood pressure in conscious, unstressed animals. Extrapolating from anesthetized data, input from the RVLM is thought to be required for maintenance of sympathetic tone, which determines resting blood pressure. Whether this supraspinal input could be provided by non-catecholaminergic spinally projecting neurons remains an open question.

Works Cited

1. Bernard, C., *Influence du grand sympathique sur la sensibilite et sur la calorification.* C R Soc Biol, 1851. **3**: p. 163-164.
2. Brown-Sequard, C.E., *Researches on the influence of the nervous system upon the function of organic life.* Med Examiner (Philadelphia), 1852. **8**: p. 486-497.
3. Goltz, F., *Uber den Tonus der Gefasse und seine Bedeuting fur die Blut deweging.* Virchows Arch, 1864. **29**: p. 394-432.
4. Dittmar, C., *Ueber die Lage des sogenannten Gefusscentrums in der Medulla oblongata.* Ber.Verh.Saechs.Akad.Wiss.Leipzig,Math.Naturwiss.Kl., 1873. **25**: p. 449-469.
5. P., O., *Die tonischen und reflectorischen Centren der Gefassnerven.* Ber.Sachs.Ges.Wiss.mat.-phys.Kl., 1871. **23**: p. 135-143.
6. Guertzenstein, P.G. and A. Silver, *Fall in blood pressure produced from discrete regions of the ventral surface of the medulla by glycine and lesions.* J Physiol, 1974. **242**(2): p. 489-503.
7. Feldberg, W. and P.G. Guertzenstein, *Vasodepressor effects obtained by drugs acting on the ventral surface of the brain stem.* J Physiol, 1976. **258**(2): p. 337-55.
8. Ross, C.A., et al., *Tonic vasomotor control by the rostral ventrolateral medulla: effect of electrical or chemical stimulation of the area containing C1 adrenaline neurons on arterial pressure, heart rate, and plasma catecholamines and vasopressin.* Journal of Neuroscience, 1984. **4**(2): p. 474-494.

9. Dampney, R.A., et al., *Role of ventrolateral medulla in vasomotor regulation: a correlative anatomical and physiological study.* Brain Res, 1982. **249**(2): p. 223-35.

10. Goodchild, A.K., R.A. Dampney, and R. Bandler, *A method for evoking physiological responses by stimulation of cell bodies, but not axons of passage, within localized regions of the central nervous system.* J Neurosci Methods, 1982. **6**(4): p. 351-63.

11. Caverson, M.M., J. Ciriello, and F.R. Calaresu, *Direct pathway from cardiovascular neurons in the ventrolateral medulla to the region of the intermediolateral nucleus of the upper thoracic cord: an anatomical and electrophysiological investigation in the cat.* J Auton Nerv Syst, 1983. **9**(2-3): p. 451-75.

12. Amendt, K., et al., *Neurones within the "chemosensitive area" on the ventral surface of the brainstem which project to the intermediolateral column.* Pflugers Arch, 1978. **375**(3): p. 289-92.

13. Ross, C.A., et al., *Adrenaline neurons in the rostral ventrolateral medulla innervate thoracic spinal cord: a combined immunocytochemical and retrograde transport demonstration.* Neurosci Lett, 1981. **25**(3): p. 257-62.

14. Ross, C.A., D.A. Ruggiero, and D.J. Reis, *Projections to the spinal cord from neurons close to the ventral surface of the hindbrain in the rat.* Neurosci Lett, 1981. **21**(2): p. 143-8.

15. Ross, C.A., et al., *Rostral ventrolateral medulla: selective projections to the thoracic autonomic cell column from the region containing C1 adrenaline neurons.* J Comp Neurol, 1984. **228**(2): p. 168-85.

16. Guyenet, P.G., *The sympathetic control of blood pressure.* Nat Rev Neurosci, 2006. **7**(5): p. 335-46.

17. Guyenet, P.G., et al., *C1 neurons: the body's EMTs.* Am J Physiol Regul Integr Comp Physiol, 2013. **305**(3): p. R187-204.

18. Wenker, I.C., et al., *Blood Pressure Regulation by the Rostral Ventrolateral Medulla in Conscious Rats: Effects of Hypoxia, Hypercapnia, Baroreceptor Denervation, and Anesthesia.* J Neurosci, 2017. **37**(17): p. 4565-4583.

2.2 The following section is a manuscript in preparation for submission investigating the questions from the previous section

Optogenetic stimulation of spinally projecting non-catecholaminergic neurons in the RVLM increases blood pressure in conscious mice

Benjamin B. Holloway[1], Ruth L. Stornetta[1], Daniel Stornetta[1], and Patrice G. Guyenet[1]

[1] ***Department of Pharmacology, University of Virginia, Charlottesville, VA 22908***

Abstract

The rostral ventrolateral medulla (RVLM) is critical brainstem region for the regulation of sympathetic activity, blood pressure, and cardiac output—though the neurons that carry out these roles remain debated. A strong candidate is barosensitive pre-sympathetic neurons, historically split into two groups, based on presence (C1) or lack of catecholamines (non-C1). C1 neurons are by far the better studied group, and the roles non-C1 neurons play in cardiovascular control—if any—remain unknown. Therefore, we sought to establish whether non-catecholaminergic pre-sympathetic neurons within the RVLM could participate in regulation of blood pressure. Here we show that optogenetic stimulation of RVLM increases blood pressure in conscious mice, even after lesion of C1 neurons (113±4 vs 143±5 mmHg, $p<0.0001$, N=9). Under anesthesia, optogenetic stimulation of spinal axons from RVLM also increases blood pressure in C1-lesioned mice (72±4 vs 96±7 mmHg, $p=0.0066$). In conscious mice with C1 intact, optogenetic stimulation of spinally-projecting RVLM neurons increases blood pressure, however stimulation of C1 alone does not (112±3 vs 129±2 mmHg, $p=0.0002$, N=4, RVLM stimulation; 103±4 vs 99±4 mmHg, N=8, $p=0.0545$ C1 stimulation). Collectively these data demonstrate that non-catecholaminergic bulbospinal neurons are capable of controlling blood pressure in conscious mice independent of C1 neurons.

Introduction

The current perception of the rostral ventrolateral medulla (RVLM) as a critical center for the maintenance of cardiovascular function in conscious animals is heavily based on the results of acute pharmacological and electrical perturbation of the region in anesthetized mammals. Pharmacological and electrical stimulation of the RVLM produce robust increases in blood pressure, while pharmacological inhibition of the RVLM lowers blood pressure to levels observed after complete autonomic blockade—indicating that all detectable influence on blood pressure by the central nervous system is dependent on the integrity of the RVLM, at least under these experimental conditions [1, 2]. Importantly, the neurons within the RVLM that are responsible blood pressure maintenance and the relevance of these results to conscious animals remain conjectural.

One of the primary candidate populations responsible for generating sympathetic tone and setting resting blood pressure is the pre-sympathetic group. Several studies have demonstrated that many neurons within the RVLM directly innervate sympathetic preganglionic neurons, and at least some spinally projecting RVLM neurons—likely pre-sympathetic—are demonstrably barosensitive [3-5]. Both supraspinal input and RVLM integrity are thought to be necessary for the maintenance of resting blood pressure, and the most straightforward pathway to explain these two observations would be that the RVLM controls blood pressure via a direct innervation of sympathetic preganglionic neurons. Both pre-sympathetic neurons and spinally-projecting barosensitive neurons (putatively pre-sympathetic) in the RVLM can be further divided based on the presence or absence of catecholaminergic biosynthetic enzymes—C1 and non-C1, respectively.

Of the two groups, C1 neurons are by far the better studied. C1 neurons compose around 72% of all bulbospinal barosensitive neurons, they are coextensive with the critical cardiovascular region, they increase blood pressure when stimulated in anesthetized and conscious rats, and their activity is required for blood pressure maintenance during certain stresses (e.g. anesthesia); though the role C1 neurons play in setting resting blood pressure remains unclear [3, 4, 6, 7]. Interestingly, optogenetic inhibition of C1 in conscious unstressed rats has yet to produce the magnitude of change in blood pressure predicted from complete pharmacological inhibition of the RVLM under anesthesia and near complete lesion of C1 neurons in rats does not affect resting blood pressure [6, 8, 9]. Further, after C1-lesion, electrical stimulation of the RVLM still increases SNA and blood pressure, and pharmacological inhibition of the RVLM lowers blood pressure the same magnitude as C1-intact animals [10]. Collectively, these data indicate that another population within the RVLM—potentially non-catecholaminergic pre-sympathetic neurons—could play an important role in generating sympathetic tone and determining resting blood pressure.

While C1 ablation does not alter resting blood pressure, when the system is stressed—such as during hypoxia (i.e. cyanide i.v.)—the lack of C1 is apparent. Therfore, it remains uncertain if blood pressure is simply compensated by non-neuronal mechanisms after C1 lesion, or if C1 neurons may play a unique role in mediating cardiovascular reflexes and stress responses while resting blood pressure is maintained through non-catecholaminergic RVLM neurons. Therefore we wished to test whether blocking sympathetic tone lowers resting blood pressure in conscious C1-intact and C1-

lesioned animals, and if stimulation of non-catecholaminergic bulbospinal neurons is sufficient to raise blood pressure in conscious animals.

Materials and Methods

Animals

All experiments were performed in accordance with guidelines approved by the University of Virginia Animal Care and Use Committee. Mice used in this study were Tg(Dbh-cre)KH212Gsat/Mmcd mice, stock no. 032081-UCD (DβH-Cre) obtained from the Mutant Mouse Regional Resource Center at the University of California, Davis, CA and maintained as hemizygous (DβHCre/0) on a C57BL/6J background. C57BL/6J mice were obtained from Jackson labs (JAX Stock #012898; STOCK Slc17a6tm1Lowl/J and C57, JAX Stock#000664). DβH0/0 littermates of hemizygous DβHCre/0 offspring were used in all experiments that did not utilize Cre recombinase.

Viral Vectors

The following viral vectors from University of North Carolina vector core were used in this work: AAV2-EF1α-DIO-hCHR2(H134R)-EYFP; AAV2-EF1α-DIO-eArch3.0-EYFP; AAV5-flex-taCasp3-TEVp; and AAV2-CaMKIIα-hChR2(H134R)-EYFP. AAVrg-pmSyn1-EBFP-Cre-bGHpA was a gift from Hongkui Zeng (Addgene viral prep # 51507-AAVrg). AAV2-EF1α-DIO-hCHR2(H134R)-EYFP and AAV2-EF1α-DIO-eArch3.0-EYFP were used to express channelrhodopsin exclusively in C1 neurons in

DβH$^{Cre/0}$ mice or in neurons expressing Cre recombinase after injection of AAVrg-pmSyn1-EBFP-Cre into the thoracic spinal cord. AAV5-flex-taCasp3-TEVp was used to selectively lesion C1 neurons in *DβH*$^{Cre/0}$ mice. AAV2-CaMKIIα-hChR2(H134R)-EYFP was used to optogenetically activate RVLM neurons in combination with C1 lesion studies.

Guided stereotaxic microinjections and optic fiber implantation

Stereotaxic injections took place in aseptic conditions as previously described. Mice were anesthetized with a mixture of ketamine (100mg/kg) and dexmedetomidine (0.2 mg/kg) injected intraperitoneally. Anesthesia was assessed by absence of corneal and hind-paw withdrawal reflex—additional anesthetic was administered as required (given at 1/5th of the original dose). Following skin shaving, the skin overlying the left mandible was cut to reveal a short segment of the mandibular branch of the facial nerve. The mice were then placed prone on a Kopf 1730 stereotaxic apparatus adapted for mouse stereotaxic injections (ear bar adaptor- model EB-5N, Narashige Scientific Instrument Lab. Bite bar- Model 926 mouse adaptor set at −2 mm; David Kopf Instruments). Body temperature was kept close to 37°C with a servo-controlled heating pad and a blanket. A 1.5 mm diameter hole was drilled into the occipital plate on the left side caudal to the parieto-occipital suture. The viral vector was loaded into a 1.2 mm internal diameter glass pipette broken to a 25 micron tip (external diameter). The facial nerve was stimulated (0.1 ms, 1–300 μA, 1Hz) to evoke antidromic field potentials within the facial motor nucleus according to a method previously used in mice and rats (OTHERS, Brown and Guyenet, 1985). These field potentials were used to map the extent of the facial motor

nucleus which was used as a landmark to precisely target specific regions of the rostral ventrolateral medulla. Strong respiration synchronous mass activity located exclusively caudal to the facial motor nucleus further helped in navigating to this region. For experiments requiring multiple injection sites along the RVLM, injections were separated by 200 microns and were aligned rostro-caudally. Injection volumes and sites varied and are addressed for each experiment.

For experiments involving optogenetic stimulation in conscious mice, a 125 μm-diameter optic fiber, consisting of a stripped, glass-clad multimode optical fiber (105 μm-core, 0.22 numerical aperture; Thorlabs, Newton, NJ, USA) glued into a zirconia ferrule (1.25 mm O.D., 126 μm bore; Precision Fiber Products, Milpitas, CA, USA), was placed with its tip ~150 μm above the injection site. For optogenetic inhibition studies, ferrules were placed bilaterally above each injection site. The ferrule-optic fiber system was secured to the skull with adhesive (either Loctite 3092 or black dental cement; Lang Dental Manufacturing, Wheeling, IL, USA).

In all mice, incisions were closed in two layers (muscle and skin) with sutures and surgical glue. Mice received post-operative boluses of atipemazole (α2-adrenergic antagonist, Antisedan, 2 mg/kg, s.c.), ampicillin (125 mg/kg, i.p.), and ketoprofen (4 mg/kg, s.c.) and were then placed in a heated environment (37°C) until consciousness was regained before being returned to a clean home cage. Ketoprofen was administered 24 and 48 hrs post-operatively.

Physiology experiments in conscious mice

For blood pressure recordings in conscious mice, animals were instrumented with radio telemetry probes (PA-C10; Data Sciences International). For probe implantation, mice were anesthetized with an i.p. injection of ketamine (120 mg/kg) and xylazine (12 mg/kg) and their body temperature kept at 37.0 ± 0.5 °C. Animals were allowed at least one week of recovery after probe implantation. Telemetric blood pressure signals were received using a PhysioTel Receiver (RLA 1020; Data Science International), then digitized by a Micro1401 board (v7.10, Cambridge Electronic Design, Ltd., Cambridge, UK) at 1kHz, and recorded using Spike2 software (v7.10, Cambridge Electronic Design, Ltd., Cambridge, UK). Mean AP and HR were calculated from pulsatile AP recordings based on values calibrated before implantation of the telemetry probe.

With the exception of 24h blood pressure recordings, all conscious studies were performed within a plethysmography chamber. Photostimulation and plethysmography experiments took place as previously described. Photostimulation was performed using a diode-pumped solid state blue laser (473 nm, CrystaLaser) controlled by TTL-pulses from a Grass model S88 stimulator (AstroMed Inc.). Prior to implantation, the light output at the tip of each optic fiber was measured with a light meter (Thorlabs, Newton, NJ) and adjusted for a final output of 10 mW. This setting was later used during the experiments. Photostimulation and plethysmography trials were carried out at least 6 wks after injections of viral vectors and implantations of the optic fiber. Breathing parameters were measured in conscious mice using unrestrained whole-body plethysmography (EMKA Technologies, Falls Church, VA ,USA) as previously described. For photostimulation within the plethysmography chamber, mice were briefly anesthetized with isoflurane while the implanted optical fiber-ferrule and the laser delivery system was

connected. Animals were allowed at least 30 minutes to recover from the brief anesthesia and ferrule attachment. The chamber was continuously flushed with dry, room-temperature air delivered at 0.5 liter/min. Chamber pressure signals were detected via a differential pressure transducer, amplified (× 500), band pass filtered (0.25Hz to 35Hz), and digitized at 1 kHz with Spike 2 software (v7.10, Cambridge Electronic Design, Ltd., Cambridge, UK). To evaluate the effects of photostimulation on f_R, 10 s-long trains of 5 ms light pulses were delivered at three frequencies (5, 10 and 15 Hz). Behavioral quiescence was determined by direct observation or via an automated function using Spike2 software. For automated acquisition, a 10s laser stimulation strain was triggered as determined by a random number generator at one of the following parameters: frequencies of 5, 10, 15, or 20 Hz and pulse widths of 5, 10, 15, or 20ms. Brief behavioral quiescence was defined as an eleven second period of breathing in which max and min f_R were less than 200 bpm and greater than 90 bpm, no sighing occurred, mean f_R was between 130 and 170 bpm, and the laser was triggered only if the preceding stimulation had occurred at a time greater than 60s prior. All automated stimulation trials were visually inspected posthoc and only those trials that had occurred during behavioral quiescence were used for analysis. The reported physiological changes during photostimulation reflect the average response of at least 5 trials per mouse at each stimulation frequency.

Physiology experiments in anesthetized mice

Mice were anesthetized with a mixture of ketamine (100 mg/kg) and dexmedetomidine (0.2 mg/kg) given i.p. The mice were placed prone on a stereotaxic

apparatus designed for rats using the mouse adaptors described above. Body temperature was kept close to 37°C with a servo-controlled heating pad and a blanket. Breathing frequency was recorded by measuring CO_2 fluctuations around the nares using a microcapnograph (CI240, Columbus Instruments; Columbus, OH, USA). For optogenetic stimulation within the brainstem, a laser was connected to the optic fiber-ferrule system as previously described in conscious experiments. For optogenetic stimulation of spinal axons, a cutaneous midline incision was made above the thoracic region of the spinal cord. Superficial tissue and muscles were retracted to expose the enlarged T2 spinal process, at which point the deep tissue caudal to the T2 spine was retracted to expose the interspinous region. Using a stereotaxic micromanipulator, a 125 µm diameter optic fiber that was attached to a second laser was placed superficial to the interspinous region, lateral to the midline in a region roughly above the intermediolateral column. We found that 473nm light achieved sufficient penetration of the disc, the dura, and the spinal cord for optogenetic stimulation, such that no further surgery was required once the intervertebral region was exposed. Once the ferrule was connected to one laser and the optic fiber connected to the second laser was positioned above the spinal cord, 10s laser trains were delivered to either the RLVM or the spinal cord at random, again using a random number generator to generate the stimulation location (i.e. RVLM or spinal cord) as well as the stimulation parameters (5, 10, 15, 20 Hz and 5, 10, 15, 20 ms). Longer stimulation trains (up to 5min) were performed manually with user-defined parameters.

CTB and retrograde AAV spinal injections

Injection of the retro-AAV was performed similar to optogenetic stimulation of spinal axons. After identification of T2 and exposure of the intervertebral space, a small puncture was made in the spinal dura using a syringe tip. A pulled glass capillary—loaded with virus and cut to a 25µm external diameter tip—was lowered onto the spinal surface using a micromanipulator. Using a picospritzer, ~80nl of virus was intermittently injected in small boli to minimize viral spread. After injection, post-surgical procedures were performed as described above for stereotaxic injections in the brainstem.

Statistical analysis

Statistical significance was set at $P<0.05$. In, text, all data are expressed as mean ± SEM. To compare two groups we used a paired t-test or Wilcoxon signed rank test. To compare multiple groups, we used the Kruskal-Wallis test or, for repeated measures, the Friedman test followed by Dunn's test to assess inter-group differences. All statistics were done using Graph Pad PRISM software (version 6, La Jolla, CA).

Results

Lesioning C1 neurons does not affect resting blood pressure in conscious mice

Bilateral injection of flex-taCasp3-TEVp AAV5 led to near complete ablation of TH-immunoreactive neurons within the RVLM (23±4 vs. 135±11 TH-ir RVLM neurons, N=13 vs. 8; caspase-injected vs. control; $p<0.0001$; Figure 1). TH-ir neurons were counted bilaterally from 7.19mm to 5.48mm caudal to bregma in 1-in-3 30µm sections.

This region overlaps with the bulbospinal rostral C1 population, which lack neuropeptide Y and were labeled with cholera-toxin B injected into the thoracic spinal cord (Figure 1). Despite a virtually complete lesion of C1 neurons, mice did not have significantly different heart rates or resting blood pressure values versus C1-intact animals during quiet-resting states—defined here as periods of at least 10 seconds where average breathing frequency was within the range of 135 to 165 breaths per minute (555±35 vs. 521±26 beats per minute, p=0.4574; 113±4 vs. 106±3 mmHg, p=0.1656; N=9 C1-lesioned vs. N=8 C1-intact mice; Figure 1).

CaMKIIα-hChR2-YFP AAV selectively labels neurons in the RVLM

Unilateral injection of CaMKIIα-hChR2-YFP led to robust expression of EYFP in the RVLM in both C1-intact and C1-lesioned mice (1573±280 vs. 2378±291 GFP-ir neurons, N=8 vs. N=13; p=0.0784; Figure 2). The vast majority of EYFP neurons lacked TH-ir in both C1-intact and C1 lesioned mice (1560±280 vs. 2340±278, 99.2% vs. 99.6%, N=8 vs. N=13; p=0.0772; Figure 2) and only a few TH-ir neurons—i.e. C1 neurons—from sections containing GFP-ir neurons expressed the ChR2-EYFP fusion protein in either group (11±3 vs. 7±2, N=8 vs. 13, C1-intact vs lesion; p=0.2583; Figure 2).

Optogenetic stimulation of RVLM neurons increases blood pressure in conscious mice, regardless of C1 lesion

Optogenetic stimulation (5ms pulses for 10 seconds) of the RVLM at least 4 weeks after unilateral injection of CaMKIIα-hChR2-YFP AAV increased in blood

pressure in conscious, C1-intact mice in a manner that was directly related to stimulation frequency—tested from 5-20Hz (Figure 2). Increasing the pulse width from 5 to 20ms did not significantly affect the increase in blood pressure (20±2 vs. 19±3 mmHg, N=8; p=0.8196), and when stimulation train lengths were increased beyond 10s, blood pressure remained elevated for the duration of the stimulation (Figure 2). In conscious C1-lesioned animals, optogenetic stimulation (5ms pulses for 10 seconds) of the RVLM again increased in blood pressure in a manner that was directly related to stimulation frequency, was independent of pulse duration, and was persistent across the stimulation length (Figure 2). For both C1-intact and C1-lesioned groups, there was no relation of stimulation frequency to change in heart rate, and the most intense stimulation produced no significant change in heart rate (ANOVA RESULT; 506±39 vs. 517±28 bpm, C1-intact, N=8, p=0.7507; 540±36 vs. 510±37 bpm, C1-lesioned, N=9, p=0.5454; Figure 2).

Optogenetic stimulation of spinally projecting axons from RVLM robustly increases blood pressure in anesthetized mice regardless of C1 lesion

In both C1-intact and C1-lesioned mice injected with CaMKIIa-ChR2-EYFP into the RVLM, YFP-expressing spinal axons densely innervated of the intermediolateral cell column (IML)—suggesting that at least some of the RVLM YFP-expressing neurons were pre-sympathetic. In C1-intact mice, many of the YFP terminals within the IML lacked detectable catecholaminergic markers—i.e. were likely from non-C1 neurons (312±49 of 376±60 terminals lacked TH-ir, ~83%)—and a strong non-catecholaminergic YFP projection of the IML remained in C1-lesioned mice, despite virtually complete ablation of C1 (342±50 of 359±53 terminals lacked TH-ir, ~96%). Neither the total

number of YFP-expressing terminals nor the number of YFP terminals lacking TH was significantly greater in C1-intact versus C1-lesioned mice (376±60 vs. 359±53, p=0.8305; & 312±49 vs. 342±50, p=0.6782; N=6 vs. N=6), while the number of TH-ir YFP terminals was significantly greater in C1-intact versus C1-lesioned mice (64±12 vs. 16±5, p=0.0044; N=6 vs. N=6). To test whether selective activation of spinal projections from the RVLM was sufficient to increase blood pressure, we directly stimulated only these fibers by illuminating the thoracic spinal cord in both C1-intact and C1-lesioned mice injected with CaMKIIa-ChR2-EYFP in the RVLM. Optogenetic stimulation of spinal fibers produced detectable increases in blood pressure that was directly related to stimulation frequency, increased with stimulation pulse duration, and was sustained through the duration of the stimulation (Figure 3).

Optogenetic stimulation of bulbospinal RVLM neurons increases blood pressure in conscious mice while selective stimulation of C1 does not

After establishing that direct activation of non-catecholaminergic bulbospinal RVLM axons was sufficient to increase blood pressure in anesthetized conditions, we wanted to test whether activation of these cells would also increase blood pressure in conscious mice. We injected the retrograde-Cre virus into the thoracic spinal cord and a DIO-EF1a-ChR2-EYFP into the RVLM, leading to the expression of ChR2-EYFP in many neurons within the same region of the RVLM as previous experiments (569±78 neurons counted in 1 in 3 sections from 7.19 to 5.57 mm caudal to bregma). C1 neurons were not ablated in these experiments, however few TH-ir neurons in the RVLM expressed YFP (11.1%; 17±3 of 152±25 C1 in sections containing YFP-expressing

neurons; N=4), and only a small portion the total YFP population was TH-ir (2.9%; 17±3 of 579±78; N=4). Optogenetic stimulation of mostly non-catecholaminergic spinally projecting RVLM cells increased blood pressure in conscious mice in manner that was directly related to stimulation frequency and increased with pulse width ($^{\Delta}$blood pressure = 0.3*stimulation frequency + 2.1; R^2=0.92; 8±2 mmHg at 5ms vs. 18±1 mmHg at 20ms; N=4, p=0.0168, conscious; R^2=0.9779 anesthetized). We then selectively and efficiently expressed ChR2-YFP in C1 neurons by injecting the same DIO-EF1a-ChR2-EYFP AAV into the RVLM of DBH-Cre$^{+/0}$ mice (102±24 of 110±25 YFP neurons, 93%, were TH-ir, and 74% of the total 137±30 TH-ir neurons expressed YFP within the 1 in 3 RVLM sections counted from six mice). Even the most intense optogenetic stimulation of C1 (20Hz, 20ms, 10s) did not increase blood pressure in conscious mice, suggesting that the increase in blood pressure due to stimulation of spinally-projecting RVLM neurons was due to non-catecholaminergic cells (102±4 mmHg prior to stimulation vs. 99±4 mmHg during stimulation, p=0.0545, $^{\Delta}$blood pressure = -4 ± 2 mmHg, N=8). Optogenetic stimulation of C1 was sufficient to activate C1 cells, as both heart rate and breathing frequency during stimulation were significantly different than prior to stimulation periods (408±23 vs. 439±28 beats/min, p=0.0047; $^{\Delta}$HR = -32 ± 8 beats/min; & 205±13 vs. 140±12 breaths/min, p=0.0001; $^{\Delta}$fR = 65 ± 9 breaths/min; N=8).

Discussion

Here we demonstrate non-catecholaminergic bulbospinal RVLM neurons are capable of controlling blood pressure independent of C1 through three primary lines of evidence (i.) optogenetic stimulation of the RVLM increases blood pressure in conscious

mice despite a nearly complete lesion of C1, (ii.) optogenetic stimulation of only the spinal axons from these C1-lesioned mice also increases blood pressure under anesthesia, and (iii.) optogenetic stimulation of bulbospinal RVLM—C1 and non-C1 included—increases blood pressure in conscious mice, while optogenetic stimulation of C1 alone does not. Collectively, these data provide the first demonstration that stimulation of non-C1 neurons is capable of regulating blood pressure in conscious animals independent of C1 neurons.

Optogenetic stimulation of the RVLM in C1-lesioned and C1-intact animals produced increases in blood pressure in conscious mice, and at least some of the neurons expressing the ChR2-YFP protein appeared to be pre-sympathetic based on fluorescent fibers in the intermediolateral cell column after C1 lesion. However, we cannot state whether the increase in blood pressure due to optogenetic stimulation was because of the activation of pre-sympathetic non-C1 neurons, whether these neurons are barosensitive, or if the pressure increase is due to, at least in part, activation of circuits other than the direct close apposition these neurons make into the intermediolateral cell column. We optogenetically stimulated only the spinally projecting fibers from RVLM neurons expressing ChR2-YFP in C1-intact and C1-lesioned mice, which produced increases in blood pressure in anesthetized mice. This demonstrates that stimulation of only the bulbospinal neurons—including activation of their potential collateral projections due to antidromic activation of spinal fibers—is sufficient to increase blood pressure independent of C1 neurons, at least under anesthetized conditions. It is likely that these same bulbospinal neurons play a role in the pressor response during conscious stimulation of the RVLM, however this remains speculative. We then tested whether

activation of bulbospinal neurons was sufficient to increase blood pressure by injecting a Cre-delivering retrograde AAV into the thoracic spinal cord and a Cre-dependent ChR2-YFP AAV into the RVLM. In these experiments, stimulation of bulbospinal neurons increased blood pressure in conscious mice, however a small portion of the labeled neurons were spinally projecting C1 neurons, which are known to play a role in activating blood pressure and sympathetic activity. We then stimulated C1 neurons specifically using DBH-Cre mice, and we were not able increase blood pressure in the same conditions, suggesting that the increase in blood pressure by activation of bulbospinal neurons is likely due to the non-catecholaminergic group. In summary, stimulation of RVLM after C1-lesion produces an increase in blood pressure, suggesting non-C1 RVLM is sufficient for this effect, stimulation of spinal axons increases blood pressure in these same mice, suggesting that pre-sympathetic non-C1 neurons are responsible for at least some of the pressor response, and stimulation of bulbospinal RVLM increases blood pressure while stimulation of C1 alone does not, indicating that this pathway is mediating much of the effect when RVLM is stimulated non-specifically.

Works Cited

1. Guertzenstein, P.G. and A. Silver, *Fall in blood pressure produced from discrete regions of the ventral surface of the medulla by glycine and lesions.* J Physiol, 1974. **242**(2): p. 489-503.
2. Ross, C.A., et al., *Tonic vasomotor control by the rostral ventrolateral medulla: effect of electrical or chemical stimulation of the area containing C1 adrenaline neurons on arterial pressure, heart rate, and plasma catecholamines and vasopressin.* J Neurosci, 1984. **4**(2): p. 474-94.
3. Schreihofer, A.M. and P.G. Guyenet, *Identification of C1 presympathetic neurons in rat rostral ventrolateral medulla by juxtacellular labeling in vivo.* J Comp Neurol, 1997. **387**(4): p. 524-36.
4. Lipski, J., et al., *Barosensitive neurons in the rostral ventrolateral medulla of the rat in vivo: morphological properties and relationship to C1 adrenergic neurons.* Neuroscience, 1995. **69**(2): p. 601-18.
5. Guyenet, P.G., et al., *Rostral Ventrolateral Medulla and Hypertension.* Hypertension, 2018. **72**(3): p. 559-566.
6. Wenker, I.C., et al., *Blood Pressure Regulation by the Rostral Ventrolateral Medulla in Conscious Rats: Effects of Hypoxia, Hypercapnia, Baroreceptor Denervation, and Anesthesia.* J Neurosci, 2017. **37**(17): p. 4565-4583.
7. Burke, P.G., et al., *Optogenetic stimulation of adrenergic C1 neurons causes sleep state-dependent cardiorespiratory stimulation and arousal with sighs in rats.* Am J Respir Crit Care Med, 2014. **190**(11): p. 1301-10.

8. Guyenet, P.G., A.M. Schreihofer, and R.L. Stornetta, *Regulation of sympathetic tone and arterial pressure by the rostral ventrolateral medulla after depletion of C1 cells in rats.* Ann N Y Acad Sci, 2001. **940**: p. 259-69.

9. Madden, C.J. and A.F. Sved, *Cardiovascular regulation after destruction of the C1 cell group of the rostral ventrolateral medulla in rats.* Am J Physiol Heart Circ Physiol, 2003. **285**(6): p. H2734-48.

10. Schreihofer, A.M., R.L. Stornetta, and P.G. Guyenet, *Regulation of sympathetic tone and arterial pressure by rostral ventrolateral medulla after depletion of C1 cells in rat.* J Physiol, 2000. **529 Pt 1**: p. 221-36.

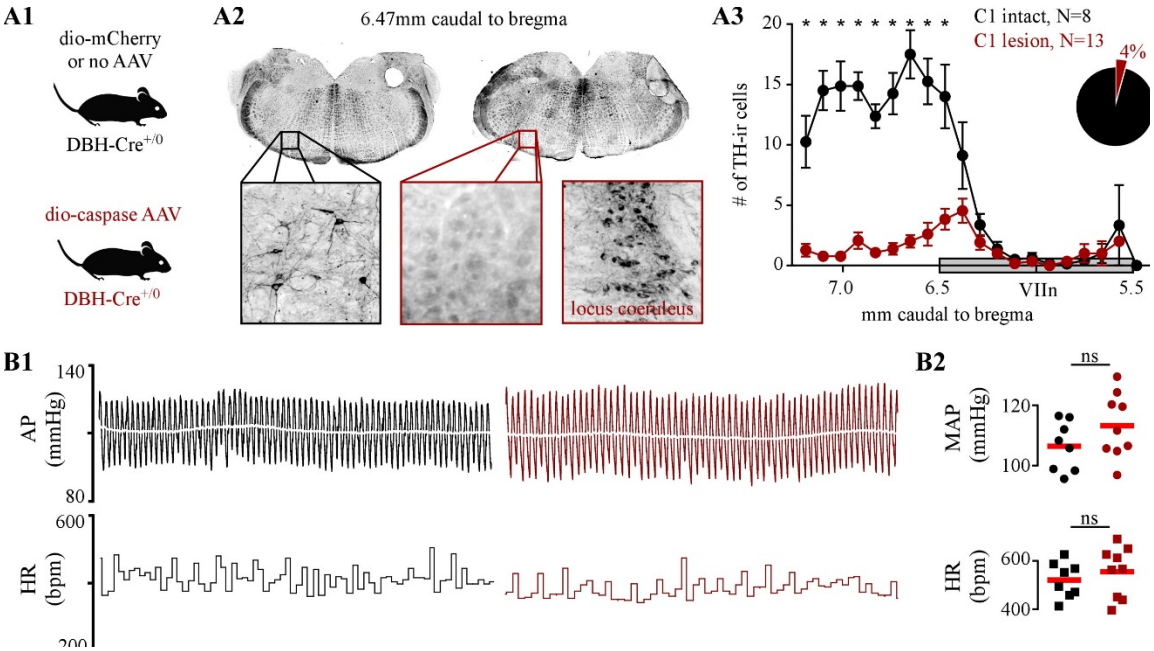
A1
dio-mCherry
or no AAV
DBH-Cre+/0
dio-caspase AAV
DBH-Cre+/0
A2
6.47mm caudal to bregma
locus coeruleus
A3
C1 intact, N=8
C1 lesion, N=13
4%
# of TH-ir cells
20
15
10
5
0
7.0
6.5
VIIn
5.5
mm caudal to bregma
B1
AP (mmHg)
140
80
HR (bpm)
600
200
B2
MAP (mmHg)
120
100
ns
HR (bpm)
600
400
ns

Figure 1: C1 lesion does not affect resting blood pressure

(A1.) Experimental approach: In the control group, DβH-Cre$^{+/0}$ mice either underwent no injection or were injected with a dio-mCherry AAV, while the experimental group was injected with a Cre-dependent caspase AAV. **(A2.)** Example brain sections from the C1-dense rostral RVLM in control and experimental groups. Magnification highlights TH-expressing neurons in tissue from the control group but the lack of TH-expressing neurons in experimental group, presumable from AAV induced caspase-mediated cell death. A magnified region from rostral sections containing locus coeruleus in the experimental group demonstrate caspase-induced death of DβH neurons was localized to the injection site. **(A3.)** Distribution of TH-ir neurons across the ventral brainstem in brain sections from control versus experimental groups. **(B1-2.)** Representative cases *(B1)* and population data *(B2.)* of resting blood pressure and heart rate in control and experimental groups

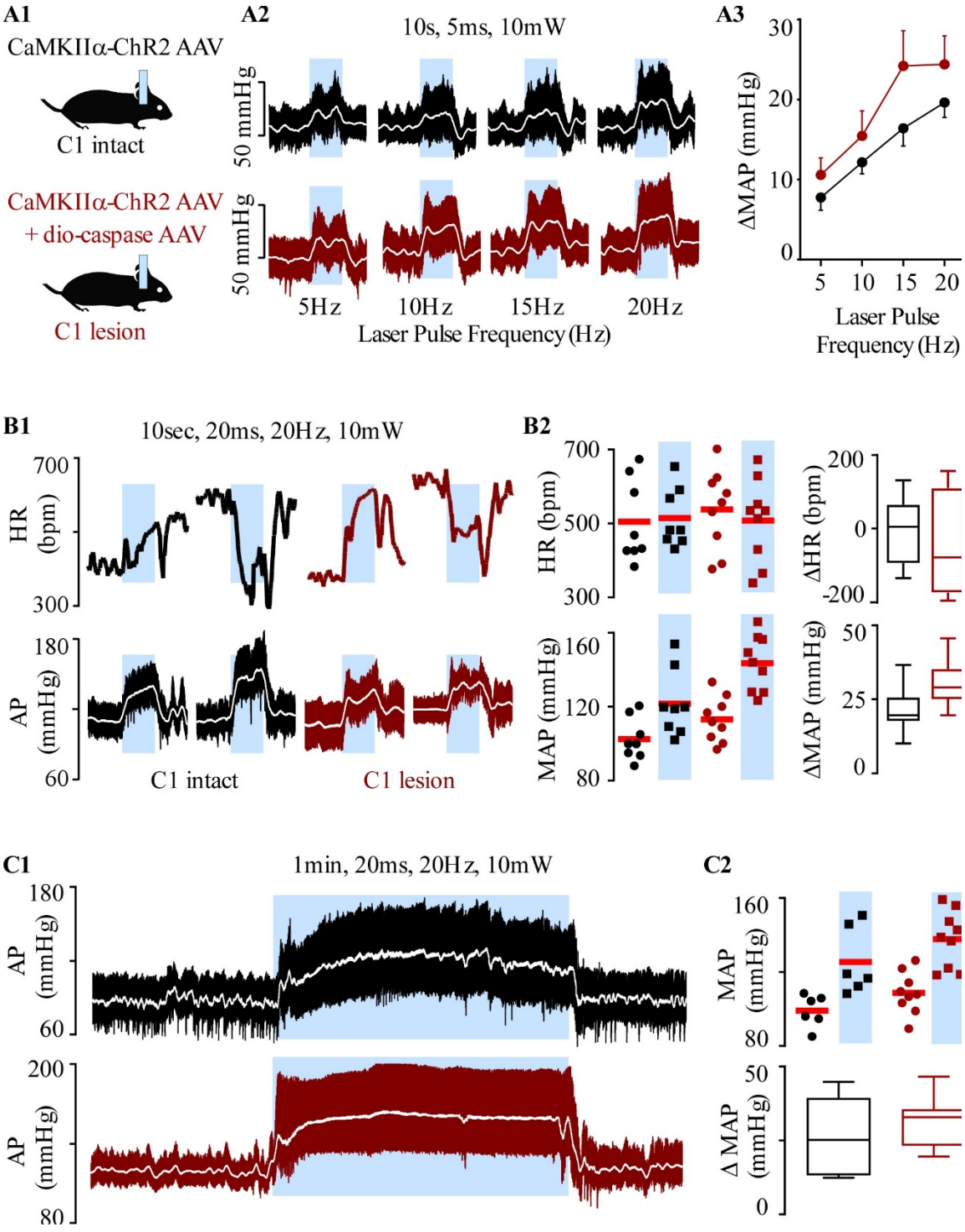
A1
CaMKIIα-ChR2 AAV
C1 intact
CaMKIIα-ChR2 AAV
+ dio-caspase AAV
C1 lesion
A2
10s, 5ms, 10mW
50 mmHg
50 mmHg
5Hz
10Hz
15Hz
20Hz
Laser Pulse Frequency (Hz)
A3
ΔMAP (mmHg)
Laser Pulse
Frequency (Hz)
B1
10sec, 20ms, 20Hz, 10mW
HR (bpm)
AP (mmHg)
C1 intact
C1 lesion
B2
HR (bpm)
ΔHR (bpm)
MAP (mmHg)
ΔMAP (mmHg)
C1
1min, 20ms, 20Hz, 10mW
AP (mmHg)
AP (mmHg)
C2
MAP (mmHg)
Δ MAP (mmHg)

Figure 2: Optogenetic stimulation of RVLM after injection of CaMIIα-ChR2 AAV increases blood pressure in conscious C1-intact and C1-lesioned mice

(A1.) To generate C1-intact control and C1-lesioned experimental groups, DβH-Cre$^{+/0}$ mice were injected unilaterally with CaMKIIα-ChR2 AAV in a single injection site within the RVLM (~80nL). The experimental group received additional bilateral injections of dio-caspase AAV across the C1 region of the brainstem. Following this, mice were implanted with an optic fiber-ferrule system for RVLM illumination **(A2-3.)** Typical examples *(A2.)* during conscious optogenetic stimulation—ten second trains of 5ms pulses—which increased blood pressure in accordance with pulse frequency (tested at 5, 10, 15, & 20Hz). Differences were calculated as average pressure 10s during- versus average during 10s prior to optogenetic stimulation *(A3.)* **(B1-3.)** Typical examples *(B1.)* and population data *(B2.)* from more intense stimulation trains (20Hz, 20ms, 10s) in conscious mice, which led to strong increases in blood pressure but produced variable effects on heart rate *(B3.)* in both groups **(C1-2.)** Longer optogenetic stimulations at 20ms, 20Hz length produced increases in blood pressure for the duration of the stimulation *(C1.)* and varying effects on heart rate *(C2.)*

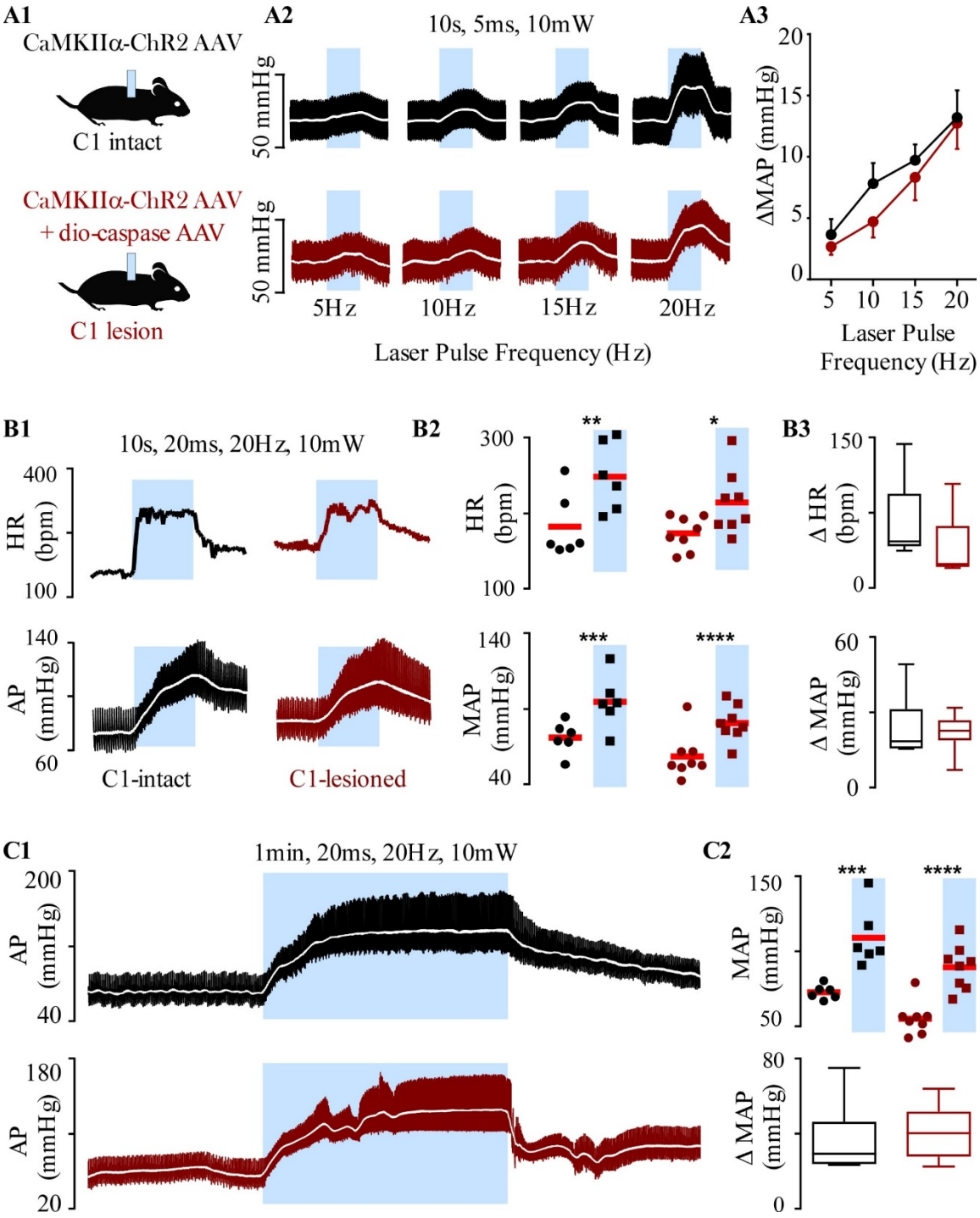
A1
CaMKIIα-ChR2 AAV
C1 intact
CaMKIIα-ChR2 AAV
+ dio-caspase AAV
C1 lesion
A2
10s, 5ms, 10mW
50 mmHg
5Hz
10Hz
15Hz
20Hz
Laser Pulse Frequency (Hz)
A3
ΔMAP (mmHg)
Laser Pulse Frequency (Hz)
B1
10s, 20ms, 20Hz, 10mW
HR (bpm)
AP (mmHg)
C1-intact
C1-lesioned
B2
HR (bpm)
MAP (mmHg)
B3
Δ HR (bpm)
Δ MAP (mmHg)
C1
1min, 20ms, 20Hz, 10mW
AP (mmHg)
C2
MAP (mmHg)
Δ MAP (mmHg)

Figure 3: Optogenetic stimulation of RVLM spinal axons increases blood pressure in anesthetized C1-intact and C1-lesioned mice

(A1.) We anesthetized mice from Figure 2, then stimulated spinal axons from CaMKII-ChR2 RVLM neurons in both C1-intact and C1-lesioned groups by illuminating the thoracic spinal cord. **(A2-3.)** Typical examples *(A2.)* during anesthetized optogenetic illumination of the spinal cord—ten second trains of 5ms pulses—which increased blood pressure in accordance with pulse frequency (tested at 5, 10, 15, & 20Hz). Differences were calculated as average pressure 10s during- versus average during 10s prior to optogenetic stimulation *(A3.)* **(B1-3.)** Typical examples *(B1.)* and population data *(B2.)* from more intense stimulation trains (20Hz, 20ms, 10s) of spinal axons in anesthetized mice, which led to strong increases in blood pressure but produced variable effects on heart rate *(B3.)* in both groups **(C1-2.)** Longer optogenetic stimulations at 20ms, 20Hz length produced large increases in blood pressure for the duration of the stimulation *(C1.)* and varying effects on heart rate *(C2.)*

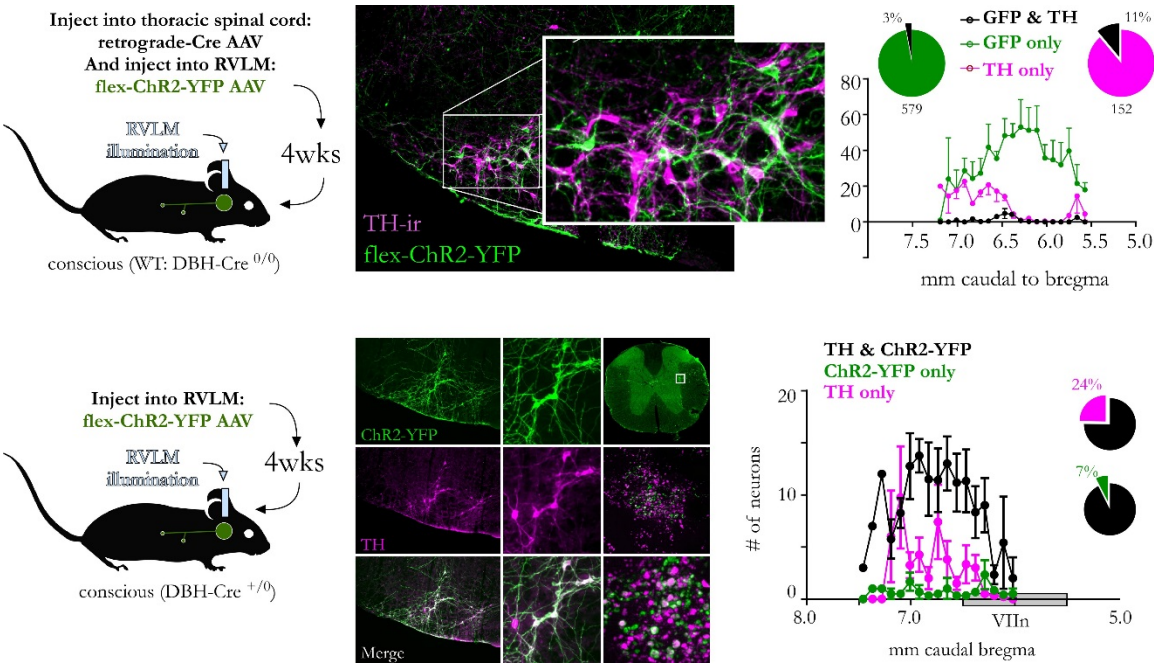

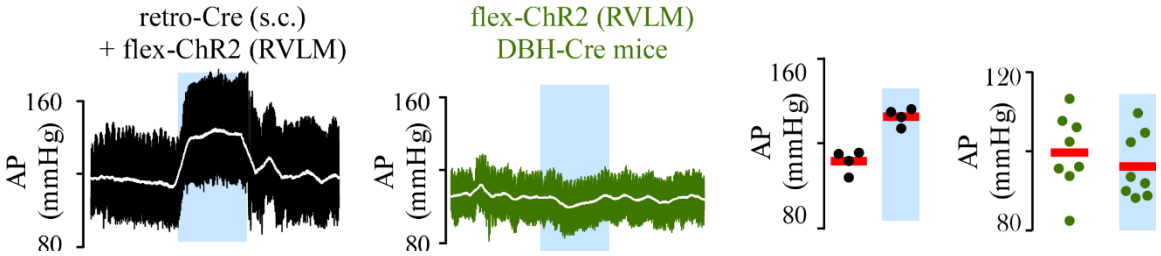

Figure 4: Optogenetic stimulation of bulbospinal C1 and non-C1 neurons increases blood pressure in conscious mice, while stimulation of C1 alone does not

(A1.) We isolated ChR2-expression to spinally projecting RVLM neurons by injecting a retrogradely-active Cre-delivering AAV into the thoracic spinal cord, and then injecting a Cre-dependent ChR2 AAV into the RVLM of WT mice. After injections, mice were implanted with an optic fiber-ferrule system above the RVLM. **(A2-3.)** Injections led to ChR2 expression in many non-C1 spinally projecting neurons and some spinally-projecting C1 neurons as well. **(B1.)** We isolated ChR2-expression to C1 neurons by injecting Cre-dependent ChR2 into DH-Cre$^{+/0}$ mice, and we then implanted an optic fiber-ferrule system above the RVLM. **(B2-3.)** Injections led to selective and comprehensive

expression of ChR2 in C1 neurons. **(C1-3.)** Optogenetic stimulation of bulbospinal neurons (non-C1 and C1) produced increases in blood pressure in conscious mice, while stimulation of C1 alone did not.

2.3 Declaration of published work: I have previously published this work in the *Journal of Neuroscience*, J Neurosci. 2013 Nov 27;33(48):18792-805. doi: 10.1523/JNEUROSCI.2916-13.2013.

Monosynaptic glutamatergic activation of locus coeruleus and other lower brainstem noradrenergic neurons by the C1 cells in mice

Benjamin B. Holloway[1], Ruth L. Stornetta[1], Genrieta Bochorishvili[1,2], Alev Erisir[2], Kenneth E. Viar[1], and Patrice G. Guyenet[1]

[1] ***Department of Pharmacology, University of Virginia, Charlottesville, VA 22908***

[2] ***Department of Psychology, University of Virginia, Charlottesville, VA 22904***

Abstract

The C1 neurons, located in the rostral ventrolateral medulla (VLM), are activated by pain, hypotension, hypoglycemia, hypoxia, and infection, as well as by psychological stress. Prior work has highlighted the ability of these neurons to increase sympathetic tone, hence peripheral catecholamine release, probably via their direct excitatory projections to sympathetic preganglionic neurons. In this study, we use channelrhodopsin-2 (ChR2) optogenetics to test whether the C1 cells are also capable of broadly activating the brain's noradrenergic system. We selectively expressed ChR2(H134R) in rostral VLM catecholaminergic neurons by injecting Cre-dependent adeno-associated viral vectors into the brain of adult dopamine-β-hydroxylase (DβH) $^{Cre/0}$ mice. Most ChR2-expressing VLM neurons (75%) were immunoreactive for phenylethanolamine N-methyl transferease, thus were C1 cells, and most of the ChR2-positive axonal varicosities were immunoreactive for vesicular glutamate transporter-2 (78%). We produced light microscopic evidence that the axons of rostral VLM catecholaminergic neurons contact LC, A1 and A2 noradrenergic neurons, and ultrastructural evidence that these contacts represent asymmetric synapses. Using optogenetics in tissue slices, we show that rostral VLM catecholaminergic neurons activate the locus coeruleus as well as A1 and A2 noradrenergic neurons monosynaptically by releasing glutamate. In conclusion, activation of rostral VLM catecholaminergic neurons, predominantly C1 cells, by somatic or psychological stresses has the potential to increase the firing of both peripheral and central noradrenergic neurons.

Introduction

The locus coeruleus (LC) is the largest cluster of CNS noradrenergic neurons. The activity of this nucleus is state-dependent and facilitates arousal and attention by increasing neuronal excitability in the cortex and elsewhere (Aston-Jones and Cohen, 2005; Carter et al., 2010; Berridge et al., 2012). Noradrenaline released by LC neurons also directly activates astrocyte metabolism (Sorg and Magistretti, 1991; Hertz et al., 2010). The ponto-medullary region contains several other much less studied clusters of noradrenergic neurons (A1, A2, A5, A7) that primarily target subcortical regions involved in nutrient intake and cardiorespiratory and hormonal regulations (Dahlstrom and Fuxe, 1964; Byrum and Guyenet, 1987; Ritter et al., 1998; Appleyard et al., 2007; Fenik et al., 2008; Bruinstroop et al., 2012).

LC unit activity is activated by hypotension in several species (Elam et al., 1984; Morilak et al., 1987b; Curtis et al., 1993) including humans (Mitchell et al., 2009). LC neurons are also activated by hypoglycemia, hypoxia, hypercapnia and bacterial infection (Elam et al., 1981; Morilak et al., 1987a; Erickson and Millhorn, 1994; Haxhiu et al., 1996; Teppema et al., 1997; Yuan and Yang, 2002; Schiltz and Sawchenko, 2007). Several observations suggest that these physiological perturbations could activate the LC via the C1 cells, a group of neurons with a dual catecholaminergic/glutamatergic phenotype which resides in the rostral ventrolateral medulla (VLM) (Guyenet et al., 2013). The C1 cells densely innervate the LC (Milner et al., 1989; Pieribone and Aston-Jones, 1991; Guyenet, 2006; Card et al., 2006; Abbott et al., 2013). C1 and LC neurons respond in a qualitatively similar manner to the above-mentioned stressors (Ritter et al., 1998; Guyenet, 2006; Moreira et al., 2006; Verberne and Sartor, 2010; Abbott et al.,

2013). Optogenetic stimulation of the C1 cells activates the LC in anesthetized rats (Abbott et al., 2012). Finally, the C1 neurons express VGLUT2 and produce glutamatergic EPSCs elsewhere (Stornetta et al., 2002a; Depuy et al., 2013). Based on light microscopy evidence, the C1 cells may also target additional clusters of lower brainstem noradrenergic neurons such as the A1 and A2 cell groups located respectively in the caudal VLM and the nucleus of the solitary tract (Card et al., 2006; Abbott et al., 2013). Finally, as is well-known, the C1 cells drive sympathetic preganglionic neurons monosynaptically, plausibly by releasing glutamate, and therefore broadly regulate the release of noradrenaline in the periphery (Morrison et al., 1989; Jansen et al., 1995; Stornetta et al., 2002b; Guyenet, 2006; Marina et al., 2011).

In the present study we test the hypothesis that the C1 neurons also broadly regulate noradrenaline release within the CNS. We focus on three clusters of noradrenergic neurons: LC neurons, A1 and A2 neurons. The existence of monosynaptic connections between the C1 cells and their noradrenergic targets is examined at the ultrastructural level and synaptic transmission between C1 and their noradrenergic neuronal targets is studied using channelrhodopsin-2 (ChR2) optogenetics in slices.

Materials and Methods

Animals

Animals were used in accordance with guidelines approved by the University of Virginia Animal Care and Use Committee. Tg(Dbh-cre)KH212Gsat/Mmcd mice, stock # 032081-UCD (DβH-Cre) were obtained from the Mutant Mouse Regional Resource

Center at the University of California, Davis, CA, USA and maintained as hemizygous (DβH$^{Cre/0}$) on a C57BL/6J background. B6.Cg-*Gt(ROSA)26Sor*$^{tm9(CAG-tdTomato)Hze}$/J mice (ROSA-tdTomato) were obtained from the Jackson Laboratory (Bar Harbor, ME) and crossed with the DβH$^{Cre/0}$ mice to produce mice (DβH$^{Cre/0}$;ROSA-tdTomato) in which noradrenergic neurons could be visualized in live slices.

Viral vectors and microinjections

The Cre-recombinase-dependent viral vectors DIO-eF1α-hChR2(H134R)-mCherry AAV and DIO-eF1α-ChR2(H134R)-eYFP AAV (both serotype 2) (Atasoy et al., 2008) were obtained from the University of North Carolina Vector core (Chapel Hill, NC) at a titer of 10^{12} viral particles per ml. Twenty-eight 6 to 13 (median 9) week-old mice (14 males, 14 females) were anesthetized with a mixture of ketamine (100 mg/kg) and dexmedetomidine (0.2 mg/kg) given i.p. After reaching an adequate plane of anesthesia (unresponsive to paw pinch and no corneal reflex) animals were placed into a modified stereotaxic device (Kopf) on a thermostatically controlled heating pad and received three injections of undiluted virus (240-360 nl total volume) into the left rostral VLM under electrophysiological guidance as described previously (Abbott et al., 2013).

Electrophysiology

Four to twelve weeks after AAV2 injection, the mice were anesthetized with a mixture of ketamine (120mg/kg) and xylazine (12mg/kg) given i.p., and after becoming completely anesthetized (unresponsive to hind paw pinch) were decapitated. The

brainstem was sectioned with a vibrating microtome in the transverse plane in ice-cold, N-Methyl-D-glucamine (NMDG)-substituted artificial cerebral spinal fluid (ACSF) containing (in mM): 92 NMDG, 2.5 KCl, 1.25 NaH_2PO_4, 10 $MgSO_4$, 0.5 $CaCl_2$, 20 HEPES, 30 $NaHCO_3$, 25 glucose, 2 thiourea, 5 Na-ascorbate, 3 Na-pyruvate (~300 mOsm/kg). After 10 minutes at 33°C, 200-300 µm thick slices were transferred to aerated physiological extracellular ACSF containing (in mM): 119 NaCl, 2.5 KCl, 1.25 NaH_2PO_4, 2 $MgSO_4$, 2 $CaCl_2$, 26 $NaHCO_3$, 12.5 glucose, 2 thiourea, 5 Na-ascorbate, 3 Na-pyruvate and maintained at room temperature (23°C). All recordings were performed at room temperature in submerged slices continuously perfused with aerated physiological ACSF. Glass pipettes (2-6 MΩ tip resistance) were filled with a solution containing (in mM): 140 K-gluconate, 10 HEPES, 10 tris-phosphocreatine, 3 ATP-Na, 0.3 GTP-Na, 1 EGTA, 2 $MgCl_2$ (pH 7.3). EPSCs were recorded at Vhold of -60mV (-74 mV after junction potential correction). In selected experiments, K-gluconate was replaced with cesium-methanesulfonate (140 mM) and recordings were made at Vhold of -70 mV and +9 mV (respectively -80 and 0 mV, after junction potential correction). The calculated E[Cl-] was -88mV. Biocytin-filled electrodes (0.2%) were used to label the recorded cells. Recordings were performed using a Multiclamp 700B amplifier and pClamp 10 software (Molecular Devices, Inc., Sunnyvale, CA, USA). Signals were low-pass filtered at 4 kHz and digitized at 10 kHz. Only cells with series resistance that remained below 25MΩ were included in the analysis. Further analysis (event-triggered averages, event-triggered histograms, EPSC detection and counting, curve fitting of PSC decay and measurement of decay time-constant) was done using Spike2 version 7.10 software (CED, Cambridge, U.K.). Photostimulation of ChR2-expressing neurons,

axons and nerve terminals was done with a 200 μm diameter optical fiber coupled to a 473nm DPSS laser (IkeCool Corporation, Anaheim, CA; 1 ms pulses, 5mW steady-state output) as previously described (Depuy et al., 2013). The optical fiber, held at forty degrees from the horizontal, was positioned such that the tip was 150μm above and 250μm lateral to each recorded neuron. This setup intensely illuminated an ellipse of approximately 0.342 mm^2, which produced an estimated average irradiance of ~14mW/mm^2 comparable to that used by others previously (Grossman et al., 2013). Delivery of optical pulses was triggered by a digitizer (Digidata 1440A, Molecular Devices) controlled by episodic protocols run in pClamp 10 (Molecular Devices). The output of the laser/fiber was calibrated for 5 mW steady-state output prior to each experiment. The following drugs were used: TTX (Fisher Scientific, final concentration 1μM); 4-aminopyridine (4-AP, Sigma, 100-200μM); kynurenic acid (Sigma, 1mM), 6-cyano-7-nitroquinoxaline-2,3-dione (CNQX, Tocris, 10 μM), D-(-)-2-Amino-5-phosphonopentanoic acid (AP-5, Sigma, 50 μM).

Slices from electrophysiological recording experiments containing biocytin-filled cells were fixed in 4% paraformaldehyde (pf) from 2 to 5 days. Sections were rinsed and incubated first in blocking solution using a triton concentration of 0.5% to enhance antibody penetration in thicker tissue and then in primary antibodies (described below) to detect tyrosine hydroxylase (TH) and dsRed or EYFP. Slices were then rinsed and incubated with appropriate secondary antibodies as well as with NeutrAvidin-Dylight-649 (Thermo Fisher Scientific, Suwanee, GA), rinsed, mounted and covered as described below.

Fluorescent light microscopy for distribution of phenylethanolamine-N-methyl transferase (*PNMT) and to confirm tdTomato expression in catecholaminergic neurons*

Lower brainstem sections from 3 DβH$^{Cre/0}$ mice injected 5 weeks prior with DIO-eF1α-eYFP AAV2 were examined to determine which proportion of the transduced neurons expressed both TH and PNMT, i.e. were C1 cells. These mice were anesthetized with an overdose of pentobarbital and perfused transcardially with 10 ml heparinized saline followed by 80 ml of 2% paraformaldehyde (pf). The brains were postfixed in 2% pf for 2 to 5 days. Brainstem sections from 3 DβH$^{Cre/0}$/ROSA26-tdTomato mice were also examined histologically to test whether the red fluorophore, tdTomato, was confined to catecholaminergic neurons. Thirty micron-thick transverse sections were cut with a vibrating microtome and collected into a cryoprotectant solution and stored at -20 °C before further processing. All histological procedures were done with free-floating sections. For fluorescent immunohistochemistry, sections were rinsed, blocked with 10% normal horse serum in 100 mM Tris-Saline containing 0.1% Triton-X-100 and incubated in primary antibodies diluted in this blocking solution for 16-18 hours at 4°C as follows: sheep anti-TH (Millipore; Billerica, MA at 1:1000), rabbit anti-dsRed (Clontech Laboratories; Mountain View, CA at 1:500) or chicken anti-GFP (AVES labs; Tigard, OR at 1:1000) and/or rabbit anti-PNMT (generously provided by Dr. Martha Bohn, Northwestern University Medical School, Chicago, IL (Bohn et al., 1987) at 1:3000). Sections were then rinsed and incubated for 45-60 min in appropriate secondary antibodies as follows: DyLight 649 anti-sheep IgG , Cy3 anti-rabbit IgG, Alexa488 anti-chicken IgY all raised in donkey and at 1:200 (Jackson ImmunoResearch Laboratories,

West Grove, PA) then rinsed, mounted on gelatinized glass slides, dehydrated through a graded series of alcohols and covered with DPX.

Light microscopy for imaging VGLUT2 in terminals from C1 neurons and to examine close appositions from C1 neurons onto A1, A2 and A6 (locus coeruleus) neurons

For fluorescent imaging of close appositions as well as for determination of VGLUT2 immunoreactivity in terminals of C1 or A1 neurons, a one in three series of 30 micron-thick coronal sections were processed as described above. A guinea pig anti-VGLUT2 antibody (Millipore, AB2251; 1:2000) was substituted for the PNMT antibody. The secondary antibody for the VGLUT2 primary was a Cy3-tagged anti-guinea pig IgG (Jackson Immunoresearch, 1:200) used exactly as the other secondaries described above.

For brightfield imaging of close appositions of terminals from ChR2-mCherry labeled C1 neurons onto TH cells in A1, A2 and A6 (locus coeruleus), sections from 3 $D\beta H^{Cre/0}$ mice previously injected with DIO-eF1α-mCherry as described above were incubated in blocking solution as described, rinsed and incubated in 1% hydrogen peroxide, then rinsed and incubated in rabbit anti-dsRed (1:500; recognizes mCherry) in 0.5% "TNB" (proprietary blocking reagent, Perkin Elmer, Waltham, MA) prepared in 100 mM Tris-Saline for 16-18 hours at 4°C. Sections were then rinsed and incubated in biotinylated donkey anti-rabbit IgG (Jackson, 1:1000) for 45-60 min, rinsed and incubated in ABC solution according to manufacturer's instructions (Vectastain "Elite"; Vector Laboratories, Burlingame, CA) for 45 min, then rinsed and incubated with 3,3'diaminobenzidine (DAB) with nickel enhancement using the DAB kit according to

the manufacturer's instructions (Vector) resulting in a black reaction product. Sections were then rinsed and incubated in sheep anti-TH (1:1000) prepared in 0.5% TNB in 100 mM Tris-Saline for 16-18 hours at 4°C. Sections were then rinsed and incubated in biotinylated donkey anti-sheep IgG (Jackson, 1:000) for 45-60 min, rinsed and incubated in ABC solution (Vector) for 45 min, then rinsed and incubated in DAB using a kit according to the manufacturer's instructions (Vector) resulting in a brown reaction product. Sections were then rinsed, mounted and covered as described above.

Light microscopic examination of putative terminals from C1 or A1 neurons

Slides were examined using a Zeiss Axioskop2 and photographed with a Zeiss MRC camera. Computer-assisted mapping of the neurons of interest was done as previously described (Bochorishvili et al., 2011; Stornetta et al., 2013). For analysis of fluorescent terminals, 10 micron Z-stacks at 0.3 micron increments were taken through the tissue with filter sets at appropriate wavelengths to discriminate the various fluorophores without "bleed through" (wavelengths listed as excitation, beam splitter, emission; for Cy3: 545, 570, 605; for Alexa 488: 500, 515, 535; for Alexa 649: 640, 660, 690.) For the 100x objective used to determine bouton double labeling and close appositions, the resulting digital images were 15.2 pixels/micron. A bouton was considered to be double labeled if both fluorophores were in focus and coincident through at least 2 levels of the Z-stack. For illustration of close appositions, Z-stack images were subjected to 3D blind deconvolution through 7 iterations using the AutoQuant X3 software (Media Cybernetics, Rockville, MD). Deconvoluted stacks were then processed with Volocity software (version 4.4, Improvision) for 3D rendering and

confirmation of close appositions. A close apposition was defined as two objects labeled with two separate fluorophores overlapping at least 7 pixels in each z-level, and at least in 2 consecutive z-levels (Corson and Erisir, 2013). The size of this overlap represents an apposition of approximately 0.45 microns in length.

Electron microscopy methods and analysis

For ultrastructural analysis, two DβH$^{Cre/0}$ mice injected 5 weeks prior with DIO-eF1α-ChR2-mCherry AAV2 were anesthetized as above and perfused transcardially, first with 20 ml of heparinized saline (1,000 U/ml), and then with fixative (25 ml of 2% pf with 3.75% acrolein, from Electron Microscope Sciences, followed by 30 ml of 2% pf). Brains from these animals were then post-fixed for at least 3 hours in 2% pf before sectioning with a vibrating microtome into 30 µm-thick transverse sections. The tissues were blocked in 0.8% BSA with 0.03% Triton-X-100 then incubated in rabbit anti-DsRed (Clontech) at 1:500 made in blocking solution at 4ºC for 16-18 hours, rinsed and incubated for 60 min in biotinylated donkey anti-rabbit IgG (1:400, Jackson). Tissues were rinsed and incubated for 60 min in ABC (Vector), rinsed and incubated in DAB (Vector) as above. Sections for immunogold-silver staining were placed in mouse anti-TH (1:1000; ImmunoStar, catalog# 22941; Hudson, WI) and incubated for 16-18 hrs at 4º C. Sections were rinsed and incubated for 30 min in washing buffer (phosphate buffered saline (PBS) containing 0.8% BSA, 0.1% fish gelatin, and 3% normal goat serum). Tissues were subsequently incubated for 2 hr in washing buffer containing 1 nm gold-conjugated donkey anti-mouse IgG (1:50; Aurion, Electron Microscopy Sciences, Hatfield, PA). The sections were next rinsed in washing buffer, followed by a rinse in

PBS, and then incubated in 2.5% glutaraldehyde in PBS for 10 min. The tissue was subsequently rinsed in PBS and transferred to sterile, untreated culture well plates for a series of 1-min rinses in PBS and then in 0.2 M sodium citrate buffer (pH 7.4). Rinses were followed by a silver enhancement reaction at room temperature using IntenSEM silver kit reagents according to manufacturer's instructions (GE Healthcare, Chalfont St. Giles, UK). The sections were handled with wooden applicator sticks and gently swirled throughout the silver enhancement procedure for 4–6 minutes. Sections were then rinsed in sodium citrate buffer and 100 mM phosphate buffer. Sections were then incubated in 1% osmium tetroxide and 1% uranyl acetate (Electron Microscopy Sciences) for 90 min. Tissues were rinsed, transferred to porcelain dishes, dehydrated through a series of increasing ethanol concentrations (30, 50, 70, and 95%), and then placed into glass vials containing 100% ethanol. Finally, the tissue sections were treated with propylene oxide (2X 10 min) and incubated in a 1:1 mixture of propylene oxide and embedding resin Embed-812 (Electron Microscopy Sciences). This mixture was then replaced with straight Embed-812 which infiltrated the sections for 16-18 hr. The tissue was embedded between sheets of plastic (Aclar), flattened and cured for at least 72 hours at 62^{o} C. Then flat-embedded sections were examined with a light microscope to detect immunogold-labeled TH-cells and DAB -labeled C1 projection fields in the A1 and A2 noradrenergic cell clusters. The regions of interest were further trimmed and repolymerized at the bottom of BEEM capsules. The block was trimmed to a 2 X 1 mm trapezoidal block that spanned the A1 or A2 and contained the TH-immunoreactive cells. Ultrathin sections (70–90 nm) were cut at a plane near-parallel to the surface of 30 μm sections using a Leica Ultracut UCT. This approach ensures that the top 5–10 μm of the sections, where

immunolabeling is present, are sectioned to yield a wide (100–200 μm) strip of labeled ultrathin tissue. Ultrathin sections were collected onto copper mesh grids in series of seven to ten sections per grid. Tissue was analyzed with a JEOL 1230 transmission electron microscope (Peabody, MA), and micrographs were captured with an ultra high resolution digital imaging (4Kx4K) camera (Scientific Instruments and Applications, Duluth, GA). Adobe Photoshop was used to adjust image contrast and illumination, and then images were exported into the Canvas drawing software (Version 10, ACD Systems, Inc.).

Antibody characterization

All antibodies used are listed in the Journal of Comparative Neurology antibody database and have been previously characterized as follows:

PNMT antibody raised in rabbits against purified rat adrenal extract was obtained from M. Bohn (Bohn et al., 1987) and showed a labeling pattern similar to that seen in rats using identical conditions as previously published (Verberne et al., 1999).

TH antibody raised in sheep (Millipore) against native tyrosine hydroxylase from rat pheochromocytoma labels one band of expected length in Western blots of mouse brain lysates (from manufacturer's information.) The labeling pattern is identical to that seen in mouse brain in previous publications from the lab using identical conditions (Depuy et al., 2013).

TH antibody raised as a mouse monoclonal antibody against TH purified from PC12 cells recognizes an epitope in the catalytic core region of the TH molecule where

extensive species homology exists. Western blots of HEK293 cells transfected with human TH probed with the antibody show one expected 60 kDa band (manufacturer's information). The labeling pattern is identical to that seen in mouse brain in previous publications from the lab using identical conditions (Depuy et al., 2013).

VGLUT2 antibody raised in guinea pig against a peptide corresponding to the C-terminal of rat VGLUT2 recognizes one band of expected size on Western blots of rat brain lysate (from manufacturer's information). Labeling is absent in terminals from neurons where VGLUT2 is eliminated by cre-mediated recombination with a floxed *VGLUT2* allele (Kaur et al., 2013). The labeling pattern is identical to that seen in mouse brain in previous publications from the lab using identical conditions (Depuy et al., 2013).

GFP antibody raised in chicken against recombinant GFP protein shows labeling only in tissue injected with viral vectors expressing eYFP. The antibody labeling matches exactly with non-amplified eYFP fluorescence.

DsRed antibody raised in rabbits against DsRed-Express, a variant of *Discosoma* sp.red fluorescent protein recognizes both N and C-terminal fusion proteins containing dsRed variants in mammalian cell extracts (from manufacturer's information). This antibody shows labeling only in tissue injected with viral vectors expressing mCherry or in tissue from tdTomato reporter mice. The antibody labeling matches exactly with non-amplified mCherry or tdTomato fluorescence.

Statistics

Statistical significance was set at $P<0.05$. Data that passed the D'Agostino-Pearson test for normality are expressed as mean ± SEM while non-normally distributed values are described by range and median. Degrees of freedom are listed for parametric tests. To compare two groups we used a paired t-test or Wilcoxon signed rank test. To compare multiple groups, we used the Kruskal-Wallis test or, for repeated measures, the Friedman test followed by Dunn's test to assess inter-group differences. All statistics were done using Graph Pad PRISM software (version 6, La Jolla, CA).

Results

Selective expression of ChR2 by rostral VLM catecholaminergic neurons.

We examined the distribution of neurons with TH-immunoreactive (ir), PNMT-ir, or both in the VLM of 6 mice using a 1-in-3 series of transverse sections. As in rats, the PNMT-ir neurons (C1 neurons) were predominantly confined to the rostral VLM, namely between the caudal end of the facial motor nucleus (FN) and the rostral pole of the lateral reticular nucleus (LRt) (Fig. 1). Caudal to the rostral pole of the LRt, the vast majority of the TH-ir cells lacked PNMT and therefore were A1 noradrenergic neurons. A small number of A1 (TH-positive and PNMT-negative) neurons were also present in the rostral VLM (Fig. 1B).

DIO-eF1α-ChR2-eYFP AAV2 was injected into the left rostral VLM of three $D\beta H^{Cre/0}$ mice. After five weeks, we mapped the location of the ChR2-eYFP-expressing neurons, also in a 1-in-3 series of transverse sections. These neurons were confined to the

VLM. None were found in the dorsal medulla, the contralateral VLM or the pons consistent with the lack of retrograde propagation of AAV serotype 2. Almost all eYFP-positive neurons were TH-ir (respectively 99, 100 and 94% colocalization in 3 mice, Fig. 1A,B) and most (69, 83 and 70% respectively) also contained PNMT immunoreactivity (Fig. 1A,B). In short, ChR2 was selectively expressed by rostral VLM catecholaminergic neurons and 74% of those catecholaminergic cells were detectably PNMT-ir hence, by definition, C1 neurons (Hokfelt et al., 1974). The balance were TH-ir neurons without detectable PNMT, therefore presumably A1 cells.

ChR2-expressing RVLM catecholaminergic neurons innervate lower brainstem noradrenergic neurons

The axonal projections of ChR2-expressing RVLM catecholaminergic neurons were examined in 2 mice using the DIO-eF1α-ChR2-mCherry AAV2 vector and in 3 mice injected with the DIO-eF1α-eYFP AAV2 vector which also labels catecholaminergic neurons selectively (>98%) when injected into the VLM of DβH$^{Cre/0}$ mice (Depuy et al., 2013; Abbott et al., 2013). A dense network of mCherry-positive axonal varicosities covered the entire locus coeruleus (Fig. 2A). Dense projections also covered the soma and dendrites of A1 and A2 neurons (Fig. 2B,C). Close appositions between eYFP-ir axonal varicosities and TH-ir somata or dendrites were commonly observed using light and immunofluorescence methods. Close appositions on A1 and A2 neurons from a 3D rendering are shown in Figure 2D,E.

Ultrastructural evidence for synapses between C1 cells and locus coeruleus neurons was not sought because it has already been provided in rats (Milner et al., 1989; Abbott et al., 2012) and we obtained optogenetic evidence for monosynaptic connectivity between these cells (shown below). We therefore focused our ultrastructural studies on the A1 and A2 neurons. For these experiments, we used tissue from three DIO-eF1α-ChR2-mCherry-AAV2 injected mice processed for simultaneous detection of mCherry and TH immunoreactivity.

Within the A1 noradrenergic neuron-rich region of the VLM (caudal to area postrema level) mCherry-ir (DAB-labeled) profiles consisted exclusively of unmyelinated axons or nerve terminals. Immunogold-silver labeling for TH was observed within perikarya, dendrites and nerve terminals. A representative asymmetric synapse between an mCherry-ir varicosity and a TH-ir dendrite (A1 region) is shown in two serial sections in Figure 3A1,A2. A total of 78 mCherry-ir axonal profiles were observed within the A1 region. Of these, 63 were axonal varicosities that directly contacted dendrites. Fifty one (80%) of these dendritic contacts showed asymmetric synaptic junctions and 12 (19%) were symmetric. The 15 other mCherry-ir profiles made close appositions but no detectable synapses.

Similar results were found in the A2 noradrenergic neuron-rich region of the nucleus of the solitary tract at and caudal to the level of the area postrema. mCherry-ir (DAB-labeled) profiles also consisted exclusively of unmyelinated axons or nerve terminals and immunogold-silver labeling for TH was observed within perikarya, dendrites and nerve terminals. The four serial sections shown in Figure 3B1-B4 show a mCherry-ir fiber establishing two synaptic junctions with a TH-ir dendrite located in the

A2 region. The synapse illustrated in top panels (Fig. 3A1-2) is a typical asymmetric synapse whereas the synapse in Figure 3B1-2 is a perforated synapse, i.e. the cross-section of a synapse that appears as two postsynaptic densities separated by a small gap. Both presynaptic and postsynaptic profiles contained silver grains and therefore were TH-ir. We identified 79 synaptic contacts between mCherry-ir varicosities and TH-ir profiles, most of which (N=70; 89%) were asymmetric and the rest symmetric (N=9, 11%). Another 11 mCherry-ir synaptic varicosities made close appositions with a TH-ir profile but no synapse was detected. Dense core vesicles (examples marked with asterisks in Fig.3) consistent with catecholamine-releasing organelles were detected within the more lightly labeled mCherry-ir varicosities.

Photostimulation of ChR2-labeled C1 axons activates LC neurons monosynaptically in slices

Seventy-nine LC neurons were recorded in transverse slices from 15 mice (9 males, 6 females). The LC was identified as the medium-sized, high-neuron density population below the third ventricle and medial to the superior cerebellar peduncle and trigeminal mesencephalic nucleus (Fig. 4A). The dense innervation of LC from C1 AAV2 transfected neurons (seen as either eYFP or mCherry fluorescent terminals) could also be visualized in the slice (Fig. 4A) and helped to guide placement of the recording electrode. Seven LC neurons were recorded and filled with biocytin in slices prepared from three DβH$^{Cre/0}$/ROSA26-tdTomato mice. These neurons exhibited red (tdTomato) fluorescence, thus were catecholaminergic LC neurons. Thirty-two biocytin-filled neurons were recorded in slices prepared from 5 DβH$^{Cre/0}$ mice previously injected with DIO-eF1α-

ChR2-mCherry AAV2. These neurons were shown to be either TH-ir and/or surrounded by other LC neurons (Fig. 5B, left column).

Pulses of laser light (1ms, 5 mW, 473nm) produced PSCs in 53 % (42/79) of the LC neurons sampled (Fig. 4B1). Occasionally, a laser pulse failed to evoke a PSC (red traces in Fig. 4B1, failure rate 19±4%, N=23). The PSC amplitude, determined by event-triggered signal averaging, including failures, was 34.8 ± 5.0 pA (range 8-107 pA; N= 23; Fig. 4B2). Failure rates, determined by peri-event histograms (Fig.4B3), were calculated for all photo-responsive LC neurons (N=23). Failure rates from LC neurons shown to be monosynaptically innervated by RVLM CA neurons, based on the recovery of synaptic transmission after addition of 4-AP and TTX (N= 9, details below), never exceeded 39% and did not differ significantly from untested LC neurons (0 to 38.7%, median 20%, N=9 vs. 0 to 73.3 %, median 6.7%; N = 14).

In 14 LC neurons, recordings were made with cesium-filled electrodes to enable voltage clamp recordings at -80 mV and at 0mV (junction potential-corrected V_{Hold}). The EPSC evoked by the 0.5Hz laser stimulation was greatly decreased in amplitude when the neurons were held at 0mV (from 32.3 ± 6.9 to 1.4 ± 0.1 pA, N=12, P=0.0005, Wilcoxon matched pairs) but always remained inward (Fig. 4B4). Thus, low frequency photostimulation of the C1 axons does not produce chloride-mediated IPSCs in LC neurons.

Higher frequency photostimulation (2, 5, 10Hz for 10 s; K-gluconate-filled pipettes) produced sustained barrages of EPSCs in LC neurons (Fig. 4C1). The EPSC rate increased during the first 2-4 seconds of the train before reaching a steady-state (Fig. 4C1). The light–evoked EPSCs tended to be desynchronized from the light pulses when

the stimulus was delivered at high frequency (10Hz, Fig. 4C2), and their rate largely exceeded the photostimulus rate (Fig. 4C1-3). This result can probably be explained by the relatively slow kinetics of ChR2(H134R) which leads to a sustained depolarization and probable intracellular calcium build-up during high frequency stimulation (Lin, 2011). The hypothesized intracellular calcium accumulation could explain the rapid but non-instantaneous return of EPSC frequency rate to base line values after the stimulus train (τ = 1.6ms, Fig. 4C3 and insert). In current clamp, high frequency photostimulation at 10 Hz reversibly activated LC neuronal firing from 1.9±0.4 Hz to 3.1±0.7 Hz (N=8, P=0.019, Friedman test; Fig. 4D).

Bath application of the broad-spectrum glutamatergic antagonist kynurenate (1mM) reversibly decreased the amplitude of the postsynaptic current (4 cells, 67.0 to 82.1% attenuation, median 76.7%; P=0.0046; Fig. 4E1,2). To determine if the excitatory C1 input to the LC was mono- or poly-synaptic, we blocked voltage-gated sodium (Na_v) channels with 1μM tetrodotoxin (TTX), then applied 100-200 μM 4-aminopyridine (4-AP) to block K_v channels (Shu et al., 2007). TTX eliminates action potential-dependent EPSCs, and thus eliminates any polysynaptic event, while 4-AP augments the light-induced, direct depolarization of ChR2-positive nerve terminals (Petreanu et al., 2009). TTX eliminated evoked EPSCs (Fig. 4F1,2), indicating that these events were action-potential dependent. The addition of 4-AP reinstated the EPSCs, though these events were typically broader (decay time constant: 20.5±5.4ms vs. 10.0±1.4ms, P=0.0547, Wilcoxon matched pairs), their onset latency delayed (14.1±1.3ms vs. 5.1±0.4ms, P=0.0039, Wilcoxon matched pairs), and their latency to peak longer (26.7±0.3ms vs. 9.5±0.7ms, df=8, P=0.006, paired t-test) than prior to drug application (Fig. 4F1). Evoked

EPSCs were virtually eliminated by blocking ionotropic glutamatergic receptors with CNQX and AP5 (Fig. 4F1,2).

In 11 LC neurons, high frequency stimulation voltage clamp experiments were done with cesium-filled electrodes. At -80 mV V_{Hold}, spontaneous EPSCs were observed, and the response to 10Hz trains of stimuli was identical to that recorded with potassium gluconate-filled electrodes. At 0 mV Vhold, however, IPSC frequency was very low and remained unchanged by the 10Hz stimulus (Fig. 6A1,B). Thus, even high frequency photostimulation of the C1 input did not produce chloride-mediated IPSCs in LC neurons. As elsewhere, sIPSCs had much slower decay kinetics than sEPSCs (N=18 and N=20, 44.4±4.1ms vs. 5.2±0.4ms, P<0.0001, Mann-Whitney Test, Fig. 6A2).

Optical stimulation of ChR2-expressing RVLM-CA neurons in brain slices

Whole-cell current and voltage clamp recordings of ChR2-eYFP-positive rostral VLM neurons were made in slices from adult DβH$^{Cre/0}$ mice to verify that these cells could be activated by light pulses. Recorded neurons (11 neurons, 5 mice) were directly visualized by the presence of eYFP fluorescence. Shortly after patching, these cells were either silent or had a slow tonic discharge pattern (0.68±0.23Hz, 0 to 2.3Hz, N=11). Each light pulse produced a depolarization leading to a single action potential about 4-8 ms after the onset of the light pulse (Fig. 7 A,D). This long delay occurred in spite of the fact that the light-evoked current, observed in voltage clamp, was instantaneous (Fig. 7 B1, B2). The latency to the peak of the action potential (5.94±0.51, N= 11) was the same as the latency of the EPSCs evoked in LC neurons by photostimulating the ChR2-expressing

axons of the rostral VLM CA neurons (5.0 ± 0.4ms, N= 23, Mann-Whitney Test, NS; Fig. 7A,C,D).

All the recorded cells were filled with biocytin and, after histological processing, every recovered biocytin-positive neuron (N= 6) was found to contain both eYFP and tyrosine-hydroxylase immunoreactivity demonstrating that they were ChR2-expressing rostral VLM catecholaminergic neurons (Fig. 7 E).

C1 rather than A1 neurons are the most probable source of the glutamatergic PSCs recorded in the locus coeruleus

After AAV2 injection into the rostral VLM, roughly 75% of the ChR2-expressing catecholaminergic neurons were C1 (PNMT-ir), and the remainder were A1 neurons (TH-ir but PNMT-negative; Fig.1). To determine which catecholaminergic cells (A1 or C1) were primarily responsible for the glutamatergic EPSCs elicited in LC neurons, ChR2-eYFP AAV2 was injected unilaterally (left side) into the caudal VLM, where no TH-ir neuron expresses PNMT. After four weeks, the locus coeruleus was examined, and the proportion of eYFP-positive axonal varicosities that were also VGLUT2-ir were counted in 1-3 coronal sections containing the LC per mouse. Injections resulted in eYFP-ir neuronal somata located no more rostral than 7.3 mm caudal to bregma, where few if any PNMT-ir neurons could be identified (Fig. 1B). For comparison, the same experiment was executed in three other mice in which the vector was injected into the rostral VLM and therefore predominantly labeled C1 cells (subset of the mice used for Fig.1). eYFP fibers were present in the locus coeruleus in both groups of animals; however, the

proportion of eYFP varicosities that were also VGLUT2-ir was much greater when the vector was injected into the C1 dense rostral VLM (78% ± 1.5%; example of double-labeled terminal in Fig. 8) than when the vector was injected into the C1 sparse caudal VLM (10.2% ± 1.1% double-labeled terminals). Thus, while the A1 cells do innervate the LC, few such cells express VGLUT2. This suggests that the glutamatergic EPSCs elicited in LC neurons by photostimulation of axons from the catecholaminergic neurons located in the rostral VLM were most likely caused by activation of C1 cells. This interpretation assumes that the A1 neurons located in the rostral VLM have the same phenotype as those located in the caudal VLM.

Photostimulation of RVLM-CA neurons activates A1 and A2 neurons in slices

In order to visualize A1 and A2 neurons in live slices, we used adult DβH$^{Cre/0}$/ROSA26-tdTomato mice. Preliminary histological experiments carried out in 3 such mice showed that tdTomato was expressed by TH-ir neurons (94 ± 1% in the A1 region of the VLM, 92 ± 1% in the nucleus of the solitary tract, i.e. A2/C2 region; Fig. 5A). Neurons immunoreactive for tdTomato and TH lacked PNMT in regions caudal to the rostral pole of the lateral reticular nucleus (Fig. 5C). Therefore, we targeted this region to record A1 neurons (location of biocytin-filled recorded neurons also shown in Fig. 5C). In the dorsal medulla, neurons immunoreactive for both tdTomato and TH lacked PNMT in regions caudal to the area postrema. These cells were therefore A2 neurons. We recorded preferentially from tdTomato-positive neurons located in this caudal region but a fraction of the recorded neurons could have been PNMT-ir C2 neurons (Fig. 5C). TdTomato was detected in 86 ± 1% of A1 and 66 ± 13% of A2

neurons, therefore the sampled neurons may not have been totally representative of this population of neurons.

For slice recordings, we injected DIO ChR2-eYFP AAV2 (8 mice) or DIO ChR2-mCherry AAV2 (4 mice) into the C1 region of DβH$^{Cre/0}$/ROSA26-tdTomato mice (6 males, 6 females). Five to fourteen weeks later, 15 tdTomato-labeled A1and 21 tdTomato-labeled A2 neurons were recorded in transverse medulla oblongata slices. Cells that received monosynaptic input from C1 neurons were filled with biocytin and processed histologically. We verified that the recorded neurons contained tdTomato and plotted the location of the recorded neurons (Fig. 5C). In some cases, the catecholaminergic nature of the recorded neurons was also verified by the presence of TH immunoreactivity in addition to the presence of tdTomato in the biocytin-labeled neuron (6 A1 neurons, 13 A2 neurons).

Low-frequency photostimulation (1ms, 5mW, 0.5Hz) elicited EPSCs in 60% (9/14) of A1 neurons sampled with a 36.3±11.7% failure rate. Average EPSC amplitude (including failures) was 24.6±10.5 pA. As in the LC, the EPSCs were virtually eliminated by the addition of tetrodotoxin (N= 5 neurons; Fig. 9A1,2), were reinstated after addition of 4-AP, and were again eliminated in presence of CNQX and AP-5 (Fig. 9A1,2). Responses of the same five A1 neurons to a high-frequency photostimulation (1ms, 5mW, 10Hz, 10s train), applied in alternation with the periods of low frequency stimulation, were also examined. The 10 Hz trains produced the same pattern of response as in the LC (compare Figs. 4C1 and 9B1), namely an increase in EPSC frequency that reached a steady-state within 5 seconds. As in the LC, the EPSCs elicited by high frequency stimulation were largely random relative to the light pulses (not illustrated),

and their steady-state frequency was several-fold higher than the stimulus frequency (2.5 fold in Fig. 9B1; range: 1.1 to 3.8 fold, median 2.8 fold; N=4). TTX reduced but did not eliminate the EPSCs evoked by high frequency stimulation (Fig. 9B1,2), although EPSC frequency rose more slowly during the photostimulation than in control. Adding 4-AP increased the frequency of EPSCs evoked by the stimulus and changed the temporal pattern of response (Fig. 9B1,2) such that the maximal EPSC frequency was elicited at the onset of the stimulus train and tended to decay thereafter. Following addition of CNQX and AP5, all observable PSCs were eliminated and the stimulus train produced no observable current (Fig. 9B1,2).

Similar results were obtained with photostimulation of C1 terminals onto the A2 neurons. Low-frequency photostimulation (0.5Hz) elicited EPSCs in 57% (12/21) of A2 cells sampled (amplitude 22.86± 5.9 pA) with occasional failures (failure rate: 27.5± 8.8 %; n=8). The EPSCs were eliminated by the addition of tetrodotoxin, reinstated by addition of 4-AP, and again abolished after addition of CNQX and AP-5 (N=8; Fig. 10A1,2). The responses of A2 neurons to 10 Hz, 10 s trains of 1ms laser pulses were identical to those observed in A1 neurons. The high frequency stimulus produced a gradual increase in PSC frequency which reached steady-state within 3 seconds and were largely random with respect to the light stimuli (not illustrated). The steady-state frequency of the evoked EPSCs was several-fold higher than the stimulus frequency (4.5 fold in B1; range: 1.7 to 5.7 fold, median 3.4 fold, N=8). TTX again reduced but did not eliminate the EPSCs (Fig. 10B1,2), which were increased after addition of 4-AP and underwent a similar temporal change as described in A1 cells (Fig. 10B1,2). The addition

of CNQX eliminated all observable EPSCs before and during the photostimulus (Fig. 10B1,2).

One catecholaminergic neuron, not included in the above description, was recorded in the intermediate reticular nucleus (asterisk in Fig. 8C), and therefore could not be classified as either A1 or A2. C1 axon photostimulation also elicited monosynaptic, glutamatergic EPSCs in this neuron.

Discussion

We show that rostral VLM catecholaminergic neurons, most likely C1 neurons, establish glutamatergic synapses with LC, A1 and A2 noradrenergic neurons. The C1 neurons activate the sympathetic nervous system in response to hypoglycemia, hypotension, pain, hypoxia, infection and psychological stress (Ericsson et al., 1994; Jansen et al., 1995; Guyenet, 2006; Marina et al., 2011; Abbott et al., 2012; Guyenet et al., 2013). The C1 cells presumably also broadly increase CNS noradrenaline release under the same conditions (summarized in Figure 11).

Glutamatergic activation of lower brainstem noradrenergic neurons by the C1 cells.

After AAV injection into the rostral VLM, ChR2 was almost exclusively expressed by catecholaminergic neurons, 75% of which were TH- and PNMT-ir, thus C1 (Hokfelt et al., 1974). A similar proportion of ChR2-labeled axonal varicosities (78%) were VGLUT2-ir whereas caudal VLM catecholaminergic neurons (A1 cells) had

generally VGLUT2-negative varicosities. Accordingly, C1 rather than A1 neurons were the principal source of the glutamatergic EPSCs observed presently. However, we confirm that A1 neurons also innervate the locus coeruleus (Robertson et al., 2013) and find that around 10% of these cells may also express VGLUT2 (see also (Stornetta et al., 2002a)). A subset of A1 cells may therefore be glutamatergic and may have contributed to the observed glutamatergic EPSCs along with C1 cells. About 10% of C1 cells express the noradrenaline transporter, representing yet another example of a potential A1/C1 intermediate phenotype (Amara and Simerly, 1994; Comer et al., 1998).

C1 axon stimulation elicited EPSCs in a majority of LC (53%) and other noradrenergic neurons sampled (62%). These percentages could be underestimated because the number of ChR2-expressing varied between animals, as did the level of expression of ChR2.

The test used to determine whether the EPSCs evoked by C1 cell stimulation were monosynaptic was based on the effects of TTX and 4-AP (Petreanu et al., 2009). When short light pulses are used, ChR2-induced depolarization, hence calcium influx and vesicular release, is critically dependent on voltage-gated sodium current, and therefore blocked by TTX (Boyden et al., 2005; Zhang and Oertner, 2007; Petreanu et al., 2009). Addition of 4-AP reinstates transmitter release by facilitating the depolarization of the stimulated nerve terminals (Petreanu et al., 2009). The long EPSC latency observed without TTX (~5ms) almost certainly reflects the gradual depolarizing action of ChR2, not the conduction velocity of the stimulated fibers. Indeed, ChR2-generated action potentials elicited by direct somatic illumination, antidromic axonal stimulation or monosynaptic transmission have very similar latencies in tissue slices although the

inward current generated in ChR2-expressing cells is instantaneous (Petreanu et al., 2007; Zhang and Oertner, 2007; Petreanu et al., 2009). We verified that these assumptions apply to the C1 cells by showing that the latency to produce a spike in ChR2-expressing C1 somata was identical to the EPSC latency observed in the noradrenergic neurons by photostimulating the axons of the C1 cells. Under TTX and 4-AP, the latency of the EPSCs was longer still, likely reflecting that when fast sodium channels are inoperative, sufficient terminal depolarization to produce calcium influx is principally dependent on ChR2 and is delayed. In sum, the observed latencies were fully compatible with monosynaptic transmission.

The EPSCs elicited by stimulating C1 axons at 10Hz had a frequency higher than the light pulses and tended to occur randomly. This characteristic likely indicates the gradual accumulation of intracellular calcium within the photostimulated axons rather than some form of polysynaptic transmission. Because of the relatively slow kinetics of ChR2(H134R), high frequency stimulation produces a tonic depolarization. Cytoplasmic calcium rise probably also accounted for the brief persistence of EPSCs after a high frequency photostimulus in the presence of TTX (e.g. Figs. 9B1, 10B1). The fact that asynchronous EPSCs could be elicited in the presence of TTX, albeit after a longer delay than without TTX (Figs. 9B1, 10B1) also suggests that they could be mediated by a presynaptic rise in intracellular calcium rather than by some form of polysynaptic transmission.

The EPSCs elicited by low or high frequency stimulation in the presence of TTX and 4-AP were virtually eliminated by standard ionotropic glutamatergic receptor antagonists demonstrating their predominantly glutamatergic nature. This result agrees

with the fact that ChR2-labelled catecholaminergic varicosities were VGLUT2-ir and formed conventional excitatory-like synapses with the brainstem noradrenergic neurons examined. Neither C1 nor A1 cells express GABAergic or glycinergic markers (Schreihofer et al., 1999; Stornetta and Guyenet, 1999; Comer et al., 1999; Stornetta et al., 2002a). In agreement, IPSCs were never evoked by C1 axon stimulation, even at high frequency. Rat LC neurons may receive input from nearby GABA interneurons (Aston-Jones et al., 2004) but these interneurons are probably not targeted by C1 cells because C1 cell stimulation did not produce IPSCs in LC neurons.

Electrical stimulation of the rostral VLM produces a biphasic response in LC neurons in vivo (excitation-inhibition) (Aston-Jones et al., 1992). The excitation was originally attributed to a non-catecholaminergic input and the inhibition supposedly due to C1 neurons. When rat ChR2-expressing rostral VLM catecholaminergic cells are selectively photoactivated in vivo, the LC response also consists of an excitation-inhibition sequence but both components are eliminated by the administration of a glutamate antagonist (Abbott et al., 2012). The inhibition could therefore be a polysynaptic effect or an intrinsic property of LC neurons. It could also result from catecholamine release by LC dendrites or by the A1 input to the LC (Egan et al., 1983; Williams et al., 1984; Huang et al., 2012).

In summary, the EPSCs evoked in LC, A1 and A2 neurons by photostimulating rostral VLM catecholaminergic neurons were glutamatergic, monosynaptic and most probably originated from C1 rather than A1 cells. The electrophysiological evidence is consistent with the presence of VGLUT2 in the terminals of rostral VLM

catecholaminergic neurons and with ultrastructural evidence for synapses between these neurons and lower brainstem noradrenergic neurons.

Is the glutamatergic phenotype of the C1 cells an artifact caused by AAV2 transfection?

VGLUT2 is down-regulated postnatally in most CNS dopaminergic neurons and up-regulated when dopaminergic neurons are lesioned or maintained in culture (Dal et al., 2008; Berube-Carriere et al., 2009; El Mestikawy S. et al., 2011). Exposure to AAV2 may reinstate VGLUT2 expression in mature dopaminergic neurons (reviewed by (El Mestikawy S. et al., 2011)). However, in adult rats never exposed to AAV, most C1 neurons express VGLUT2mRNA and VGLUT2 immunoreactivity is detectable in most PNMT-immunoreactive varicosities. In addition, in TH-Cre rats, the AAV2 vector used presently does not change the VGLUT2 immunoreactivity present in C1 neuron axonal varicosities (Stornetta et al., 2002a; Depuy et al., 2013). For technical reasons we could not replicate this evidence in mice. However, unless VGLUT2 up-regulation by AAV2 vectors is unique to the mouse and unless, among VLM catecholaminergic neurons it is unique to the rostral VLM, the glutamatergic component of C1 cell transmission observed in the present study is not an AAV-induced artifact.

Do the C1 cells release catecholamines?

The C1 cells express vesicular monoamine transporter-2 (Sevigny et al., 2008). They also synthesize numerous neuropeptides (reviewed in (Guyenet et al., 2013)) and their terminals contain dense-core vesicles likely mediating the release of these

substances (present data). Our failure to detect any residual synaptic event after glutamate receptor blockade, even during high frequency stimulation, is consistent with our prior study on vagal motor neurons (Depuy et al., 2013) and likely means that our tests were not suited to detect responses mediated by peptides and catecholamines. In subcortical regions, noradrenaline often produces long-term potentiation or even metaplasticity (Neverova et al., 2007; Inoue et al., 2013). These phenomena develop over a much longer time period than the acute responses that we examined. Finally, the catecholamines released by the C1 cells could have limited effects on neurons and instead activate glia (O'Donnell et al., 2012).

Control of CNS noradrenergic neurons by the C1 cells: functional significance

The C1 cells are activated by hypoglycemia, hypotension, hypercapnia, infection, hypoxia and pain and contribute to the increased sympathetic tone and corticosterone release elicited by these stimuli (Madden and Sved, 2003; Abbott et al., 2009; Marina et al., 2011; Guyenet et al., 2013). These stimuli also activate LC neurons (Elam et al., 1981; Morilak et al., 1987a; Morilak et al., 1987b; Curtis et al., 1993; Murase et al., 1994; Guyenet et al., 2013). The present results suggest that the C1 cells likely relay these stimuli to LC, A1 and A2 noradrenergic neurons as well as to sympathetic preganglionic neurons (Figure 11). The A5 neurons, not examined in the present study, are excited by C1 neurons in vivo and are probably also directly innervated by these cells (Card et al., 2006; Abbott et al., 2012; 2013).

C1 cell activation by hypotension or by any of the above-mentioned stresses is therefore likely to produce widespread increases of CNS noradrenaline release with broad consequences on neuronal excitability, glial cell metabolism and, potentially, cerebral blood flow (Bekar et al., 2008; Attwell et al., 2010; Gordon et al., 2011).

Works Cited

Abbott SB, Depuy SD, Nguyen T, Coates MB, Stornetta RL, Guyenet PG (2013) Selective optogenetic activation of rostral ventrolateral medullary catecholaminergic neurons produces cardiorespiratory stimulation in conscious mice. J Neurosci 33:3164-3177.

Abbott SB, Kanbar R, Bochorishvili G, Coates MB, Stornetta RL, Guyenet PG (2012) C1 neurons excite locus coeruleus and A5 noradrenergic neurons along with sympathetic outflow in rats. J Physiol 590:2897-2915.

Abbott SB, Stornetta RL, Socolovsky CS, West GH, Guyenet PG (2009) Photostimulation of channelrhodopsin-2 expressing ventrolateral medullary neurons increases sympathetic nerve activity and blood pressure in rats. J Physiol 587:5613-5631.

Amara SG, Simerly RB (1994) Cell-type-specific expression of catecholamine transporters in the rat brain. J Neurosci 14:4903-4914.

Appleyard SM, Marks D, Kobayashi K, Okano H, Low MJ, Andresen MC (2007) Visceral afferents directly activate catecholamine neurons in the solitary tract nucleus. J Neurosci 27:13292-13302.

Aston-Jones G, Astier B, Ennis M (1992) Inhibition of noradrenergic locus coeruleus neurons by C1 adrenergic cells in the rostral ventral medulla. Neurosci 48:371-382.

Aston-Jones G, Cohen JD (2005) An integrative theory of locus coeruleus-norepinephrine function: adaptive gain and optimal performance. Annu Rev Neurosci 28:403-450.

Aston-Jones G, Zhu Y, Card JP (2004) Numerous GABAergic afferents to locus ceruleus in the pericerulear dendritic zone: possible interneuronal pool. J Neurosci 24:2313-2321.

Atasoy D, Aponte Y, Su HH, Sternson SM (2008) A FLEX switch targets Channelrhodopsin-2 to multiple cell types for imaging and long-range circuit mapping. J Neurosci 28:7025-7030.

Attwell D, Buchan AM, Charpak S, Lauritzen M, MacVicar BA, Newman EA (2010) Glial and neuronal control of brain blood flow. Nature 468:232-243.

Bekar LK, He W, Nedergaard M (2008) Locus coeruleus alpha-adrenergic-mediated activation of cortical astrocytes in vivo. Cereb Cortex 18:2789-2795.

Berridge CW, Schmeichel BE, Espana RA (2012) Noradrenergic modulation of wakefulness/arousal. Sleep Med Rev 16:187-197.

Berube-Carriere N, Riad M, Dal BG, Levesque D, Trudeau LE, Descarries L (2009) The dual dopamine-glutamate phenotype of growing mesencephalic neurons regresses in mature rat brain. J Comp Neurol 517:873-891.

Bochorishvili G, Stornetta RL, Coates MB, Guyenet PG (2011) Pre-Botzinger complex receives glutamatergic innervation from galaninergic and other retrotrapezoid nucleus neurons. J Comp Neurol 520:1047-1061.

Bohn MC, Dreyfus CF, Friedman WJ, Markey KA (1987) Glucocorticoid effects on phenylethanolamine N-methyltransferase (PNMT) in explants of embryonic rat medulla oblongata. Brain Res 465:257-266.

Boyden ES, Zhang F, Bamberg E, Nagel G, Deisseroth K (2005) Millisecond-timescale, genetically targeted optical control of neural activity. Nat Neurosci 8:1263-1268.

Bruinstroop E, Cano G, VanderHorst VG, Cavalcante JC, Wirth J, Sena-Esteves M, Saper CB (2012) Spinal projections of the A5, A6 (locus coeruleus), and A7 noradrenergic cell groups in rats. J Comp Neurol 520:1985-2001.

Byrum CE, Guyenet PG (1987) Afferent and efferent connections of the A5 noradrenergic cell group in the rat. J Comp Neurol 261:529-542.

Card JP, Sved JC, Craig B, Raizada M, Vazquez J, Sved AF (2006) Efferent projections of rat rostroventrolateral medulla C1 catecholamine neurons: Implications for the central control of cardiovascular regulation. J Comp Neurol 499:840-859.

Carter ME, Yizhar O, Chikahisa S, Nguyen H, Adamantidis A, Nishino S, Deisseroth K, De Lecea L (2010) Tuning arousal with optogenetic modulation of locus coeruleus neurons. Nat Neurosci 13:1526-1533.

Comer AM, Gibbons HM, Qi J, Kawai Y, Win J, Lipski J (1999) Detection of mRNA species in bulbospinal neurons isolated from the rostral ventrolateral medulla using single-cell RT-PCR. Brain Res Brain Res Protoc 4:367-377.

Comer AM, Qi J, Christie DL, Gibbons HM, Lipski J (1998) Noradrenaline transporter expression in the pons and medulla oblongata of the rat: localisation to noradreneric and some C1 adrenergic neurones. Mol Brain Res 62:65-76.

Corson JA, Erisir A (2013) Monosynaptic convergence of chorda tympani and glossopharyngeal afferents onto ascending relay neurons in the nucleus of the solitary

tract: a high-resolution confocal and correlative electron microscopy approach. J Comp Neurol 521:2907-2926.

Curtis AL, Drolet G, Valentino RJ (1993) Hemodynamic stress activates locus coeruleus neurons of unanesthetized rats. Brain Res Bull 31:737-744.

Dahlstrom A, Fuxe K (1964) Demonstration of monoamines in the cell bodies of brain stem neurons. Acta Physiol Scand 62 (suppl. 232):1-55.

Dal BG, Berube-Carriere N, Mendez JA, Leo D, Riad M, Descarries L, Levesque D, Trudeau LE (2008) Enhanced glutamatergic phenotype of mesencephalic dopamine neurons after neonatal 6-hydroxydopamine lesion. Neurosci 156:59-70.

Depuy SD, Stornetta RL, Bochorishvili G, Deisseroth K, Witten I, Coates MB, Guyenet PG (2013) Glutamatergic neurotransmission between the C1 neurons and the parasympathetic preganglionic neurons of the dorsal motor nucleus of the vagus. J Neurosci 33:1486-1497.

Egan TM, Henderson G, North RA, Williams JT (1983) Noradrenaline-mediated synaptic inhibition in rat locus coeruleus neurones. J Physiol 345:477-488.

El Mestikawy S., Wallen-Mackenzie A, Fortin GM, Descarries L, Trudeau LE (2011) From glutamate co-release to vesicular synergy: vesicular glutamate transporters. Nat Rev Neurosci 12:204-216.

Elam M, Yao T, Svensson TH, Thoren P (1984) Regulation of locus coeruleus neurons and splanchnic, sympathetic nerves by cardiovascular afferents. Brain Res 290:281-287.

Elam M, Yao T, Thoren P, Svensson TH (1981) Hypercapnia and Hypoxia: chemoreceptor-mediated control of locus coeruleus neurons and splanchnic sympathetic nerve. Brain Res 222:373-381.

Erickson JT, Millhorn DE (1994) Hypoxia and electrical stimulation of the carotid sinus nerve induce c-Fos-like immunoreactivity within catecholaminergic and serotinergic neurons of the rat brainstem. J Comp Neurol 348:161-182.

Ericsson A, Kovacs KJ, Sawchenko PE (1994) A functional anatomical analysis of central pathways subserving the effects of interleukin-1 on stress-related neuroendocrine neurons. J Neurosci 14:897-913.

Fenik VB, Rukhadze I, Kubin L (2008) Inhibition of pontine noradrenergic A7 cells reduces hypoglossal nerve activity in rats. Neurosci 157:473-482.

Gordon GR, Howarth C, MacVicar BA (2011) Bidirectional control of arteriole diameter by astrocytes. Exp Physiol 96:393-399.

Grossman N, Simiaki V, Martinet C, Toumazou C, Schultz SR, Nikolic K (2013) The spatial pattern of light determines the kinetics and modulates backpropagation of optogenetic action potentials. J Comput Neurosci 34:477-488.

Guyenet PG (2006) The sympathetic control of blood pressure. Nat Rev Neurosci 7:335-346.

Guyenet PG, Stornetta RL, Bochorishvili G, Depuy SD, Burke PG, Abbott SB (2013) Invited Review EB 2012: C1 neurons: the body's EMTs. Am J Physiol Regul Integr Comp Physiol doi: 10.1152/ajpregu.00054.2013-

Haxhiu MA, Yung K, Erokwu B, Cherniack NS (1996) CO_2-induced c-fos expression in the CNS catecholaminergic neurons. Resp Physiol 105:35-45.

Hertz L, Lovatt D, Goldman SA, Nedergaard M (2010) Adrenoceptors in brain: cellular gene expression and effects on astrocytic metabolism and [Ca(2+)]i. Neurochem Int 57:411-420.

Hokfelt T, Fuxe K, Goldstein M, Johansson O (1974) Immunohistochemical evidence for the existence of adrenaline neurons in the rat brain. Brain Res 66:235-251.

Huang HP, Zhu FP, Chen XW, Xu ZQ, Zhang CX, Zhou Z (2012) Physiology of quantal norepinephrine release from somatodendritic sites of neurons in locus coeruleus. Front Mol Neurosci 5:29.-doi: 10.3389/fnmol.2012.00029.

Inoue W, Baimoukhametova DV, Fuzesi T, Cusulin JI, Koblinger K, Whelan PJ, Pittman QJ, Bains JS (2013) Noradrenaline is a stress-associated metaplastic signal at GABA synapses. Nat Neurosci 16:605-612.

Jansen ASP, Nguyen XV, Karpitskiy V, Mettenleiter TC, Loewy AD (1995) Central command neurons of the sympathetic nervous system:basis of the fight-or flight response. Science 270:644-646.

Kaur S, Pedersen NP, Yokota S, Hur EE, Fuller PM, Lazarus M, Chamberlin NL, Saper CB (2013) Glutamatergic signaling from the parabrachial nucleus plays a critical role in hypercapnic arousal. J Neurosci In press:

Lin JY (2011) A user's guide to channelrhodopsin variants: features, limitations and future developments. Exp Physiol 96:19-25.

Madden CJ, Sved AF (2003) Cardiovascular regulation after destruction of the C1 cell group of the rostral ventrolateral medulla in rats. Am J Physiol Heart Circ Physiol 285:H2734-H2748.

Marina N, Abdala AP, Korsak A, Simms AE, Allen AM, Paton JF, Gourine AV (2011) Control of sympathetic vasomotor tone by catecholaminergic C1 neurones of the rostral ventrolateral medulla oblongata. Cardiovasc Res 91:703-710.

Milner TA, Abate C, Reis DJ, Pickel VM (1989) Ultrastructural localization of phenylethanolamine N- methyltransferase-like immunoreactivity in the rat locus coeruleus. Brain Res 478:1-15.

Mitchell DA, Lambert G, Secher NH, Raven PB, van LJ, Esler MD (2009) Jugular venous overflow of noradrenaline from the brain: a neurochemical indicator of cerebrovascular sympathetic nerve activity in humans. J Physiol 587:2589-2597.

Moreira TS, Takakura AC, Colombari E, Guyenet PG (2006) Central chemoreceptors and sympathetic vasomotor outflow. J Physiol 577:369-386.

Morilak DA, Fornal CA, Jacobs BL (1987b) Effects of physiological manipulations on locus coeruleus neuronal activity in freely moving cats. II. Cardiovascular challenge. Brain Res 422(1):24-31.

Morilak DA, Fornal CA, Jacobs BL (1987a) Effects of physiological manipulations on locus coeruleus neuronal activity in freely moving cats. III. Glucoregulatory challenge. Brain Res 422:32-39.

Morrison SF, Callaway J, Milner TA, Reis DJ (1989) Glutamate in the spinal sympathetic intermediolateral nucleus: localization by light and electron microscopy. Brain Res 503:5-15.

Murase S, Inui K, Nosaka S (1994) Baroreceptor inhibition of the locus coeruleus noradrenergic neurons. Neurosci 61:635-643.

Neverova NV, Saywell SA, Nashold LJ, Mitchell GS, Feldman JL (2007) Episodic stimulation of alpha1-adrenoreceptors induces protein kinase C-dependent persistent changes in motoneuronal excitability. J Neurosci 27:4435-4442.

O'Donnell J, Zeppenfeld D, McConnell E, Pena S, Nedergaard M (2012) Norepinephrine: a neuromodulator that boosts the function of multiple cell types to optimize CNS performance. Neurochem Res 37:2496-2512.

Paxinos G, Franklin KBJ (2004) The Mouse Brain in Stereotaxic Coordinates. Amsterdam: Elsevier.

Petreanu L, Huber D, Sobczyk A, Svoboda K (2007) Channelrhodopsin-2-assisted circuit mapping of long-range callosal projections. Nat Neurosci 10:663-668.

Petreanu L, Mao T, Sternson SM, Svoboda K (2009) The subcellular organization of neocortical excitatory connections. Nature 457:1142-1145.

Pieribone VA, Aston-Jones G (1991) Adrenergic innervation of the rat nucleus locus coeruleus arises predominantly from the C1 adrenergic cell group in the rostral medulla. Neurosci 41:525-542.

Ritter S, Llewellyn-Smith I, Dinh TT (1998) Subgroups of hindbrain catecholamine neurons are selectively activated by 2-deoxy-D-glucose induced metabolic challenge. Brain Res 805:41-54.

Robertson SD, Plummer NW, de MJ, Jensen P (2013) Developmental origins of central norepinephrine neuron diversity. Nat Neurosci 16:1016-1023.

Schiltz JC, Sawchenko PE (2007) Specificity and generality of the involvement of catecholaminergic afferents in hypothalamic responses to immune insults. J Comp Neurol 502:455-467.

Schreihofer AM, Stornetta RL, Guyenet PG (1999) Evidence for glycinergic respiratory neurons: Bötzinger neurons express mRNA for glycinergic transporter 2. J Comp Neurol 407:583-597.

Sevigny CP, Bassi J, Teschemacher AG, Kim KS, Williams DA, Anderson CR, Allen AM (2008) C1 neurons in the rat rostral ventrolateral medulla differentially express vesicular monoamine transporter 2 in soma and axonal compartments. Eur J Neurosci 28:1536-1544.

Shu Y, Yu Y, Yang J, Mccormick DA (2007) Selective control of cortical axonal spikes by a slowly inactivating K+ current. Proc Natl Acad Sci USA 104:11453-11458.

Sorg O, Magistretti PJ (1991) Characterization of the glycogenolysis elicited by vasoactive intestinal peptide, noradrenaline and adenosine in primary cultures of mouse cerebral cortical astrocytes. Brain Res 563:227-233.

Stornetta RL, Guyenet PG (1999) Distribution of glutamic acid decarboxylase mRNA-containing neurons in rat medulla projecting to thoracic spinal cord in relation to monoaminergic brainstem neurons. J Comp Neurol 407:367-380.

Stornetta RL, Macon CJ, Nguyen TM, Coates MB, Guyenet PG (2013) Cholinergic neurons in the mouse rostral ventrolateral medulla target sensory afferent areas. Brain Struct Funct 218:455-475.

Stornetta RL, Sevigny CP, Guyenet PG (2002a) Vesicular glutamate transporter DNPI/VGLUT2 mRNA is present in C1 and several other groups of brainstem catecholaminergic neurons. J Comp Neurol 444:191-206.

Stornetta RL, Sevigny CP, Schreihofer AM, Rosin DL, Guyenet PG (2002b) Vesicular glutamate transporter DNPI/GLUT2 is expressed by both C1 adrenergic and nonaminergic presympathetic vasomotor neurons of the rat medulla. J Comp Neurol 444:207-220.

Teppema LJ, Veening JG, Kranenburg A, Dahan A, Berkenbosch A, Olievier C (1997) Expression of *c-fos* in the rat brainstem after exposure to hypoxia and to normoxic and hyperoxic hypercapnia. J Comp Neurol 388:169-190.

Verberne AJ, Sartor DM (2010) Rostroventrolateral medullary neurons modulate glucose homeostasis in the rat. Am J Physiol Endocrinol Metab 299:E802-E807.

Verberne AJM, Stornetta RL, Guyenet PG (1999) Properties of C1 and other ventrolateral medullary neurones with hypothalamic projections in the rat. J Physiol 517:477-494.

Williams JT, North RA, Shefner SA, Nishi S, Egan TM (1984) Membrane properties of rat locus coeruleus neurones. Neurosci 13:137-156.

Yuan PQ, Yang H (2002) Neuronal activation of brain vagal-regulatory pathways and upper gut enteric plexuses by insulin hypoglycemia. Am J Physiol Endocrinol Metab 283:E436-E448.

Zhang YP, Oertner TG (2007) Optical induction of synaptic plasticity using a light-sensitive channel. Nat Methods 4:139-141.

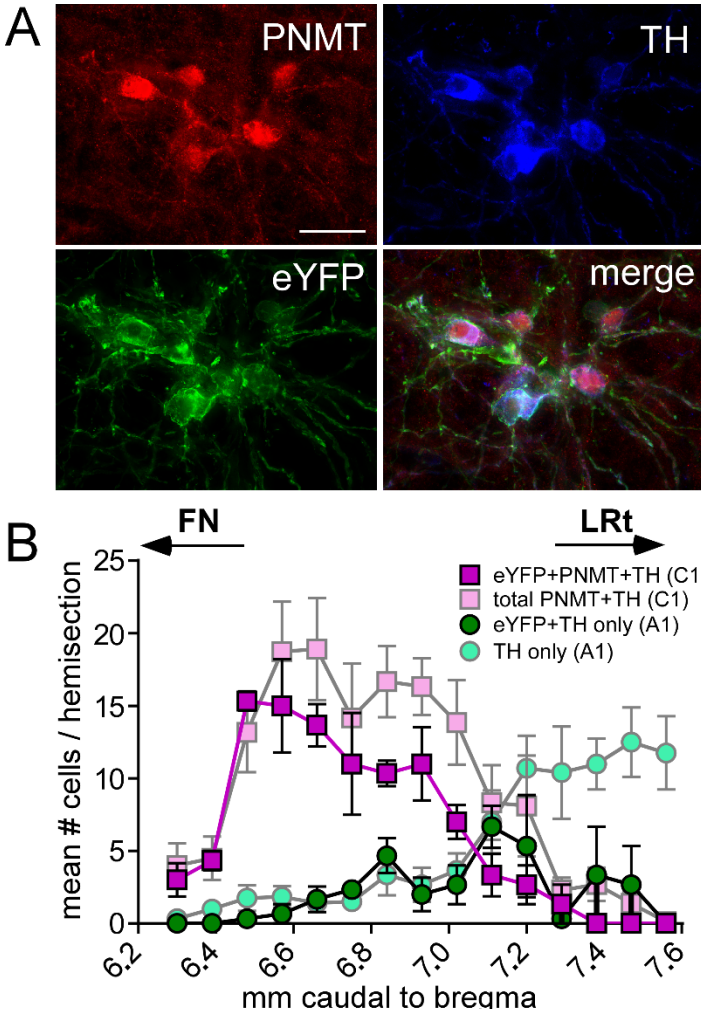
A
PNMT
TH
eYFP
merge
B
FN
LRt
eYFP+PNMT+TH (C1
total PNMT+TH (C1)
eYFP+TH only (A1)
TH only (A1)
mean # cells / hemisection
0
5
10
15
20
25
6.2
6.4
6.6
6.8
7.0
7.2
7.4
7.6
mm caudal to bregma

Figure 1: Selective expression of ChR2-eYFP in C1 cells

A, cluster of ChR2-eYFP-positive RVLM neurons that were immunoreactive for both TH and PNMT and therefore qualified as C1 neurons. Scale: 30 μm. This transverse section was located approximately 6.6 mm caudal to bregma (after Paxinos and Franklin (2004)). B, rostrocaudal distribution of C1 (immunoreactive for both PNMT and TH; light pink symbols with gray lines and error bars) and presumptive A1 neurons (immunoreactive for TH only; light green with gray lines and error bars) (mean ± SE of 6 mice). Rostrocaudal distribution of ChR2-eYFP-positive C1 neurons (PNMT- and TH-ir; purple squares with purple lines and black errors bars, average of 3 mice) and ChR2-eYFP-positive A1 neurons (TH-ir and eYFP-ir, but PNMT-negative; dark green with black lines and error bars, same 3 mice). Note that the percentage of C1 cells expressing ChR2-eYFP in the rostral VLM is much higher than expression of ChR2-eYFP in the TH-ir only (A1) neurons at more caudal levels.

Abscissa indicates the level of the transverse sections in mm caudal to bregma after Paxinos and Franklin (2004). The location of the facial motor nucleus (FN) and that of the lateral reticular nucleus (LRt) are indicated for orientation (for LRt, starting point of arrow defines level where the anterior portion of this nucleus ends). Arrows indicate that these structures extend beyond the levels represented.

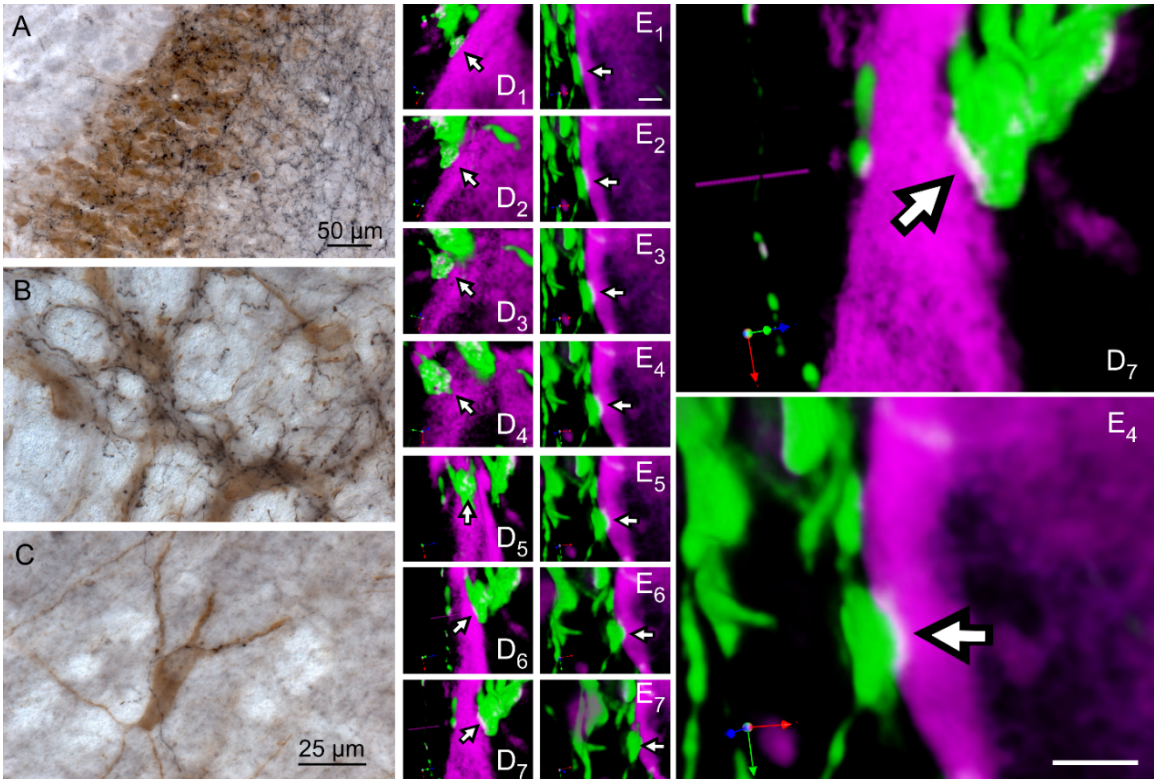
A
50 µm
B
C
25 µm
D1
E1
D2
E2
D3
E3
D4
E4
D5
E5
D6
E6
D7
E7
D7
E4

Figure 2: Innervation of lower brainstem noradrenergic neurons by the C1 cells

A, mCherry-ir axonal varicosities (black diaminobenzidine, DAB, reaction product) cover the cell body-rich portion of the LC (light brown DAB: TH-immunoreactivity) and the region medial to it where most LC dendrites reside. scp, left superior cerebellar peduncle. B, close appositions between mCherry-ir terminals (black DAB) and A1 neurons (light brown DAB: TH-immunoreactivity). C, close appositions, i.e. putative synapses (arrows) between mCherry-ir terminals (black DAB) and one A2 neuron (light brown DAB: TH-immunoreactivity). D, E, examples of synapse (arrow) between eYFP-ir terminal (green) and A1 neuron (TH-ir, magenta) (D) or A2 neuron (TH-ir, magenta) (E). D1-7 and E1-7 represent different angles of observation of the putative synaptic contact revealed through velocity 3D rendering software using deconvoluted images of either 57 (D) or 34 (E) serial 0.3 μm Z-stacks. The overlapping region of the two fluorophores is seen as a white band (arrow) and represents the putative contact zone. D7 and E5 are enlarged in the far right panels. Scale in A : 50μm, C: 25 μm applies to B,C; E, enlargement of D7 : 1 μm applies to D, E, enlargements of D7 and E5.

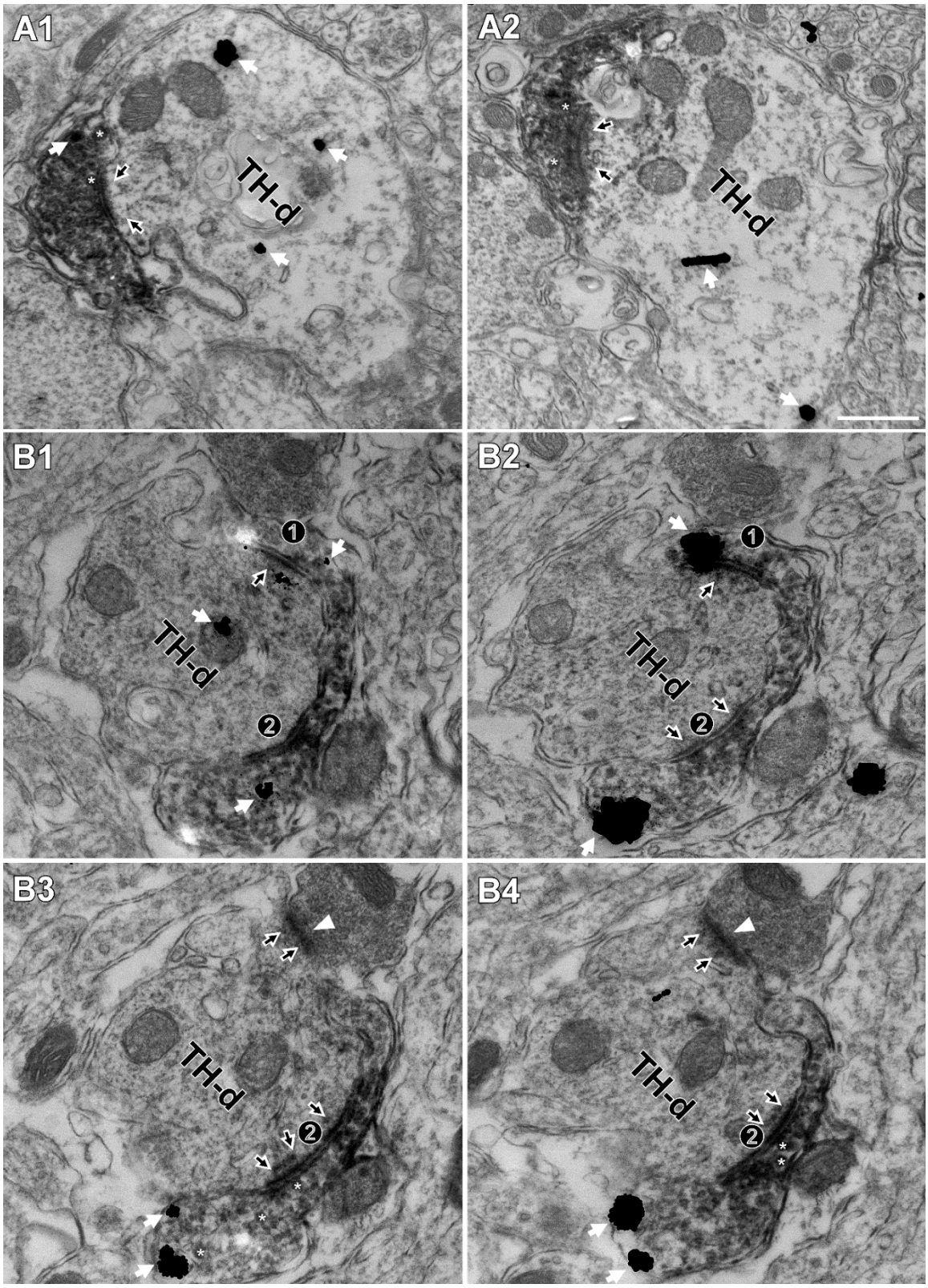
A1
TH-d
A2
TH-d
B1
1
TH-d
2
B2
1
TH-d
2
B3
TH-d
2
B4
TH-d
2

Figure 3: Ultrastructural evidence for synaptic contacts between putative C1 cells and A1/A2 catecholaminergic neurons

Electron micrographs display a number of asymmetric synapses formed between mCherry-ir terminals and catecholaminergic dendrites (TH-d) in adjacent sections. The terminal is identified by the presence of eYFP revealed by immunohistochemistry with a DAB reaction product (fine DAB precipitate) and the TH-d by black grains indicating the TH immunoreactivity revealed by a silver-gold reaction (silver-intensified immunogold particles, white arrows). The presynaptic terminal is also TH-ir as evidenced by the presence of immunogold reaction product (white arrows). A1-A2, a labeled A1 (TH-ir) neuronal dendrite shown in serial sections contains immunogold-silver particles (white arrows) and receives an asymmetric synapse (black rimmed arrows point to PSDs) from an mCherry-ir terminal. In B1-B4, four adjacent serial sections with labeled dendritic profiles forming one conventional synaptic junction (1) and a perforated synapse (2) from labeled terminals with small round vesicles and dense core vesicles (asterisks) in the A2 catecholaminergic cell group. The perforated synapse exhibits PSD profiles (white rimmed arrows) that have a discontinuity. Synapses were also formed between unlabeled terminals with small clear round vesicles and TH-ir dendrites (example in B3,4 indicated by white arrowhead). Scale 0.5 μm.

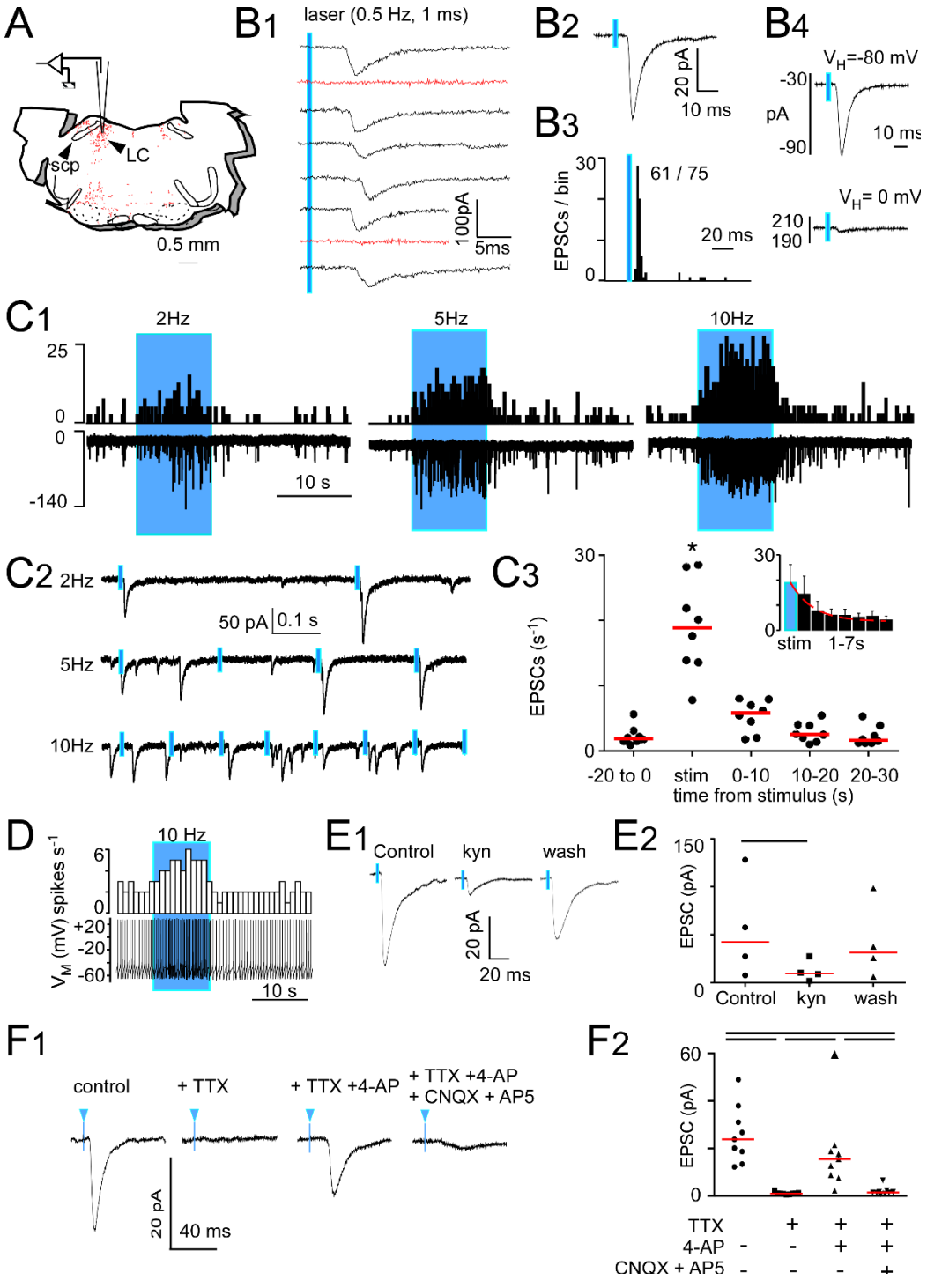
A
scp
LC
0.5 mm
B1
laser (0.5 Hz, 1 ms)
100pA
5ms
B2
20 pA
10 ms
B3
EPSCs / bin
30
0
61 / 75
20 ms
B4
V_H=-80 mV
-30
pA
-90
10 ms
V_H= 0 mV
210
190
C1
2Hz
5Hz
10Hz
25
0
0
-140
10 s
C2
2Hz
50 pA
0.1 s
5Hz
10Hz
C3
EPSCs (s-1)
30
0
*
stim
1-7s
-20 to 0
stim
0-10
10-20
20-30
time from stimulus (s)
D
10 Hz
6
0
+20
-20
-60
V_M (mV)
spikes s-1
10 s
E1
Control
kyn
wash
20 pA
20 ms
E2
150
0
EPSC (pA)
Control
kyn
wash
F1
control
+ TTX
+ TTX +4-AP
+ TTX +4-AP
+ CNQX + AP5
20 pA
40 ms
F2
60
0
EPSC (pA)
TTX
4-AP
CNQX + AP5

Figure 4: Monosynaptic glutamatergic input from C1 neurons to LC

A, Experimental design. The LC was identified in transverse slices by its location medial to the superior cerebellar peduncle (scp) and by the presence of a dense network of mCherry or EYFP fluorescent axons emanating from the C1 neurons (small red dots represent individual boutons originating from C1 neurons after Abbott et al. (2013)). B, EPSCs evoked in LC neurons by low frequency photostimulation of the axons of C1 cells (B1, single responses; red traces are failures). Blue vertical line or filled box represents the period of laser stimulation throughout the figure. B2, average of 75 consecutive stimulations. B3, event triggered histogram showing that 61 out of 75 stimuli resulted in an EPSC; B1-B3: same neuron). B4, recording made with cesium-filled electrode at Vhold -85 mV and 0 mV. Average of 75 stimuli. Note lack of outward current at Vhold = 0 mV). C, responses elicited by higher frequency photostimulation of C1 axons (2-10 Hz) (C1, representative example: bottom, original traces; top EPSC frequency binned every 0.5 s. C2, expanded scale traces. Note that at 10 Hz, the evoked EPSCs are no longer synchronized with the light pulses. C3, EPSC frequency at rest, during the last 5 seconds of a 10 s, 10 Hz stimulation train and at three recovery times in 7 LC neurons; red horizontal lines indicate the median response; non-parametric ANOVA, Dunn's posthoc test; group identified by an asterisk is significant from all others at $P<0.05$); C3 Inset, Blue square represents the mean EPSC frequency (per sec) during the stimulation period and the open circles represent the mean EPSC frequency binned in each 1s interval following the end of the stimulus. Decay time constant was 1.6s with a 95% interval of 1.1 to 2.8s. D, Current clamp recording: 10 Hz stimulation (1 ms pulses) more than doubles the firing rate of the neuron. E, reversible attenuation of the evoked EPSC by

1mM kynurenate (E1; representative example; E2, summary data from 4 neurons; red horizontal lines indicate the median response, black horizontal bars at top of panel indicate $P<0.05$ between control and kynurenate by Dunn's test following non-parametric ANOVA. F, test for monosynaptic connection (F1, representative experiment. Each trace is the average of 75 evoked responses. F2, group data from 9 neurons/6 mice; red horizontal lines indicate the median response; black horizontal bars at top of panele link groups that are significantly different at $P<0.05$ using non-parametric ANOVA followed by Dunn's test.

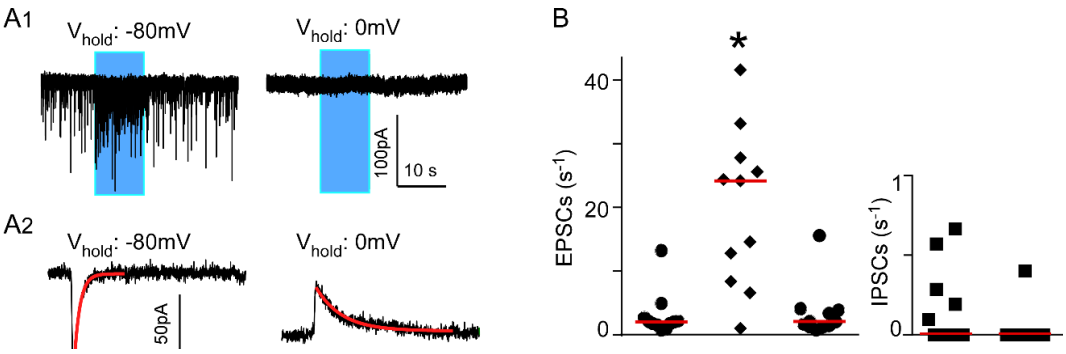
A1
V_{hold}: -80mV
V_{hold}: 0mV
100pA
10 s
A2
V_{hold}: -80mV
V_{hold}: 0mV
50pA
B
EPSCs (s^{-1})
40
20
0
*
IPSCs (s^{-1})
1
0

Figure 5: Identification and location of recorded brainstem noradrenergic neurons

A, Identification of noradrenergic neurons in DβH$^{Cre/0}$/ROSA26-tdTomato mice. Fluorescence photomicrograph centered on the left dorsal vagal complex (transverse 30 μm-thick section). Left: tyrosine-hydroxylase (TH); middle: tdTomato; right: merged image. Wide rimmed arrows in middle panel: catecholaminergic tdTomato-labeled neurons. White arrows in right panel: TH-immunoreactive (ir) neurons devoid of tdTomato fluorescence. This representative section contained 17 TH-ir neurons, 12 of which were positive for tdTomato. Some of the TH-ir neurons devoid of tdTomato could be dopaminergic. Scale: 100 μm.

B, left column, top two panels: low power photomicrograph showing a recorded LC neuron filled with biocytin (blue) and its location in the nucleus (LC neurons identified by TH immunoreactivity, green). Bottom two panels, higher magnification showing more clearly that the recorded neuron was TH-ir. B, middle column, A1 neuron located in the caudal VLM, labeled with biocytin (top panel, blue) and identified as noradrenergic by the presence of tdTomato fluorescence (second panel from top, red). The neuron was surrounded by axonal processes labeled with ChR2-eYFP which originated from C1 neurons (green, third panel down). Lower panel shows the merged image. B, right column: A2 neuron located in the nucleus of the solitary tract, filled with biocytin after recording (top panel, blue) and identified as noradrenergic by the presence of tdTomato fluorescence. The neuron is surrounded by axonal processes originating from C1 neurons (eYFP, in green). Bottom panel, merged image. Scale in A: 190 μm in left column, top two panels; 30 μm in all other panels. Scale in B: 500 μm.

C, location of the recorded noradrenergic (tdTomato-positive) A1 and A2 neurons (represented by blue-filled circles) recovered following histology plotted on representative sections that also illustrate the typical location of noradrenergic (TH+ PNMT- cells represented by red squares) and adrenergic neurons (PNMT+ cells represented by gray diamonds). Drawings are computer-assisted plots; numbers next to sections indicate the location of the transverse plane in relation to bregma after Paxinos and Franklin (2004). IO, inferior olive; LRt, lateral reticular nucleus; NA, nucleus ambiguous; NTS, nucleus of the solitary tract; 12, hypoglossal nucleus.

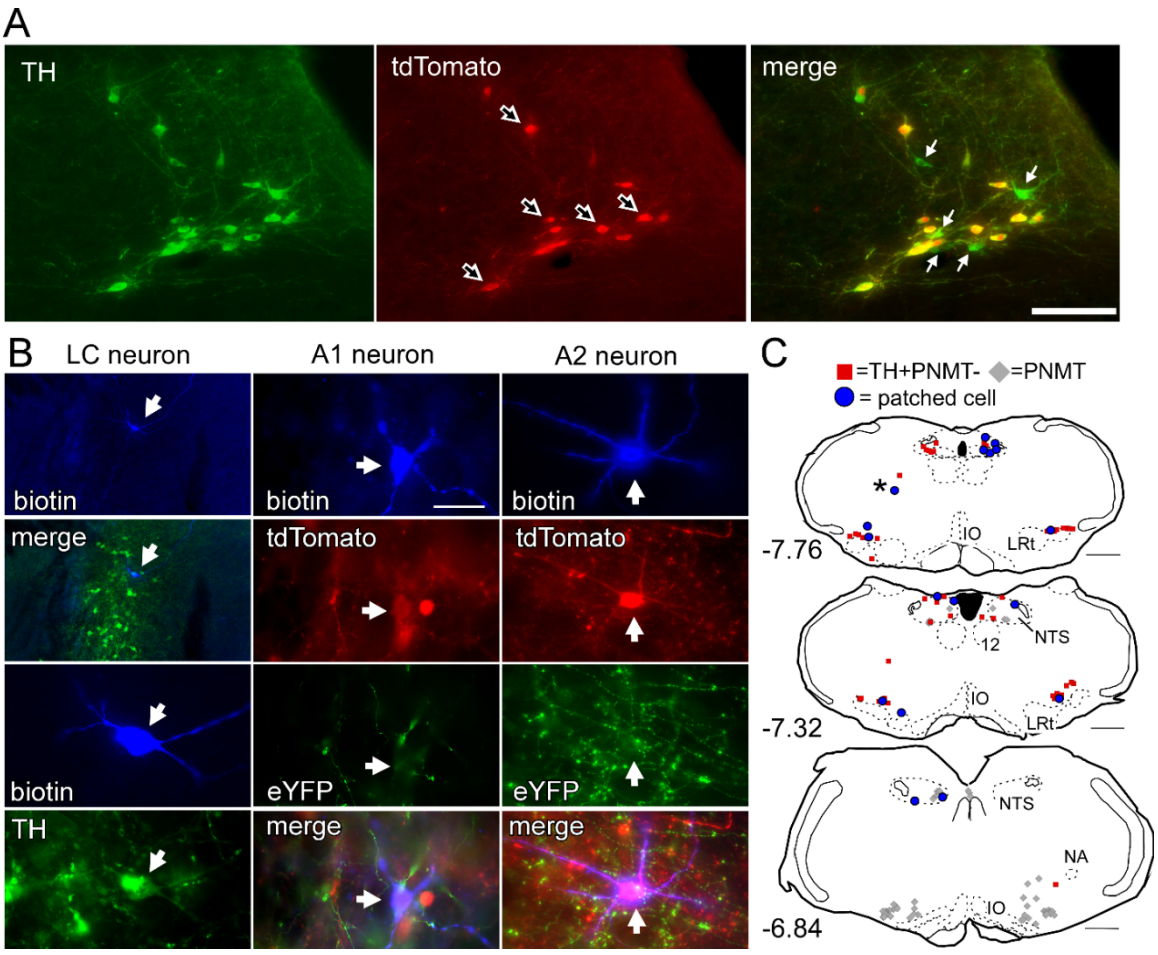
A
TH
tdTomato
merge
B
LC neuron
A1 neuron
A2 neuron
biotin
biotin
biotin
merge
tdTomato
tdTomato
biotin
eYFP
eYFP
TH
merge
merge
C
=TH+PNMT-
=PNMT
= patched cell
-7.76
IO
LRt
12
NTS
-7.32
IO
LRt
NTS
NA
IO
-6.84

Figure 6: Photostimulation of C1 cell axons does not elicit IPSCs in LC neurons

Whole cell recordings were obtained with cesium-filled electrodes in 11neurons from 5mice. Pulses of laser light (1ms, 5mW, 10Hz) were applied for 10s (blue box). A1, EPSCs were elicited when the neuron was clamped at -80 mV but no detectable current was elicited at 0mV. A2, high resolution example of single EPSC recorded at -80 mV (left) and single IPSC recorded at 0mV (right). The red lines are a single exponential fit of the PSC decay. EPSC decay 4.3ms, IPSC decay 21.2ms. B, left. EPSC frequency before (Ctrl) during (stim) and after photostimulation at 10 Hz (rec). Red horizontal lines indicate the median response in both panels. The asterisk indicates P<0.05 relative to the control and recovery period (non-parametric ANOVA, Dunn's post-hoc test). B, right. IPSCs were very infrequent and their frequency was unaffected by photostimulation

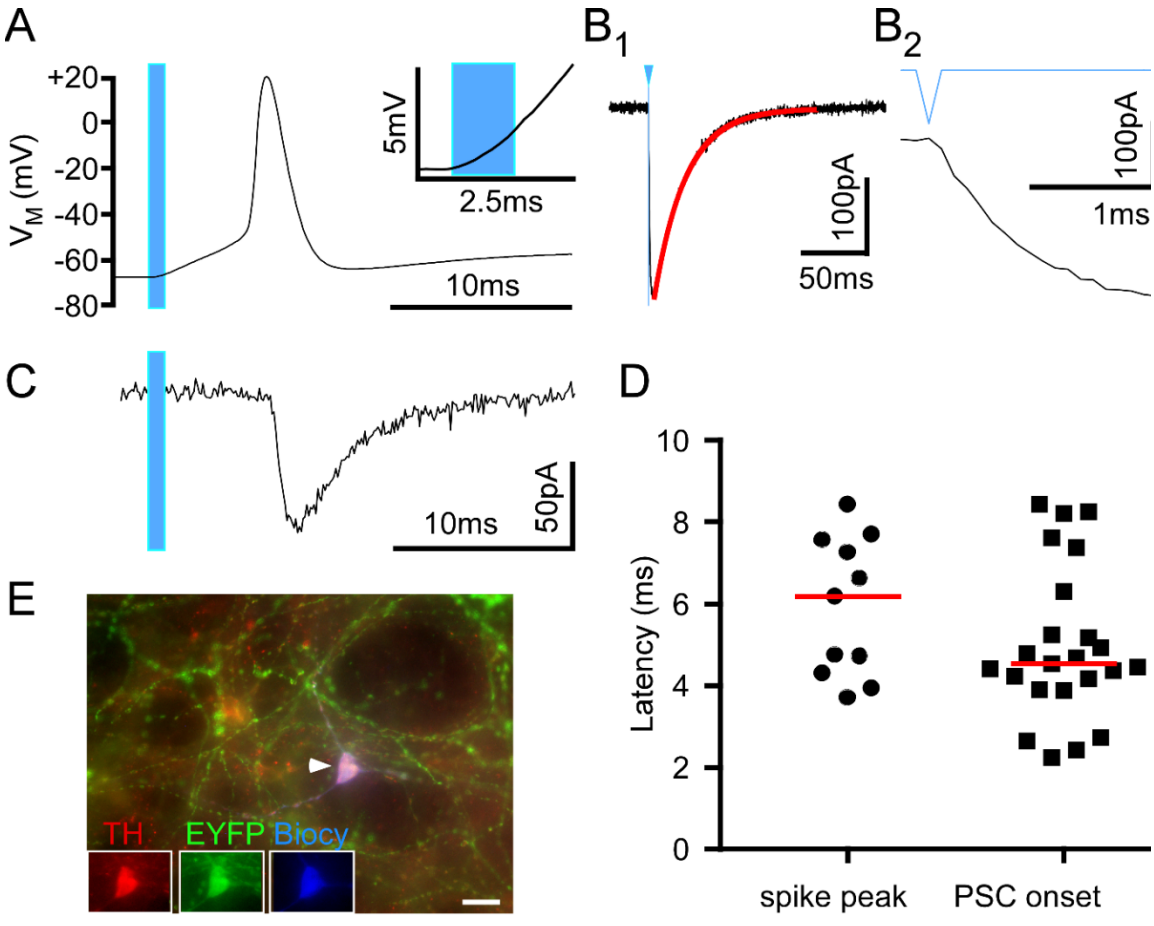

Figure 7

Figure 7: ChR2-mediated excitation of rostral VLM catecholaminergic neurons

A, action potential elicited in a ChR2-expressing rostral VLM neuron by a 1ms laser pulse (blue bar). Note the long latency of the action potential. The inset at higher resolution shows that the slow depolarization begins rapidly after laser onset. B1, voltage clamp recording of the same neuron showing that the inward current generated by the laser pulse (0.1ms-long) is virtually instantaneous and decays exponentially (red line; τ = 23ms). B2, higher resolution of the initial response showing that the inward current is instantaneous. C, typical EPSC elicited in a LC neurons by photoactivating the severed axons of rostral VLM catecholaminergic neurons (1ms pulse). Panels A and C are aligned to emphasize the similarity between the latency of the action potential recorded at the level of a cell body and the latency of the EPSC evoked by stimulating the axons of the same cells. D, group data (latency to peak of action potentials recorded from the somata of 11 C1 cells from 5mice and EPSC latencies recorded in 9 LC neurons from 6 mice. E, example of a recorded ChR2-expressing rostral VLM catecholaminergic neuron (white arrow; scale bar: 20 μm. TH (red), eYFP (green), and biocytin (blue). Inset shows individual channels.

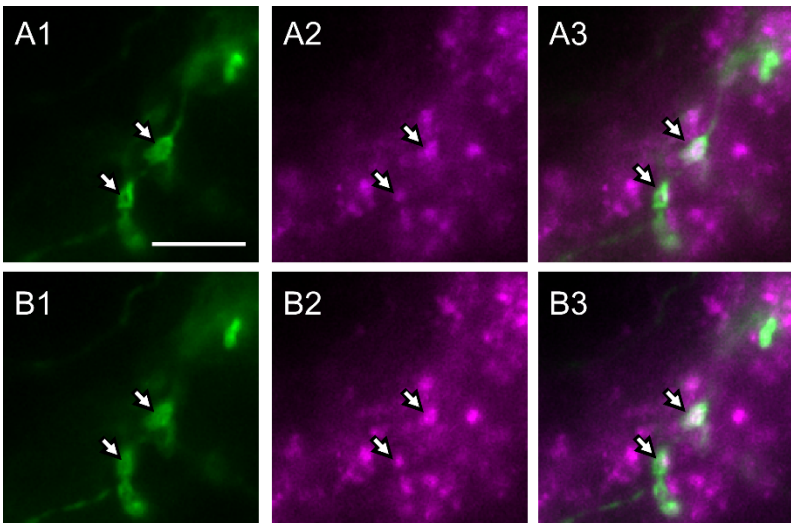
A1
A2
A3
B1
B2
B3

Figure 8: Terminals from rostral VLM catecholaminergic neurons in locus coeruleus are glutamatergic

A, B, serial 0.3 μm Z-stack sections of axonal varicosities from rostral VLM catecholaminergic neurons. A1, B1, eYFP immunoreactivity (green); A2,B2, VGLUT2 (magenta); A3,B3, merged image. Scale: 5 μm.

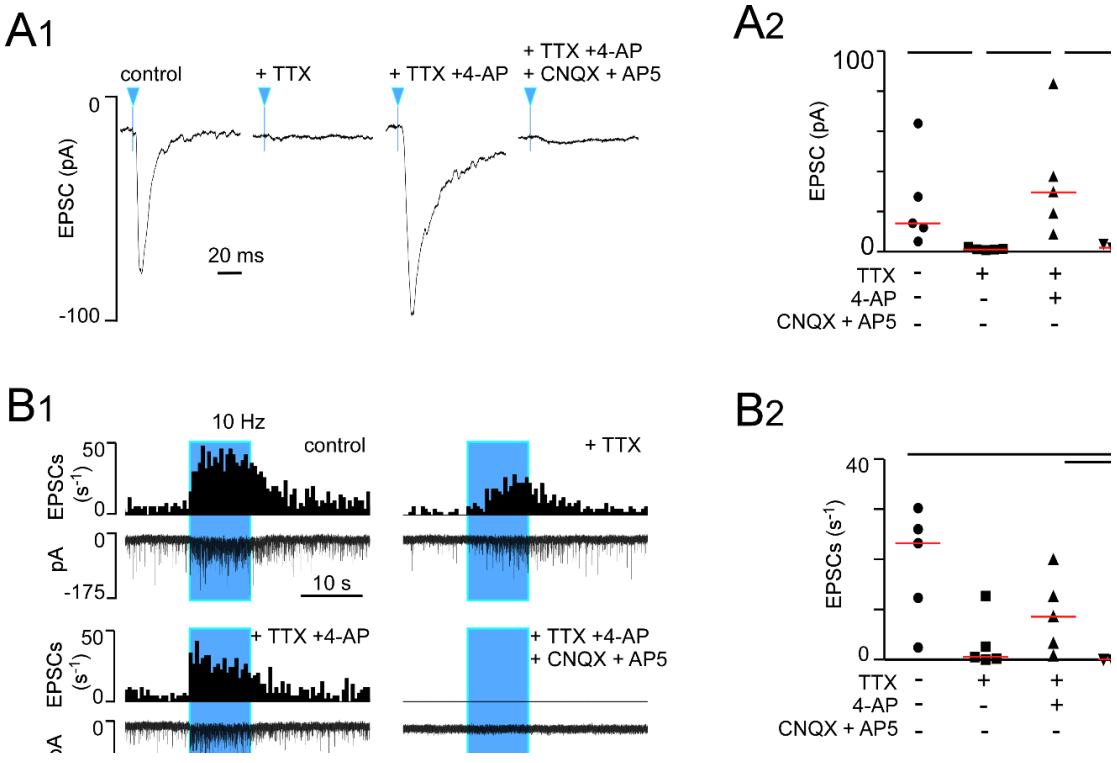
A1
control
+ TTX
+ TTX +4-AP
+ TTX +4-AP
+ CNQX + AP5
0
EPSC (pA)
-100
20 ms
A2
100
EPSC (pA)
0
TTX - + +
4-AP - - +
CNQX + AP5 - - -
B1
10 Hz
control
+ TTX
50
EPSCs (s-1)
0
pA
0
-175
10 s
+ TTX +4-AP
+ TTX +4-AP
+ CNQX + AP5
50
EPSCs (s-1)
0
0
B2
40
EPSCs (s-1)
0
TTX - + +
4-AP - - +
CNQX + AP5 - - -

Figure 9: A1 neurons receive monosynaptic glutamatergic input from C1 neurons

A, effect of TTX, 4-AP and glutamate receptor antagonists on the EPSCs elicited by low frequency (0.5Hz) photostimulation of the axons of rostral VLM catecholaminergic neurons (A1, representative example; 0.5 Hz, 1 ms photostimulation at blue arrows; each trace is the average of 75 stimuli. A2, group data from 5neurons and 4mice; Red horizontal lines indicate the median response; black horizontal bars at top of figure link groups that are significantly different at $P<0.05$ determined using a non-parametric ANOVA with Dunn's posthoc test. B, effect of TTX, 4-AP and glutamate receptor antagonists on the responses elicited by high frequency photostimulation (10 Hz, 1 ms pulses; photostimulation periods represented by the blue boxes). B1, representative example; bottom traces: original recordings, Vhold -85 mV. B2, group data; red horizontal lines indicate the median response; black horizontal bars at top of figure link groups that are significantly different at $P<0.05$ determined using a non-parametric ANOVA with Dunn's posthoc test.

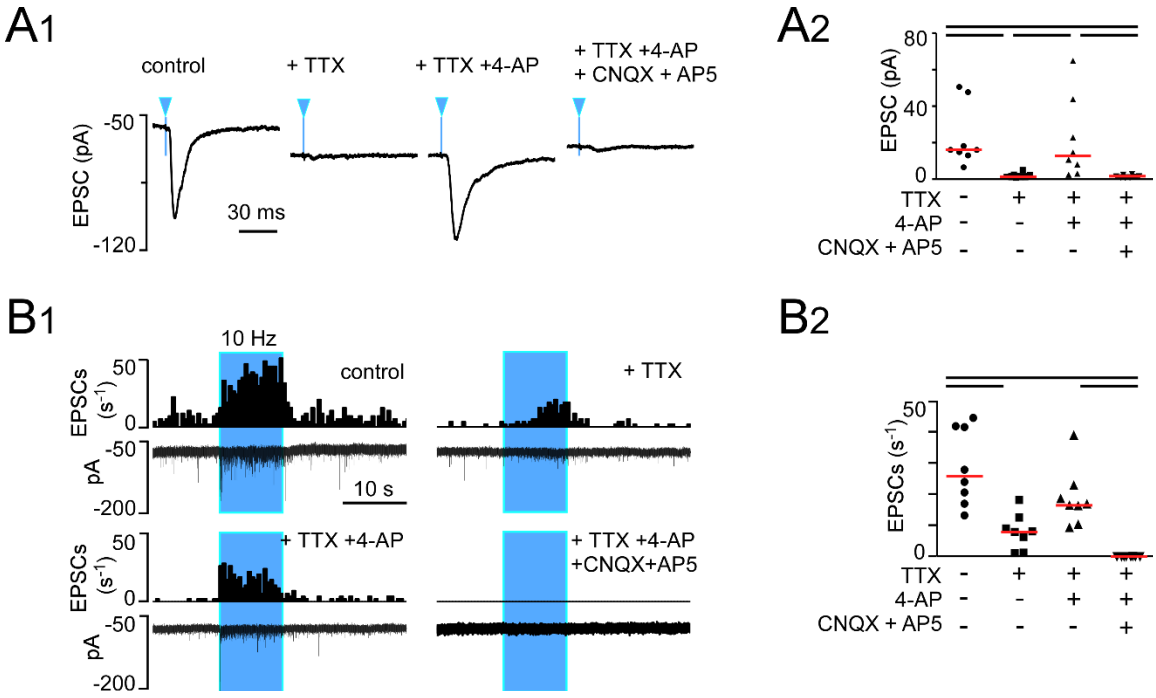
A1
control
+ TTX
+ TTX +4-AP
+ TTX +4-AP
+ CNQX + AP5
EPSC (pA)
-50
-120
30 ms
A2
EPSC (pA)
80
40
0
TTX - + + +
4-AP - - + +
CNQX + AP5 - - - +
B1
10 Hz
control
+ TTX
EPSCs (s-1)
50
0
pA
-50
-200
10 s
+ TTX +4-AP
+ TTX +4-AP
+CNQX+AP5
B2
EPSCs (s-1)
50
0
TTX - + + +
4-AP - - + +
CNQX + AP5 - - - +

Figure 10: A2 neurons receive monosynaptic glutamatergic input from C1 neurons

A, effect of TTX, 4-AP and glutamate receptor antagonists on the EPSCs elicited by low frequency (0.5Hz) photostimulation of the axons of rostral VLM catecholaminergic neurons (A1, representative example; 0.5 Hz, 1 ms photostimulation at blue arrows; each trace is the average of 75 stimuli. A2, group data from 8 neurons and 7 mice; red horizontal lines represent the median response; black horizontal bars at top of figure link groups that are significantly different at $P<0.05$ determined using a non-parametric ANOVA with Dunn's posthoc test). B, effect of TTX, 4-AP and glutamate receptor antagonists on the responses elicited by high frequency photostimulation of the axons of rostral VLM catecholaminergic neurons (10 Hz, 1 ms pulses; photostimulation period represented by the blue boxes). B1, representative example; bottom traces: original recordings, Vhold -85 mV. B2, group data; red horizontal lines represent the median response; black horizontal bars at top of figure link groups that are significantly different at $P<0.05$ determined using a non-parametric ANOVA with Dunn's posthoc test.

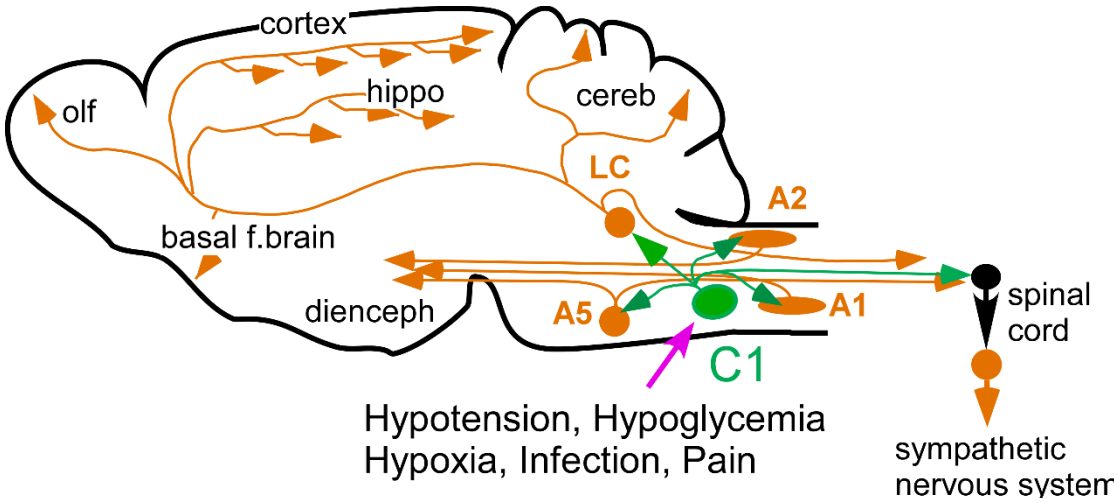
cortex
olf
hippo
cereb
LC
A2
basal f.brain
dienceph
A5
A1
C1
spinal
cord
Hypotension, Hypoglycemia
Hypoxia, Infection, Pain
sympathetic
nervous system

Figure 11: The C1 cells regulate peripheral and CNS noradrenaline release

C1 cells (green) directly innervate and activate sympathetic preganglionic neurons (black) plus every major group of CNS noradrenergic neurons (orange). The C1 cells thus have the capacity to activate noradrenergic release throughout the body and the brain under conditions such as hypotension, hypoxia etc.. Abbreviations: basal f. brain, basal forebrain, cereb, cerebellum, dienceph, diencephalon, hippo, hippocampus, olf, olfactory bulb.

Chapter 3: Regulation of breathing via the RVLM

Along with blood pressure regulation, the RVLM is also an important region for the neural control of breathing. One of the principle populations involved in this regulation is the retrotrapezoid nucleus neurons (RTN). RTN are chemosensitive, and they are thought to adjust breathing in a CO_2-dependent manner, whether through direct, indirect, or combinatorial chemosensitive mechanisms. Some evidence indicates that RTN neurons may also be involved in the neural control of breathing in general, i.e. non-chemosensitive pathways. Much of the research on RTN has been performed at the cellular level—characterizing the chemosensitive channels of RTN, or at the physiological level—measuring the effect on breathing during RTN perturbation or after RTN lesion. One of the primary obstacles in researching RTN is specificity. Currently, the most selective technique developed for targeting RTN neurons is the use of the artificial promoter PRSx8—a multimer of the Phox2a/b-recognition site. Within the RVLM, injections of viral vectors containing this promoter lead to specific expression of viral payload in noradrenergic neurons (namely C1) and RTN neurons. Studies of RTN at the cellular level have side-stepped this issue by either demonstrating intrinsic chemosensitivity—the hallmark of RTN—or identifying the RNA or protein fingerprints of RTN neurons post-hoc. For conscious studies, however, there is no transgenic or promoter-based technique to specifically target RTN versus C1, and no approach to overcome the limitations of the PRSx8 labelling of C1 neurons has been developed. This severely limits interpretation of physiological consequences during putative RTN perturbation, which may in fact be the results of C1 activity, or a muddy combination of

RTN and C1 stimulation. Therefore, I attempted to design an approach to specifically stimulate RTN in conscious mice.

The following two articles detail our investigations into the how the RVLM regulates breathing. The first publication in this section—in which I am not the first but a contributing author—is included as the results are critical in the strategic design of the second article in this section. My goal in this project was to determine the consequence of optogenetically stimulating RTN neurons alone. Thus, I designed a research strategy to isolate the effects of RTN versus C1/RTN optogenetic stimulation using available technologies.

3.1 Declaration of published work: I am a contributing author to this previously published work, accepted in the *European Journal of Neuroscience,* Eur J Neurosci. 2014 Jan;39(1):98-106. doi: 10.1111/ejn.12421. Epub 2013 Nov 18.

VGLUT2 is required for the respiratory and parasympathetic activation produced by optogenetic stimulation of catecholaminergic neurons in the rostral ventrolateral medulla of mice *in vivo*.

Stephen B. G. **Abbott**, Benjamin B. **Holloway,** Kenneth E. **Viar**, and Patrice G. **Guyenet**

Department of Pharmacology, University of Virginia, Charlottesville, VA 22908

Address correspondence to:

Patrice G. Guyenet, PhD

University of Virginia Health System

P.O. Box 800735, 1300 Jefferson Park Avenue

Charlottesville, VA 22908-0735.

Tel: (434) 924-7433; Fax: (434) 982-3878; E-mail: pgg@virginia.edu

Running title: VGLUT2 in RVLM-CA neurons

Pages-20; Figure-4; Tables-0; Equations-0

Word count: total= 6383; abstract=238; introduction; 409

Keywords: conditional knockout, Channelrhodopsin 2, C1 neuron, glutamate

Abstract

Catecholaminergic neurons of the rostral ventrolateral medulla (RVLM-CA neurons) contribute to the sympathetic, parasympathetic and neuroendocrine responses elicited by physical stressors such as hypotension, hypoxia, hypoglycemia and infection. Most RVLM-CA neurons express vesicular glutamate transporter 2 (VGLUT2) and may use glutamate as ionotropic transmitter but the importance of this mode of transmission *in vivo* is uncertain. To address this question we genetically deleted VGLUT2 from dopamine-β-hydroxylase-expressing neurons in mice ($D\beta H^{Cre/0}$;$VGLUT2^{flox/flox}$, henceforth cKO mice). Then we compared the effects produced *in vivo* by selectively stimulating RVLM-CA neurons in cKO vs. control mice ($D\beta H^{Cre/0}$) using channelrhodopsin-2 (ChR2-mCherry) optogenetics. ChR2-mCherry was expressed by similar numbers of RVLM neurons in each strain (~400 neurons), with identical selectivity for CA neurons (90-99 % colocalization with tyrosine hydroxylase). RVLM-CA neurons had similar morphology and axonal projections in $D\beta H^{Cre/0}$ and cKO mice. Each light pulse (up to 20 Hz) activated ChR2- mCherry expressing RVLM-CA neurons in slices of adult $D\beta H^{Cre/0}$ mice and likewise activated presumptive RVLM-CA neurons recorded in anesthetized $D\beta H^{Cre/0}$ and cKO mice. Photostimulation in conscious mice produced frequency–dependent (5-20 Hz) respiratory activation in $D\beta H^{Cre/0}$ mice but no effect in cKO mice. Similarly, photostimulation under urethane anesthesia strongly activated efferent vagal nerve activity in $D\beta H^{Cre/0}$ mice only. Vagal responses were unaffected by α1-adrenergic receptor blockade. In short, two responses evoked by RVLM-CA neuron stimulation in vivo were shown to depend on the expression of

VGLUT2 by these neurons suggesting that the acute autonomic responses elicited by these neurons in vivo are mediated by glutamate.

Introduction

Catecholaminergic neurons located in the rostral ventrolateral medulla (RVLM-CA neurons), are activated by a variety of stresses (pain, hypotension, hypoxia, hypoglycemia and infection) and contribute to the autonomic and neuroendocrine responses elicited by these stimuli (Guyenet et al, 2013). Most RVLM-CA neurons are C1 neurons which, by definition, express all the catalytic enzymes required for the production of adrenaline (tyrosine hydroxylase, TH, dopamine-β-hydroxylase, DβH, and phenylethanolamine N-methyl transferase, PNMT) (Hokfelt et al, 1974;Ross et al, 1983;Phillips et al, 2001). Despite a catecholaminergic phenotype, evidence suggests that C1 neurons release glutamate as a primary neurotransmitter in adult rodents. PNMT-containing terminals form asymmetric synaptic contacts consistent with the ultrastructure of classical excitatory synapses (Milner et al, 1987;Milner et al, 1988;Milner et al, 1989;Agassandian et al, 2012;Depuy et al, 2013). Glutamate uptake by synaptic vesicles is mediated by one of three vesicular glutamate transporters (VGLUT1-3) (Bellocchio et al, 2000;Takamori et al, 2000;Gras et al, 2002;Fremeau et al, 2004), of which, only vesicular glutamate transporter 2 (VGLUT2) transcripts and protein are detectable in C1 neurons of rats and mice (Stornetta et al, 2002a;Herzog et al, 2004;Rosin et al, 2006;Abbott et al, 2012). Further, optogenetic activation of the C1 axons elicits monosynaptic glutamatergic EPSCs in parasympathetic preganglionic neurons in vitro

(Depuy et al, 2013), which is consistent with prior *in vivo* pharmacological evidence (Morrison et al, 1991;Morrison 2003;Abbott et al, 2012).

Evidence that C1 neurons use glutamate as a fast transmitter is substantial, but for the most part indirect (histological, pharmacological) or *in vitro*. Glutamate release by the C1 neurons should rely on VGLUT2 but this has not been directly tested. The aim of the present study is to determine the contribution of glutamatergic transmission to RVLM-CA neuron signaling in intact mice and determine significance of VGLUT2 in this process. To accomplish this aim, we crossed DβH$^{Cre/0}$ mice, in which noradrenergic and adrenergic neurons express Cre-recombinase, with mice in which exon 2 of the VGLUT2 gene is flanked by LoxP sites (Tong et al, 2007;Abbott et al, 2013). In the resulting progeny (VGLUT2$^{flox/flox}$;DβH$^{Cre/0}$, henceforth cKO), VGLUT2 is largely eliminated from the terminals of RVLM-CA neurons (Depuy et al, 2013). To determine the contribution of VGLUT2 and glutamate release in RVLM-CA neuron signaling *in vivo*, we compared the effects of stimulating these neurons on respiration and vagus nerve efferent activity in DβH$^{Cre/0}$ and cKO mice using a Cre-dependent channelrhodopsin-2(ChR2)-based optogenetic method.

Materials and Methods

Animals

Animal use was in accordance with NIH Guide for the Care and Use of Laboratory Animals and approved by the University of Virginia Animal Care and Use Committee. DβH$^{Cre/0}$ mice were obtained from the Mutant Mouse Regional Resource

Center at the University of California, Davis, CA, USA [Tg(DβH-cre)KH212Gsat/Mmcd; stock # 032081-UCD]. DβH$^{Cre/0}$ mice were maintained as hemizygous (Cre/0) on a C57BL/6J background. Homozygous VGLUT2$^{(flox/flox)}$ mice (JAX Stock #012898; STOCK Slc17a6$^{tm1Lowl/J}$)(Tong et al., 2007) were bred with DβH $^{Cre/0}$ mice to generate DβH$^{Cre/0}$; VGlut2$^{flox/0}$ mice and subsequently crossed with Vglut2$^{flox/flox}$ mice for 2 generations to generate cKO mice in which VGLUT2 is absent from any Cre-expressing neurons (Depuy et al, 2013). A total of 11 DβH$^{Cre/0}$ mice (5 male, 6 female) and 10 cKO mice (5 male, 5 female) aged between 10-22 weeks were used for these experiments.

Virus injection and optical fiber implantation

AAV2- DIO-EF1α-ChR2(H134R)-mCherry or AAV2- DIO-EF1α-ChR2(H134R)-eYFP (abbreviated AAV2-ChR2-mCherry or AAV2-ChR2-eYFP, titer- 10^{12} virus molecules per ml) was purchased from the University of North Carolina vector core, (constructs courtesy of K. Deisseroth (Stanford)). This vector features an enhanced version of the photosensitive cationic channel channelrhodopsin-2 (ChR2 H134R) fused to the fluorescent reporter, mCherry, under the control of the promoter for elongation factor 1α (EF1α). The ChR2-mCherry sequence is flanked by double lox sites (LoxP and lox 2722).

Unilateral microinjections of AAV2-ChR2-mCherry into the left RVLM and placement of a fiber optic were performed under aseptic conditions in mice anesthetized with a mixture of ketamine (100 mg/kg) and dexmedetomidine (0.2 mg/kg; i.p.) as previously described (Abbott et al, 2013). Adequate anesthesia was judged by the absence

of the corneal and hind-paw withdrawal reflex. Additional anesthetic was administered as necessary (20% of the original dose, i.p.). Following injections of AAV2-ChR2-mCherry (~400 nl) into the left RVLM, an implantable 200 µm-diameter fiber optic was placed with its tip 400 µm above the injection site (~4.7 mm from the dorsal surface of the brain) and the fiber optic was secured to the skull with cyanoacrylate adhesive. The implantable fiber optic consisted of a desheathed optical fiber (Thorlabs, 200 µm-core, 0.39 numerical aperture) glued into a zirconia ferrule (1.25 mm O.D., 230 µm bore, Precision Fiber Products). A subset of mice ($D\beta H^{Cre/0}$ N=3, cKO N=2) injected with AAV2-ChR2-mCherry were not implanted with a fiber optic and were later used to determine the response of single presumed C1 neurons to photostimulation under anesthesia. Mice received post-operative boluses of atipemazole (✔ 2-adrenergic antagonist, 2 mg/kg, s.c.), ampicillin (125 mg/kg, i.p.), and ketoprofen (4 mg/kg, s.c.). Ampicillin and ketoprofen were readministered 24 hours post-operatively. Mice were housed in the UVa vivarium for >4 weeks after virus injection. During this time mice gained weight normally and appeared unperturbed by the implanted fiber optic.

Single-unit recording and optical stimulation of putative ChR2-expressing RVLM-CA neurons

Extracellular recordings of RVLM neurons were obtained in a subset of freely-breathing anesthetized mice ($D\beta H^{Cre/0}$ and cKO) using a modification of a method previously developed for rats (Abbott et al, 2012). These mice were anesthetized with urethane (1.6 g/kg dissolved in H_2O delivered i.p. 20% W/V sol^n) and placed in the stereotaxic frame in a prone position. RVLM neurons located in the C1 region i.e.

immediately caudal to the facial motor nucleus and at a depth of 5-5.3 mm from the surface of the brain were recorded using glass pipettes introduced vertically in the brain. Light (5 ms, 8-9 mW) was delivered to the RVLM through a fiber optic inserted into the brain at a 15 degree angle from the vertical in the transverse plane so that its tip was within 500 μm from the region explored by unit recording. Faithful pulse-by-pulse neuronal activation up to 20Hz was taken as evidence that the recorded cells were directly photostimulated and therefore probably RVLM-CA neurons.

Whole cell recording of ChR2-expressing RVLM- CA neurons in slices

Slice preparation was essentially as described in (Depuy et al, 2013). Briefly, six weeks after AAV2 injection, 3 $D\beta H^{Cre/0}$ mice were anesthetized with a mixture of ketamine (120mg/kg) and xylazine (12mg/kg) given i.p., and after becoming completely anesthetized (unresponsive to hind paw pinch) were decapitated. The brainstem was sectioned with a vibrating microtome in the transverse plane in ice-cold, N-Methyl-D-glucamine (NMDG)-substituted artificial cerebral spinal fluid (ACSF) containing (in mM): 92 NMDG, 2.5 KCl, 1.25 NaH_2PO_4, 10 $MgSO_4$, 0.5 $CaCl_2$, 20 HEPES, 30 $NaHCO_3$, 25 glucose, 2 thiourea, 5 Na-ascorbate, 3 Na-pyruvate (~300 mOsm/kg). After 10 minutes at 33ºC, brain slices were transferred to aerated physiological extracellular ACSF containing (in mM): 119 NaCl, 2.5 KCl, 1.25 NaH_2PO_4, 2 $MgSO_4$, 2 $CaCl_2$, 26 $NaHCO_3$, 12.5 glucose, 2 thiourea, 5 Na-ascorbate, 3 Na-pyruvate, and maintained at room temperature (23ºC). All recordings were performed at room temperature in submerged slices continuously perfused with aerated (95% O_2, 5% CO_2) physiological ACSF. Glass pipettes (2-6 MΩ tip resistance) were filled with a solution containing (in

mM): 140 K-gluconate, 10 HEPES, 10 tris-phosphocreatine, 3 ATP-Na, 0.3 GTP-Na, 1 EGTA, 2 $MgCl_2$, and 0.2% biocytin. The junction potential was 14.8 mV and corrected membrane potentials are reported in the text and figures. Recordings were performed using a Multiclamp 700B amplifier and pClamp 10 software (Molecular Devices, Inc., Sunnyvale, CA, USA). Signals were low-pass filtered at 4 kHz and digitized at 10 kHz. Only cells with series resistance that remained below 25MΩ were included in the analysis. Further analysis was done using Spike2 v7.10 (CED, Cambridge, U.K.). Photostimulation of visually identified ChR2-eYFP expressing neurons was done with a 200 μm diameter optical fiber coupled to a 473nm DPSS laser (IkeCool Corporation, Anaheim, CA) as previously described (Depuy et al, 2013). The optical fiber, held at an angle of forty degrees from the horizontal axis, was positioned such that the tip was 150 μm above and 250 μm lateral to the recorded neuron. The optical fiber intensely illuminated an ellipse of approximately 0.342 mm^2 and produced an estimated average irradiance of ~15mW/mm^2. Delivery of optical pulses (5 ms duration) was triggered by a digitizer (Digidata 1440A, Molecular Devices) controlled by episodic protocols run in pClamp 10 (Molecular Devices). The optical fiber was calibrated for 5 mW steady-state output prior to each experiment.

Combination optogenetics and whole-body plethysmography in conscious mice

Photostimulation of the RVLM was performed as described before (Abbott et al, 2013). Prior to implantation, the light output of each implanted optical fiber was measured with a light meter (Thorlabs) and the laser setting was adjusted to deliver 8-9 mW. This setting was later used during experiments.

Breathing patterns were measured in conscious mice using unrestrained whole-body plethysmography (EMKA Technologies) as previously described (Abbott et al, 2013). The chamber was continuously flushed with dry room-temperature air delivered at 0.5 standardized liters/min. Fluctuations in chamber pressure were amplified (x500) and acquired at 1 KHz with Spike 2 software (v7.06, CED). Respiratory frequency (f_R; breaths/min) was calculated based on the onset of inspiration during periods of behavioral quiescence. Mice were briefly anesthetized with isoflurane while the connection between the implanted fiber optic and the laser delivery system was established. Recordings were initiated at least 30 min after the mice had regained consciousness. To evaluate the effects of photostimulation on f_R, 10 s trains of light pulses (5 ms duration) were delivered at various frequencies (5-25 Hz) during behavioral quiescence. The reported changes in f_R reflect the average response of 2-3 trials at each stimulus frequency per mouse (inter-trial variability during 20 Hz trials, $D\beta H^{Cre/0}$= 44.7 ± 11.3 breaths/min; cKO = 3.6 ± 3.6 breaths/min, N=8 each).

Recording of vagus nerve efferent activity in urethane-anesthetized mice

Recordings of the vagus nerve were performed under urethane anesthesia (1.6 g/kg dissolved in H_2O delivered i.p. 20% W/V sol^n). Depth of anesthesia was assessed by an absence of the corneal and hind-paw withdrawal reflex. Additional anesthetic was administered as necessary (10% of the original dose, i.p.). Body temperature was maintained at 37.2 ± 0.5 °C with a servo-controlled temperature pad (TC-1000, CWE Inc.). Following induction of anesthesia, the fiber optic was connected to the laser, and mice were then placed in a stereotaxic frame in the supine position. A tracheostomy was

performed and animals were mechanically ventilated with pure oxygen (MiniVent type 845, Hugo-Sachs Electronik). Fine Teflon-coated silver wires were placed subcutaneously in the chest area to record electrocardiogram and heart rate. To record vagus nerve efferent activity, approximately 15 mm of the vagus nerve was dissected free from the carotid arteries in the neck and the distal end of the isolated nerve segment was crushed, amounting to a vagotomy. Following vagotomy, the central respiratory pattern became desynchronized from the ventilator thereby establishing the loss of afferent vagus nerve activity. At this point, the rate and volume of mechanical ventilation was adjusted to eliminate spontaneous breathing (170-220 rpm at 7-8 µl/g), the adequacy of anesthesia was rechecked and the paralyzing agent vecuronium was administered (0.1 mg/kg, i.p.). After this point adequate anesthesia was determined by the absence of changes in HR in response to a firm hind paw pinch. The vagus nerve ipsilateral to the implanted fiber optic, and anterior to section of the nerve crushed earlier, was placed on a bipolar platinum-iridium wire electrode (part no. 778000, A-M Systems) and embedded in silicone (Kwik-Sil, WPI). Physiological signals filtered and amplified (ECG: 10-1000 Hz, x1000. Vagus: 30-3000 Hz, x10000) (BMA-400, CWE Inc.) and acquired in Spike 2 software (v7.06, CED). Post-hoc high-pass filtering of vagus nerve recordings (high pass-100 Hz, transition-50 Hz) was used in cases exhibiting ECG contamination. Three cases were excluded from analysis due to failed nerve recordings. The vagus nerve response to RVLM photostimulation was analyzed by measuring the area under the curve (AUC) relative to prestimulus AUC of waveform averages of rectified vagus nerve activity triggered from the first light pulse of 10-20 stimulation trials (1 s train of 5 ms pulses at 5, 10 and 20 Hz) delivered at 0.1 Hz. The resulting value was defined as the evoked

vagus nerve activity during photostimulation (in arbitrary units, a.u.). To account for potential differences in the quality of the vagus nerve recording between animals, the evoked vagus nerve activity during photostimulation was normalized with respect to respiratory-related oscillations in vagus nerve activity (rectified and smoothed (τ=0.01)) during administration of CO_2 (6-7%) to the inspired gas. These oscillations reflect the periodic changes in parasympathetic preganglionic neuron activity elicited by the central respiratory pattern generator. Thus;

Normalized evoked vagus nerve activity during photostimulation (a.u.) =

((AUC vagus nerve activity during stimulation) - (AUC vagus nerve activity during prestimulus period)) / (range of respiratory-related oscillations in vagus nerve activity during CO_2)

For presentation purposes, the range of respiratory-related vagus nerve activity was assigned a scale of 0-100 a.u. and traces of nerve recordings and waveform averages were scaled accordingly. Note that zero a.u. in vagus nerve recordings does not reflect absolute zero activity. The paired-pulse stimulation was evaluated in $D\beta H^{Cre/0}$ mice by generating waveform averages of paired 50 ms laser pulses delivered at 0.2 Hz. Prazosin (1 mg/kg i.p.) was administered in $D\beta H^{Cre/0}$ and cKO mice to evaluate the effects of central α1-adrenoreceptor blockade on the observed vagal response to photostimulation.

Histological procedures

Following the completion of the *in vivo* experiments, mice were lethally anesthetized with urethane and transcardially perfused with 50 ml of heparinized saline followed by 100 ml of freshly prepared 2% paraformaldehyde (pf) in 100 mM sodium phosphate buffer, pH 7.4**.** Brains were extracted and post-fixed at 4º C for 24-48 hours in the same fixative. Coronal sections were cut at 30 μm on a vibrating microtome and stored in a cryoprotectant solution (20% glycerol plus 30% ethylene glycol in 50 mM phosphate buffer, pH 7.4) at -20° C.

Immunohistochemical procedures and microscopy was performed as previously described using antibodies of proven selectivity (Abbott et al, 2013). The following antibodies were used; mCherry protein was detected using anti-DsRed (rabbit polyclonal, 1:500, Clontech #632496, Clontech Laboratories) followed by Cy3-tagged anti-rabbit-IgG (1:200, Jackson ImmunnoResearch Laboratories). TH was detected using a sheep polyclonal antibody (1:1000 , Millipore #AB1542, EMD Millipore) followed by Alexafluor488-tagged donkey anti-sheep antibody (1:200, Jackson ImmunoResearch Laboratories). eYFP was detected using a chicken polyclonal antibody (1:2000, Aves labs Inc. Tigard, USA) followed by Alexafluor488-tagged donkey anti-chicken antibody (1:200, Jackson code 703-545-155).

The slices used for whole cell recordings *in vitro* were rinsed and incubated first in blocking solution using a triton concentration of 0.5% to enhance antibody penetration and then in primary antibodies for TH and eYFP as described above. Slices were then rinsed and incubated with secondary antibodies (above described) as well as with

NeutrAvidin-Dylight-649 (Thermo Fisher Scientific, Suwanee, GA) to identify biocytin. Slices were finally rinsed, mounted and coverslips were affixed.

All brain sections were examined under bright field and epifluorescence using a Zeiss AxioImager Z.1 microscope with computer controlled stage using the Neurolucida software (v10, MBF Bioscience). Cell counts were performed in a 1:3 series aligned to the caudal extent of the facial motor nucleus, designated as -6.48 mm from bregma after an atlas (Paxinos & Franklin 2004). Images were obtained with a Zeiss MRC camera as TIFF files (1388 x 1040 pixels) and imported into Canvas software (v10, ACD Systems) for composition of figures. Output levels were adjusted to include all information-containing pixels. Balance and contrast were adjusted to reflect true rendering as much as possible. No other "photo-retouching" was done.

Statistical analyses

Microsoft Excel 2010 and Graphpad Prism 6 was used to collate and analyze data. The distribution of the data was tested for normality (D'Agostino and Pearson omnibus), and significant differences between samples were determined using one-way ANOVA (Kruskal-Wallis for non-Gaussian data) and two-way ANOVAs, and unpaired two-tailed t-tests (Mann-Whitney test for non- Gaussian data) with a threshold of $\alpha=0.05$. Results are presented as mean ± SEM unless noted otherwise.

Results

ChR2-mCherry expression by RVLM-CA neurons in DβH$^{Cre/0}$ and cKO mice and optrode placements

In DβH$^{Cre/0}$ mice (N=8), 146 ± 19 ChR2-mCherry+ neurons were identified in the RVLM (1/3 series, actual numbers of ChR2-mCherry+ neurons approximately three times larger). Most ChR2-mCherry+ neurons were detectably catecholaminergic (i.e. expressed TH) (95.4 ± 0.9%; range: 91.7- 99.4%), accounting for 68.4 ± 2.3% of the TH+ neurons in the ipsilateral VLM in sections containing ChR2-mCherry+ neurons (Figure 1A1,A2,C1). In cKO mice (N=8), 127 ± 16 ChR2-mCherry+ neurons were identified in the RVLM, of which 94.9 ± 1.0% (range: 90.4 – 99.3%) were TH+, accounting for 57.3 ± 5.0 % of the TH+ neurons observed in sections containing ChR2-mCherry+ neurons (Figure 1B1,B2,C2). Comparatively speaking, the RVLM of DβH$^{Cre/0}$ and cKO mice contained a similar number ChR2-mCherry+ neurons ($t_{14}=0.78, P=0.45$), and a similar percentage of these neurons were TH+ ($t_{14}=1.38, P=0.74$). Also, the rostro-caudal distribution of ChR2-mCherry+ neurons in RVLM was indistinguishable in the between DβH$^{Cre/0}$ and cKO mice ($F_{16,214}=0.23, P=0.99$ for the interaction between genotype and bregma level) (Figure 1C1, C2). The absolute number of RVLM TH+ neurons was equivalent between strains ($t_{14}=2.61, P=0.81$), as was the rostro-caudal distribution of TH+ neurons in the RVLM ($F_{16,214}=1.23, P=0.24$). Finally, the proportion of RVLM TH+ neurons expressing ChR2-mCherry was not different ($t_{14}=4.59, P=0.063$). Importantly, the distribution and density of the ChR2-mCherry labeled terminals were similar in DβH$^{Cre/0}$ and cKO mice, indicating that the absence of VGLUT2 did not alter the gross morphology and projections of RVLM-CA neurons (Figure 1A3, B3).

The tips of the optical fibers were typically found 300-500 µm from above the ventral surface of the VLM and had a similar distribution in DβH$^{Cre/0}$ and cKO mice (Figure 1D).

Optical stimulation of RVLM-CA neurons in slices and in vivo

Optical stimulation of RVLM-CA neurons in brain slices

Whole-cell current clamp recordings of ChR2-eYFP+ RVLM neurons were made in slices from adult DβH$^{Cre/0}$ mice to verify that these cells could be activated by light pulses, and to determine the frequency which these neurons could be reliably driven. Recorded neurons (9 neurons, 3 mice) were directly visualized by the presence of eYFP fluorescence. Shortly after patching these cells were either silent or had a slow tonic discharge pattern (0.73±0.32Hz, 0 to 2.3Hz, N=9), each light pulse produced a strong depolarization leading to a single action potential (Figure 2A). Higher frequencies produced a tonic depolarization without clear evidence of action potential generation (not illustrated). For this reason, we used a frequency of stimulation of less than 25Hz in all our subsequent *in vivo* experiments. Spike amplitude was gradually reduced during train stimulation. This phenomenon was evident during 10 Hz stimulation (Figure 2A) and especially marked at 20Hz (Figure 2A, top and bottom traces). Fast sodium channel inactivation caused by tonic depolarization is the likely cause of the reduction of action potential amplitude. This tonic depolarization is due to the slow kinetics of ChR2 currents and has been well described previously in other systems (Boyden et al, 2005;Lin et al, 2009) . All the recorded cells were filled with biocytin and, after histological processing,

every recovered biocytin-positive neuron (N= 6) was found to contain eYFP and tyrosine-hydroxylase immunoreactivity demonstrating that they were ChR2-expressing RVLM-CA neurons. Figure 2B shows an example of 3 such cells recorded in a single slice.

Optical stimulation of putative RVLM-CA neurons in vivo

These experiments were designed to compare the response of putative RVLM-CA neurons to photostimulation in DβH$^{Cre/0}$ and cKO mice. We recorded from tonically active neurons located immediately caudal to the facial motor nucleus, in a region corresponding to the site of virus injection. We found 4 cells in 3 DβH$^{Cre/0}$ mice and 2 cells in 2 cKO mice that were faithfully entrained by light up to 20 Hz (Figure 2C,D). These neurons had a tonic discharge rate, as opposed to the ON-OFF respiratory synchronous discharge that is typical of most non-catecholaminergic neurons in this region of the brain (Schreihofer & Guyenet 1997). In both strains, the amplitude of the extracellular action potential was reduced during photostimulation at frequencies above 5Hz (Figure 2C,D). The decrease in spike amplitude was gradual reaching steady-state after 3-10 pulses (Figure 2D), was fully reversible upon interruption of the stimulus (Figure 2C and D) and was observed in every photoactivated neuron. The same phenomenon has been previously described for ChR2-expressing C1 cells in rats (Abbott et al, 2009). The decrease in extracellular spike amplitude is consistent with the reduced action potential amplitude observed by intracellular recording in slices (Figure 2A). The silent period that followed high frequency stimulation in vivo was presumably caused by hyperpolarization, also clearly present in the intracellular recordings in slices. Together,

the evidence suggests that ChR2-mCherry+ neurons are reliably entrained to stimulus frequencies up to 20 Hz and that the stimulus-response relationship of putative ChR2-mCherry+ RVLM-CA neurons is comparable in DβH$^{Cre/0}$ and cKO mice.

In summary, the anatomical and electrophysiological evidence revealed no differences between DβH$^{Cre/0}$ and cKO mice with regard to the morphology and distribution of RVLM-CA neurons, the level of expression of ChR2-mCherry by these cells, and their response to light pulses.

Respiratory effects produced by optogenetic stimulation of RVLM-CA neurons in DβH$^{Cre/0}$ and cKO mice.

During behavioral quiescence, DβH$^{Cre/0}$ and cKO mice had a similar respiratory frequency, f_R, (DβH$^{Cre/0}$ vs. cKO, 131 ± 10 vs. 148 ± 3 breaths/min, $t_{12}=1.7$, $P=0.12$). Photostimulation increased f_R in DβH$^{Cre/0}$ mice (Fig. 2A), as reported previously (Abbott et al, 2013). The increase in f_R increased with light-pulse frequency up to a stimulus frequency of 15 Hz (+54.1 ± 11.6 breaths/min, N=7). In contrast, photostimulation had no effect on f_R in cKO mice (+3.1 ± 6.7 breaths/min, N=7) ($F_{4,48}=6.62$, $P=0.0003$ for the interaction between stimulation frequency and genotype; Figure 3A,B).

Vagal efferent activity elicited by optogenetic stimulation of RVLM-CA neurons in DβH$^{Cre/0}$ and cKO mice.

RVLM-CA neurons densely innervate the dorsal motor nucleus of the vagus, which contains parasympathetic preganglionic neurons (Fig. 1A3,B3) (Depuy et al, 2013). Optogenetic experiments in slices maintained at room temperature indicate that this connection is monosynaptic and primarily glutamatergic (Depuy et al, 2013).

In urethane-anesthetized DβH$^{Cre/0}$ mice, photostimulation of RVLM-CA neurons at 20 Hz activated vagus nerve efferents (Fig. 3A1), with an onset latency of 24.1 ± 1.3 ms and latency to the peak of 37.5 ± 1.7 ms from the start of the light pulse train. Stimulation at 5 Hz and 10 Hz produced faithful short-latency responses that followed each light pulse (Figure 4B1). Unlike the sympathetic nerve response (Abbott et al, 2012) the vagus nerve response to photostimulating RVLM-CA neurons showed negligible paired-pulse depression when 50 ms pulses were delivered at intervals spanning 1000 ms, with a minimum interval 250 ms ($F_{3,4}=3.36, P=0.14,$ Figure 4C). However, during 20 Hz stimulation, a modest accommodation in vagus nerve response was observed over the duration of the stimulus (1 s).

In contrast to the observations in DβH$^{Cre/0}$ mice, photostimulation evoked no detectable vagal response in 4/7 cKO mice tested (Figure 4A2, B2), and a small discharge during 20 Hz stimulation in 3/7 cKO mice (Figure 4D2). The discharge observed in responsive cKO mice had the same kinetics as the vagal response in DβH$^{Cre/0}$ mice, but the amplitude of the response was much smaller when normalized to the fluctuations of vagal activity present during exposure of the mice to elevated CO_2 (Figure 4D).

Regardless of strain, administration of the α1-adrenoreceptor antagonist, prazosin, at a concentration sufficient to block central α1-adrenroreceptors (Menkes et al, 1981) did not alter the vagal activation caused by phtotostimulation (DβH$^{Cre/0}$ vs. responsive

cKO, +2.2 ± 14.0 vs. -0.4 ± 12.7% change in vagal response after prazosin, $F_{1,9}=0.21$, $P=0.66$ for the effect of prazosin) (Figure 4D). Thus, the evoked vagal response observed in DβH$^{Cre/0}$ and responsive cKO mice are unlikely to be generated by catecholamine release.

In summary, RVLM-CA neuron photostimulation produced a much greater activation of the vagus nerve in DβH$^{Cre/0}$ mice than cKO mice at all stimulation frequencies examined ($F_{2,22}=13.11$, $P=0.0002$ for the interaction between stimulus frequency and genotype) (Figure 4E).

Discussion

The present results show that VGLUT2 deletion from RVLM-CA neurons has no detectable impact on the number and morphology of these neurons but virtually eliminates the short-term effects of activating these neurons *in vivo*. This work highlights the importance of VGLUT2 and, by inference, glutamate release in the physiological effects of RVLM-CA neuron stimulation in the intact mouse.

Evidence for deletion of VGLUT2 from RVLM-CA neurons

In an earlier study we have demonstrated that VGLUT2 immunoreactivity is virtually absent from virally-labeled RVLM-CA neuron terminals in the brain of cKO mice (Depuy et al, 2013). In that study, only 8% of virally-labeled axonal varicosities originating from RVLM-CA neurons contained detectable VGLUT2 immunoreactivity in

cKO mice, compared to 97% in DβH$^{Cre/0}$ mice (Depuy et al, 2013). At the resolution of light microscopy the appearance of VGLUT2 immunoreactivity in the terminals of RVLM-CA in cKO mice may reflect superposition of virally-labeled terminals and glutamatergic boutons of an unknown source. Other investigators have shown that VGLUT2 expression and function is effectively eliminated in Cre-expressing neurons when various Cre-driver mouse lines are crossed with the VGLUT2$^{flox/flox}$ mouse line (Tong et al, 2007;Liu et al, 2010;Fortin et al, 2012). On this basis, we conclude that VGLUT2 was effectively deleted from most but probably not all Cre-expressing noradrenergic and adrenergic neurons in our cKO mice.

cKO mice had no obvious abnormalities in the number, morphology and projection pattern of virally-labeled RVLM-CA neurons, suggesting that VGLUT2-dependent vesicular glutamate release is not essential for the development of these neurons. This result is consistent with prior evidence that RVLM-CA neurons have normal embryological development in VGLUT2-null mutant mice (Wallen-Mackenzie et al, 2006), and contrasts with evidence that VGLUT2 expression is important for the survival and the development of mesencephalic dopamine neurons after birth (Fortin et al, 2012).

Photostimulation of RVLM-CA in slices and in vivo

The present whole cell recordings demonstrated that ChR2-expressing RVLM-CA neurons respond to light pulses in conventional manner. As in other neurons, the relatively slow kinetics of the current elicited by ChR2(H134R) enables reliable neuronal

activation only up to 20Hz (Wang et al, 2007;Lin et al, 2009). At frequencies above 10Hz, fast sodium channel inactivation, presumably caused by the tonic depolarization, produced a gradual reduction in action potential amplitude which translated into smaller amplitude extracellular spikes in vivo.

We did not obtain proof that the RVLM neurons that were light-activated on a pulse by pulse basis in vivo were ChR2-expressing CA neurons. Conceivably, these cells could have been non-CA neurons that were driven synaptically with extremely high fidelity by the ChR2-expressing CA neurons. This interpretation, unlikely in the case of the DβH$^{Cre/0}$, is implausible in the case of cKO mice in which the RVLM-CA neurons have lost their fast transmitter.

Glutamate mediates the stimulatory effects of the C1 cells on respiration and the parasympathetic outflow in vivo

Up to 99% of the ChR2-mCherry expressing neurons were demonstrably catecholaminergic in DβH$^{Cre/0}$ and cKO mice. The RVLM contains catecholamine neurons primarily of the C1 phenotype (i.e. PNMT-expressing neurons), along with a small proportion of A1 neurons (i.e. noradrenergic neurons devoid of PNMT). Thus given the location of ChR2-mCherry expressing neurons in this study, most of them were likely C1 rather than A1 neurons. A1 neurons rarely express transcripts for VGLUTs in rats (Stornetta et al, 2002a) and are thought to use noradrenaline as a primary neurotransmitter. The fact that α1-adrenergic receptor blockade did not reduce the vagal response in DβH$^{Cre/0}$ mice indicates that the release of noradrenaline from A1 (or C1)

neurons or downstream targets was not essential to the observed responses. Accordingly, the robust and consistent respiratory and vagal stimulation produced by activating RVLM-CA neurons in the DβH$^{Cre/0}$ mice was almost certainly caused by the activation of RVLM-CA neurons that normally express VGLUT2. Also, given that cKO mice were virtually unresponsive to identical stimulation of a similar population of RVLM-CA neurons, the combined evidence indicates that VGLUT2 and thereby glutamate release is necessary for physiological responses to C1 neuron stimulation.

The circuit responsible for the respiratory stimulation elicited by photostimulation of RVLM-CA neurons is unknown. A direct connection of the C1 cells to the pre-Bötzinger complex is anatomically plausible but many other routes are conceivable given the complexity of the projection pattern of the RVLM-CA neurons (Card et al, 2006;Abbott et al, 2013). RVLM-CA neurons activate the preganglionic neurons of the dorsal vagal complex monosynaptically in mouse brain slices (Depuy et al, 2013). This direct pathway likely contributed to the vagal efferent responses evoked by RVLM photostimulation in the present *in vivo* experiments but more indirect circuits may also have been recruited.

A minority of cKO mice retained a weak vagal response that resembled the response observed in DβH$^{Cre/0}$ mice. The fast kinetics of the residual vagal response in cKO mice is inconsistent with the actions of a slow acting metabotropic transmitter be it a catecholamine or peptide. As already mentioned, noradrenaline release from stimulated C1 or A1 neurons is unlikely to explain the vagal response in cKO mice, as it was insensitive to α1-adrenergic receptor blockade. Other possible explanations for the small residual effect seen in a fraction of the cKO mice are the release of an unidentified

transmitter from RVLM-CA, and the up-regulation of either VGLUT1 or 3. However, a greater proportion of cKO mice should have had an appreciable response to photostimulation to justify these possibilities.

Failed or incomplete deletion of the VGLUT2 gene in a minority of RVLM-CA neurons sufficiently explains the small vagal response found in a minority of cKO mice. By experimental design, both the expression of ChR2-mCherry and the deletion of VGLUT2 were contingent on the presence of genomic Cre driven from the DβH-promoter. For this reason, we predicted that RVLM-CA neurons expressing Cre-dependent ChR2-mCherry would be neurons that express sufficiently high levels of Cre to also eliminate VGLUT2 in the cKO mouse, theoretically bypassing issues arising from variegated expression of Cre in the $D\beta H^{Cre/0}$ mouse line. However, the efficacy of Cre-recombination of LoxP sites within the VGLUT2 gene may be influenced by the chromosomal location of the LoxP sites and the distance between these sites (Schmidt-Supprian & Rajewsky 2007;Liu et al, 2013). Considering this, differences in the recombination efficiency of the virally-delivered floxed transgene vs. the floxed VGLUT2 gene may result in the expression of ChR2-mCherry in a subset of RVLM-CA neurons that retain functional VGLUT2 expression in the cKO mouse. This possibility could account for the reduced amplitude of the vagal response in cKO mice, as well as for the similarities in the kinetics of the vagal response in both strains. It would also account for the small fraction of virally-labeled RVLM-CA terminals that appear VGLUT2 immunoreactive in cKO mice (Depuy et al, 2013).

Altogether the evidence supports the conclusion that VGLUT2 and glutamate release are required for the effects of RVLM-CA neuron stimulation *in vivo*. This

interpretation is consistent with the presence of VGLUT2 mRNA and protein in C1 neurons in rodents (Stornetta et al, 2002b;Herzog et al, 2004;Stornetta et al, 2005;Abbott et al, 2013) and the fact that optogenetic activation of RVLM-CA terminals in slices produces fast EPSCs that are blocked by ionotropic glutamate antagonists (Depuy et al, 2013).

Do C1 neurons release catecholamines?

In mesencephalic dopaminergic neurons, VGLUT2 may serve to facilitate the vesicular packaging of catecholamine (Hnasko et al, 2010). The same mechanism could potentially exist in C1 neurons, which co-express vesicular monoamine transporter 2 and VGLUT2 (Sevigny et al, 2008;Depuy et al, 2013). If vesicular packaging of catecholamine depends on VGLUT2 in C1 neurons, the ability of these neurons to release catecholamine could be severely curtailed in cKO mice, which could explain the absence of detectable catecholamine release during RVLM-CA neuron stimulation in cKO mice. However, this interpretation requires that the responses elicited in $D\beta H^{Cre/0}$ mice should have a prominent catecholaminergic component, which does not appear to be true ((Depuy et al, 2013;Abbott et al, 2013) and present results). We did not explore the effect of β-adrenergic receptor blockade on the vagal response in the present study because the excitatory effect of catecholamines on dorsal vagal motoneurons are described as entirely mediated by α1-adrenergic receptors (Martinez-Pena y Valenzuela et al, 2004). Furthermore, we have previously shown that β-adrenoreceptor blockade does not attenuate the respiratory response to RVLM-CA neuron stimulation (Abbott et al, 2013). Together, the lack of effect of α1-adrenergic receptors indicates that catecholamine

release makes at most a very minor contribution to the acute respiratory and parasympathetic effects produced by RVLM-CA neuron stimulation *in vivo*. Clearly, this observation does not eliminate the possibility that catecholamines are released from C1 neurons in other conditions.

An uninvestigated possibility is that catecholamines released by C1 neurons have effects that are delayed. Indeed catecholamines often produce long-term potentiation or even metaplasticity that develop over a much longer time period than the acute responses that we have examined (Neverova et al, 2007;Inoue et al, 2013). A similar argument can be made for any one of the neuropeptides known to be expressed by C1 neurons (for review see (Guyenet et al, 2013)). Another possibility is that the catecholamines released by C1 neurons activate the surrounding glia and have only minor effects on synaptic transmission (O'Donnell et al, 2012).

In conclusion, we have shown that genetic deletion of VGLUT2 from RVLM-CA neurons abolishes the acute respiratory and parasympathetic activation produced by selectively stimulating these neurons in mice. The collective evidence indicates that C1 neurons regulate the autonomic nervous system through the synaptic release of glutamate, which is consistent with their role in mediating rapid counter-regulatory responses to physical stresses.

Acknowledgements

The authors would like to acknowledge R.L. Stornetta, S.D. Depuy and M. B Coates for assistance with microscopy and mouse breeding. This work was supported by the following grants from the National Institutes of Health (HL28785 and HL74011 to PGG), and a postdoctoral fellowship to SBGA from the American Heart Association (11post7170001).

Abbreviations

Catecholaminergic neurons of the rostral ventrolateral medulla, RVLM-CA neurons; $D\beta H^{Cre/0}$;$VGLUT2^{flox/flox}$ mice, cKO mice; Tyrosine hydroxylase, TH; Dopamine-β-hydroxylase, DβH; Phenylethanolamine N-methyl transferase, PNMT; Vesicular glutamate transporters, VGLUT; Channel channelrhodopsin-2, ChR2; Elongation factor 1α, EF1α; Respiratory frequency, $f_{R;}$ Area under the curve, AUC.

Works Cited

1. Abbott,S.B., Depuy,S.D., Nguyen,T., Coates,M.B., Stornetta,R.L. & Guyenet,P.G. (2013) Selective optogenetic activation of rostral ventrolateral medullary catecholaminergic neurons produces cardiorespiratory stimulation in conscious mice. *J. Neurosci.*, **33**, 3164-3177.

2. Abbott,S.B., Kanbar,R., Bochorishvili,G., Coates,M.B., Stornetta,R.L. & Guyenet,P.G. (2012) C1 neurons excite locus coeruleus and A5 noradrenergic neurons along with sympathetic outflow in rats. *J. Physiol.*, **590**, 2897-2915.

3. Abbott,S.B., Stornetta,R.L., Socolovsky,C.S., West,G.H. & Guyenet,P.G. (2009) Photostimulation of channelrhodopsin-2 expressing ventrolateral medullary neurons increases sympathetic nerve activity and blood pressure in rats. *J. Physiol*, **587**, 5613-5631.

4. Agassandian,K., Shan,Z., Raizada,M., Sved,A.F. & Card,J.P. (2012) C1 catecholamine neurons form local circuit synaptic connections within the rostroventrolateral medulla of rat. *Neurosci.*, **227**, 247-259.

5. Bellocchio,E.E., Reimer,R.J., Fremeau,R.T., Jr. & Edwards,R.H. (2000) Uptake of glutamate into synaptic vesicles by an inorganic phosphate transporter. *Science*, **289**, 957-960.

6. Boyden,E.S., Zhang,F., Bamberg,E., Nagel,G. & Deisseroth,K. (2005) Millisecond-timescale, genetically targeted optical control of neural activity. *Nat Neurosci*, **8**, 1263-1268.

7. Card,J.P., Sved,J.C., Craig,B., Raizada,M., Vazquez,J. & Sved,A.F. (2006) Efferent projections of rat rostroventrolateral medulla C1 catecholamine neurons: Implications for the central control of cardiovascular regulation. *J. Comp. Neurol.*, **499**, 840-859.

8. Depuy,S.D., Stornetta,R.L., Bochorishvili,G., Deisseroth,K., Witten,I., Coates,M.B. & Guyenet,P.G. (2013) Glutamatergic neurotransmission between the C1 neurons and the parasympathetic preganglionic neurons of the dorsal motor nucleus of the vagus. *J. Neurosci.*, **33**, 1486-1497.

9. Fortin,G.M., Bourque,M.J., Mendez,J.A., Leo,D., Nordenankar,K., Birgner,C., Arvidsson,E., Rymar,V.V., Berube-Carriere,N., Claveau,A.M., Descarries,L., Sadikot,A.F., Wallen-Mackenzie,A. & Trudeau,L.E. (2012) Glutamate corelease promotes growth and survival of midbrain dopamine neurons. *J. Neurosci.*, **32**, 17477-17491.

10. Fremeau,R.T., Voglmaier,S., Seal,R.P. & Edwards,R.H. (2004) VGLUTs define subsets of excitatory neurons and suggest novel roles for glutamate. *Trends Neurosci*, **27**, 98-103.

11. Gras,C., Herzog,E., Bellenchi,G.C., Bernard,V., Ravassard,P., Pohl,M., Gasnier,B., Giros,B. & El Mestikawy,S. (2002) A third vesicular glutamate

transporter expressed by cholinergic and serotoninergic neurons. *J. Neurosci.*, **22**, 5442-5451.

12. Guyenet,P.G., Stornetta,R.L., Bochorishvili,G., Depuy,S.D., Burke,P.G. & Abbott,S.B. (2013) Invited Review EB 2012: C1 neurons: the body's EMTs. *Am. J. Physiol Regul. Integr. Comp Physiol*, doi: 10.1152/ajpregu.00054.2013.

13. Herzog,E., Gilchrist,J., Gras,C., Muzerelle,A., Ravassard,P., Giros,B., Gaspar,P. & El Mestikawy,S. (2004) Localization of VGLUT3, the vesicular glutamate transporter type 3, in the rat brain. *Neurosci.*, **123**, 983-1002.

14. Hnasko,T.S., Chuhma,N., Zhang,H., Goh,G.Y., Sulzer,D., Palmiter,R.D., Rayport,S. & Edwards,R.H. (2010) Vesicular glutamate transport promotes dopamine storage and glutamate corelease in vivo. *Neuron*, **65**, 643-656.

15. Hokfelt,T., Fuxe,K., Goldstein,M. & Johansson,O. (1974) Immunohistochemical evidence for the existence of adrenaline neurons in the rat brain. *Brain Res*, **66**, 235-251.

16. Inoue,W., Baimoukhametova,D.V., Fuzesi,T., Cusulin,J.I., Koblinger,K., Whelan,P.J., Pittman,Q.J. & Bains,J.S. (2013) Noradrenaline is a stress-associated metaplastic signal at GABA synapses. *Nat. Neurosci.*, **16**, 605-612.

17. Lin,J.Y., Lin,M.Z., Steinbach,P. & Tsien,R.Y. (2009) Characterization of engineered channelrhodopsin variants with improved properties and kinetics. *Biophys. J.*, **96**, 1803-1814.

18. Liu,J., Willet,S.G., Bankaitis,E.D., Xu,Y., Wright,C.V. & Gu,G. (2013) Non-parallel recombination limits cre-loxP-based reporters as precise indicators of conditional genetic manipulation. *Genesis.*, **51**, 436-442.

19. Liu,Y., Abdel,S.O., Zhang,L., Duan,B., Tong,Q., Lopes,C., Ji,R.R., Lowell,B.B. & Ma,Q. (2010) VGLUT2-dependent glutamate release from nociceptors is required to sense pain and suppress itch. *Neuron*, **68**, 543-556.

20. Martinez-Pena y Valenzuela,I., Rogers,R.C., Hermann,G.E. & Travagli,R.A. (2004) Norepinephrine effects on identified neurons of the rat dorsal motor nucleus of the vagus. *Am. J. Physiol Gastrointest. Liver Physiol*, **286**, G333-G339.

21. Menkes,D.B., Baraban,J.M. & Aghajanian,G.K. (1981) Prazosin selectively antagonizes neuronal responses mediated by alpha-1-adrenoceptors in brain. *Naunyn-Schmied. Arch. Pharmacol.*, **317**, 273-275.

22. Milner,T.A., Abate,C., Reis,D.J. & Pickel,V.M. (1989) Ultrastructural localization of phenylethanolamine N- methyltransferase-like immunoreactivity in the rat locus coeruleus. *Brain Res.*, **478**, 1-15.

23. Milner,T.A., Morrison,S.F., Abate,C. & Reis,D.J. (1988) Phenylethanolamine N-methyltransferase-containing terminals synapse directly on sympathetic preganglionic neurons in the rat. *Brain Res*, **448**, 205-222.

24. Milner,T.A., Pickel,V.M., Park,D.H., Joh,T.H. & Reis,D.J. (1987) Phenylethanolamine N-methyltransferase-containing neurons in the rostral ventrolateral medulla of the rat. I. Normal ultrastructure. *Brain Res*, **411**, 28-45.

25. Morrison,S.F. (2003) Glutamate transmission in the rostral ventrolateral medullary sympathetic premotor pathway. *Cell Mol. Neurobiol*, **23**, 761-772.

26. Morrison,S.F., Callaway,J., Milner,T.A. & Reis,D.J. (1991) Rostral ventrolateral medulla--a source of the glutamatergic innervation of the sympathetic intermediolateral nucleus. *Brain Res*, **562(1)**, 126-135.

27. Neverova,N.V., Saywell,S.A., Nashold,L.J., Mitchell,G.S. & Feldman,J.L. (2007) Episodic stimulation of alpha1-adrenoreceptors induces protein kinase C-dependent persistent changes in motoneuronal excitability. *J. Neurosci.*, **27**, 4435-4442.

28. O'Donnell,J., Zeppenfeld,D., McConnell,E., Pena,S. & Nedergaard,M. (2012) Norepinephrine: a neuromodulator that boosts the function of multiple cell types to optimize CNS performance. *Neurochem. Res.*, **37**, 2496-2512.

29. Paxinos,G. & Franklin,K.B.J. (2004) *The Mouse Brain in Stereotaxic Coordinates* Elsevier, Amsterdam.

30. Phillips,J.K., Goodchild,A.K., Dubey,R., Sesiashvili,E., Takeda,M., Chalmers,J., Pilowsky,P.M. & Lipski,J. (2001) Differential expression of catecholamine biosynthetic enzymes in the rat ventrolateral medulla. *J. Comp. Neurol.*, **432**, 20-34.

31. Rosin,D.L., Chang,D.A. & Guyenet,P.G. (2006) Afferent and efferent connections of the rat retrotrapezoid nucleus. *J. Comp. Neurol.*, **499**, 64-89.

32. Ross,C.A., Ruggiero,D.A., Joh,T.H., Park,D.H. & Reis,D.J. (1983) Adrenaline synthesizing neurons in the rostral ventrolateral medulla: a possible role in tonic vasomotor control. *Brain Res.*, **273**, 356-361.

33. Schmidt-Supprian,M. & Rajewsky,K. (2007) Vagaries of conditional gene targeting. *Nat. Immunol.*, **8**, 665-668.

34. Schreihofer,A.M. & Guyenet,P.G. (1997) Identification of C1 presympathetic neurons in rat rostral ventrolateral medulla by juxtacellular labeling in vivo. *J. Comp. Neurol.*, **387**, 524-536.

35. Sevigny,C.P., Bassi,J., Teschemacher,A.G., Kim,K.S., Williams,D.A., Anderson,C.R. & Allen,A.M. (2008) C1 neurons in the rat rostral ventrolateral medulla differentially express vesicular monoamine transporter 2 in soma and axonal compartments. *Eur. J. Neurosci.*, **28**, 1536-1544.

36. Stornetta,R.L., Rosin,D.L., Simmons,J.R., McQuiston,T.J., Vujovic,N., Weston,M.C. & Guyenet,P.G. (2005) Coexpression of vesicular glutamate transporter-3 and gamma-aminobutyric acidergic markers in rat rostral medullary raphe and intermediolateral cell column. *J Comp Neurol.*, **492**, 477-494.

37. Stornetta,R.L., Sevigny,C.P. & Guyenet,P.G. (2002a) Vesicular glutamate transporter DNPI/VGLUT2 mRNA is present in C1 and several other groups of brainstem catecholaminergic neurons. *J. Comp. Neurol.*, **444**, 191-206.

38. Stornetta,R.L., Sevigny,C.P., Schreihofer,A.M., Rosin,D.L. & Guyenet,P.G. (2002b) Vesicular glutamate transporter DNPI/GLUT2 is expressed by both C1

adrenergic and nonaminergic presympathetic vasomotor neurons of the rat medulla. *J. Comp. Neurol.*, **444**, 207-220.

39. Takamori,S., Rhee,J.S., Rosenmund,C. & Jahn,R. (2000) Identification of a vesicular glutamate transporter that defines a glutamatergic phenotype in neurons. *Nature*, **407**, 189-194.

40. Tong,Q., Ye,C., McCrimmon,R.J., Dhillon,H., Choi,B., Kramer,M.D., Yu,J., Yang,Z., Christiansen,L.M., Lee,C.E., Choi,C.S., Zigman,J.M., Shulman,G.I., Sherwin,R.S., Elmquist,J.K. & Lowell,B.B. (2007) Synaptic glutamate release by ventromedial hypothalamic neurons is part of the neurocircuitry that prevents hypoglycemia. *Cell Metab*, **5**, 383-393.

41. Wallen-Mackenzie,A., Gezelius,H., Thoby-Brisson,M., Nygard,A., Enjin,A., Fujiyama,F., Fortin,G. & Kullander,K. (2006) Vesicular glutamate transporter 2 is required for central respiratory rhythm generation but not for locomotor central pattern generation. *J. Neurosci.*, **26**, 12294-12307.

42. Wang,H., Peca,J., Matsuzaki,M., Matsuzaki,K., Noguchi,J., Qiu,L., Wang,D., Zhang,F., Boyden,E., Deisseroth,K., Kasai,H., Hall,W.C., Feng,G. & Augustine,G.J. (2007) High-speed mapping of synaptic connectivity using photostimulation in Channelrhodopsin-2 transgenic mice. *Proc. Natl. Acad. Sci. U. S. A*, **104**, 8143-8148.

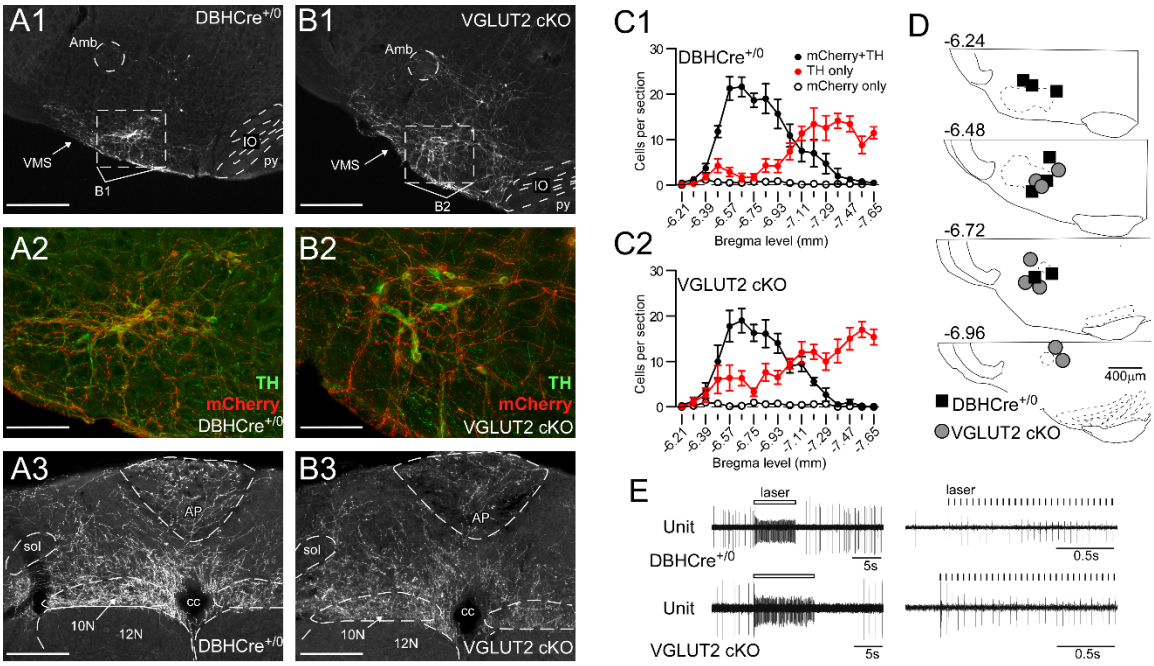
A1
DBHCre+/0
Amb
VMS
IO
py
B1
B1
VGLUT2 cKO
Amb
VMS
IO
py
B2
A2
TH
mCherry
DBHCre+/0
B2
TH
mCherry
VGLUT2 cKO
A3
AP
sol
cc
10N
12N
DBHCre+/0
B3
AP
sol
cc
10N
12N
VGLUT2 cKO
C1
DBHCre+/0
mCherry+TH
TH only
mCherry only
Cells per section
Bregma level (mm)
C2
VGLUT2 cKO
Cells per section
Bregma level (mm)
D
-6.24
-6.48
-6.72
-6.96
400μm
DBHCre+/0
VGLUT2 cKO
E
laser
Unit
DBHCre+/0
5s
0.5s
Unit
VGLUT2 cKO
5s
0.5s

Figure 1. Distribution of ChR2-mCherry neurons in the rostral ventrolateral medulla (RVLM), placement of fiber optic in DβH$^{Cre/0}$ and cKO mice

A1) Low magnification image of ChR2-mCherry expression in a coronal section of the RVLM from a DβH$^{Cre/0}$ mouse (approx.-6.64 mm from bregma). Scale bar: 400 µm. A2) Higher magnification of the region outlined in A1 showing immunofluorescence for ChR2-mCherry (in red) and tyrosine hydroxylase (TH in green). Colocalization of ChR2-mCherry and TH appears orange. Scale bar: 100 µm. A3) ChR2-mcherry immunoreactive axons within the dorsal medulla of a DβH$^{Cre/0}$ mouse (approx.-7.48 mm from bregma). Scale bar: 200 µm. B1-3) Descriptions and scale bars same as A1-3 except that sections are from a cKO mouse. C1-2) Rostro-caudal distribution of neurons expressing ChR2-mCherry, TH or both in the ipsilateral RVLM of DβH$^{Cre/0}$ (C1, N=8) and cKO mice (C2, N=8). D) Location of the tip of implanted fiber optics in DβH$^{Cre/0}$ and cKO mice. Abbreviations: 10N- dorsal motor nucleus of the vagus, 12N- Hypoglossal motor nucleus, AP- area postrema, Amb- compact formation of the nucleus ambiguous, cc- central canal, IO- inferior olive, py- pyramidal tract, VMS- ventral medullary surface.

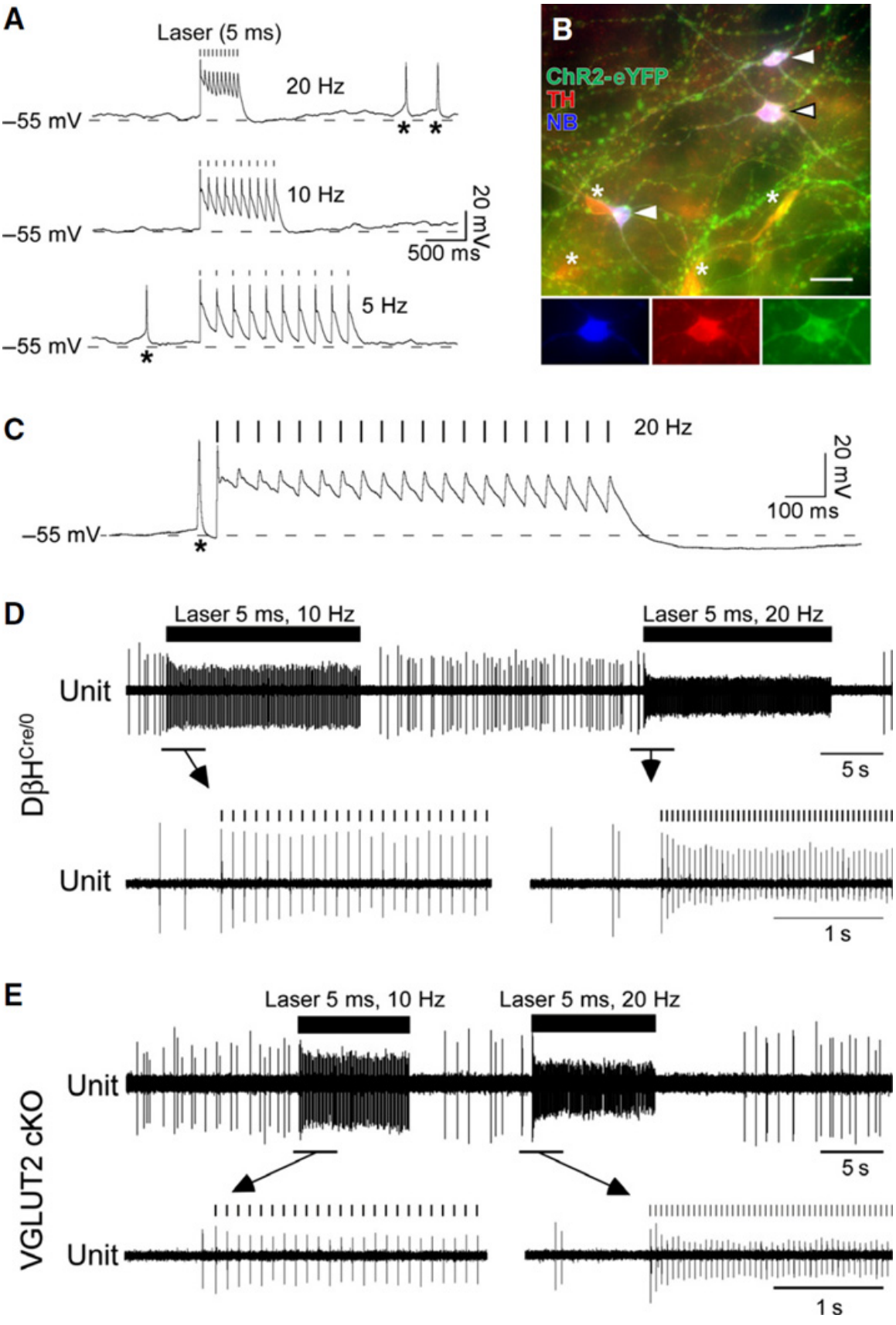
A
Laser (5 ms)
20 Hz
–55 mV
10 Hz
–55 mV
20 mV
500 ms
5 Hz
–55 mV
B
ChR2-eYFP
TH
NB
C
20 Hz
–55 mV
20 mV
100 ms
D
Laser 5 ms, 10 Hz
Laser 5 ms, 20 Hz
Unit
DβH Cre/0
5 s
Unit
1 s
E
Laser 5 ms, 10 Hz
Laser 5 ms, 20 Hz
Unit
VGLUT2 cKO
5 s
Unit
1 s

Figure 2. Light activation of ChR2-mCherry-expressing neurons in DβH$^{Cre/0}$ and cKO mice.

A) Current-clamp recording of a ChR2-eYFP+ RVLM neuron in a slice (DβH$^{Cre/0\ mouse}$) Top three traces: 20, 10 and 5 Hz stimulation (10 x 5 ms pulses). Each light pulse is followed by a short-latency depolarization and an action potential. Asterisks indicates spontaneous action potentials. The lower trace shows the cell response to a 1 s stimulus train and illustrates the reduction in action potential size after the first light-induced spike and the hyperpolarization that follows the stimulus train. B) example of biocytin-filled RVLM-CA neurons that were activated photo-responsive (arrowheads). All three neurons contained ChR2-EYFP and TH immunoreactivity. The inserts correspond to the middle cell (black rimmed arrowhead) and shows immunofluorescence for each marker separately C) Extracellular recording of a single putative ChR2-mCherry+ RVLM-CA neuron during photostimulation (5 ms pulse duration at 10 and 20 Hz during open bar) in an anesthetized DβH$^{Cre/0}$ mouse. Expanded traces (below) show the pulse-by-pulse activation typical of ChR2-expressing neurons, the gradual reduction in spike amplitude tentatively attributed to fast sodium channel inactivation and the silent period following the stimulus train. D) Identical experiment in a cKO mouse.

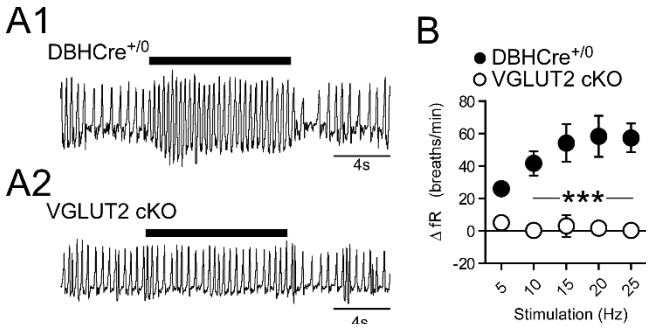
A1
DBHCre+/0
4s
A2
VGLUT2 cKO
4s
B
DBHCre+/0
VGLUT2 cKO
Δ fR (breaths/min)
80
60
40
20
0
-20
***
5
10
15
20
25
Stimulation (Hz)

Figure 3. Effect of stimulating RVLM-CA neurons on respiratory frequency in DβH$^{Cre/0}$ and cKO mice

A) Original plethysmography traces (inspiration upward) of a DβH$^{Cre/0}$ (upper trace) and a cKO mouse (lower trace) during photostimulation (5ms pulse duration at 20 Hz, 10 s train). B) Relationship between photostimulus frequency and increase in respiratory frequency (f_R) in DβH$^{Cre/0}$ (N=7) and cKO (N=7) mice. *** P<0.001 for DβH$^{Cre/0}$ vs. cKO (Bonferroni post-hoc test following repeated measures ANOVA).

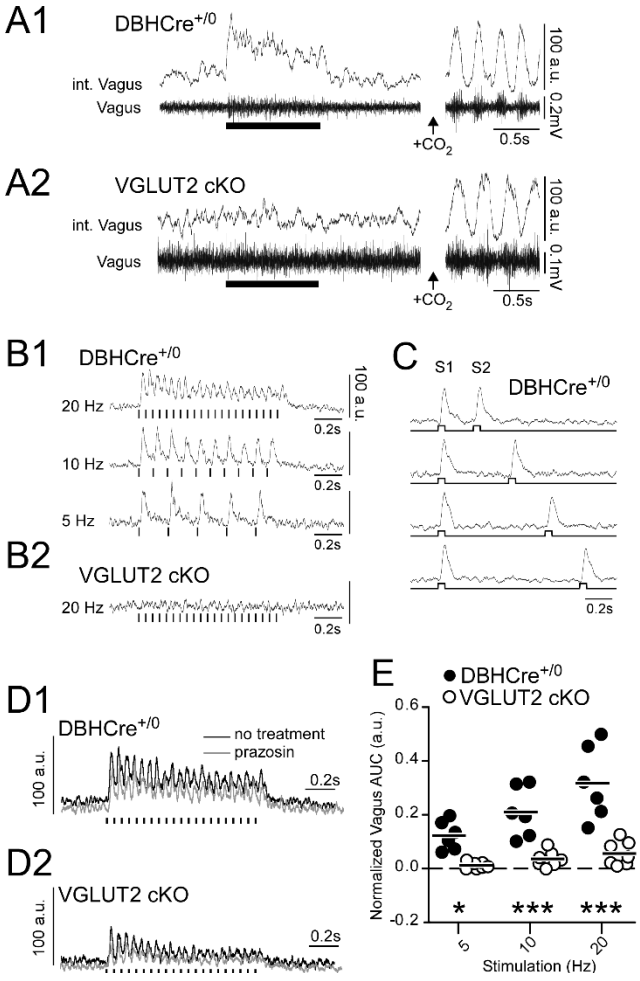
A1
DBHCre+/0
int. Vagus
Vagus
+CO2
0.5s
100 a.u. 0.2mV
A2
VGLUT2 cKO
int. Vagus
Vagus
+CO2
0.5s
100 a.u. 0.1mV
B1
DBHCre+/0
20 Hz
10 Hz
5 Hz
0.2s
100 a.u.
B2
VGLUT2 cKO
20 Hz
0.2s
C
S1
S2
DBHCre+/0
0.2s
D1
DBHCre+/0
no treatment
prazosin
100 a.u.
0.2s
D2
VGLUT2 cKO
100 a.u.
0.2s
E
DBHCre+/0
VGLUT2 cKO
Normalized Vagus AUC (a.u.)
0.6
0.4
0.2
0.0
-0.2
*
***
***
5
10
20
Stimulation (Hz)

Figure 4. Effect of stimulating RVLM-CA neurons on efferent vagus nerve activity in DβH$^{Cre/0}$ and cKO mice

A1-2) Integrated (upper trace) and raw (lower trace) recording of multiunit vagus nerve activity in a urethane-anesthetized DβH$^{Cre/0}$ (A1) and cKO (B2) mouse showing activation by photostimulation (5 ms pulse duration at 20 Hz, 1 s train; left panel). Respiratory-related oscillations in vagus nerve activity caused hypercapnia in the same mouse (7% CO_2; right panel). The amplitude of oscillations in vagus activity during elevated inspired CO_2 (i.e. peak to trough) was assigned a value of 100 arbitrary units (a.u) to normalize recordings between experiments. Integrated vagus nerve activity is rectified and smoothed with 0.03 s time constant. B1-2) Normalized waveform averages of the vagal response to photostimulation (5 ms pulse duration, 15-20 trials per trace, averaging triggered from the onset of 1 s stimulus train) in a DβH$^{Cre/0}$ mouse (B1) and a cKO (B2) mouse. C) Waveform average of the vagal response to paired-pulse stimulation (50 ms pulses) in a DβH$^{Cre/0}$ mouse, note that the magnitude of the second burst was similar regardless of the delay of the second pulse of light down to 250 ms. D) Example of the of the vagal response to photostimulation (5 ms pulse duration at 20 Hz) in a DβH$^{Cre/0}$ (D1) and cKO (D2) mouse before and after α1-adrenergic receptor blockade (prazosin 1 mg/kg). Waveforms generated by averaging 10-15 trials per trace. Note the cKO mouse used in the example had the largest response of all cKO mice tested. E) Group data of the normalized vagus nerve activity during photostimulation (see methods) in DβH$^{Cre/0}$ (N=6) and cKO (N=7) mice. * $P<0.05$, *** $P<0.001$ for DβH$^{Cre/0}$ vs. cKO by Bonferroni post-test.

3.2 **Declaration of published work: I have previously published this work in the *European Journal of Neuronscience, Eur J Neurosci.* 2015 Sep;42(6):2271-82. doi: 10.1111/ejn.12996. Epub 2015 Jul 23**

The retrotrapezoid nucleus stimulates breathing by releasing glutamate in adult conscious mice

Benjamin B. **Holloway**, Kenneth E. **Viar**, Ruth L. **Stornetta** and Patrice G. **Guyenet**

Department of Pharmacology, University of Virginia, Charlottesville, VA 22908

Keywords: breathing, central respiratory chemoreceptors, glutamate, optogenetics.

Abstract

The retrotrapezoid nucleus (RTN) is a bilateral cluster of neurons located at the ventral surface of the brainstem below the facial nucleus. RTN is activated by hypercapnia and stabilizes blood PCO_2 by adjusting lung ventilation in a feedback manner. RTN neurons contain *Vglut2* transcripts *(*vesicular glutamate transporter-2, *Slc17a6)*, and their synaptic boutons contain Vglut2 immunoreactivity. Here, we use optogenetics to test whether RTN increases ventilation in conscious adult mice by releasing glutamate.

Neurons located below the facial motor nucleus were transduced unilaterally to express channelrhodopsin-2-(ChR2-)eYFP using lentiviral vectors that employ the Phox2b-activated artificial promoter, PRSx8. The targeted population consisted of two types of Phox2b-expressing neurons: non-catecholaminergic neurons (putative RTN chemoreceptors) and catecholaminergic (C1) neurons. Opto-activation of a mix of ChR2-expressing RTN and C1 neurons produced a powerful stimulus frequency-dependent (5-15 Hz) stimulation of breathing in control conscious mice. Respiratory stimulation was comparable in mice in which dopamine-*β*-hydroxylase-positive *(*$D\beta H^{+}$) neurons no longer expressed Vglut2 ($D\beta H^{Cre/0};;Vglut2^{fl/fl}$). In a third group of mice, we injected a mixture of PRSx8-Cre lentiviral vector and a Cre-dependent ChR2-AAV2 unilaterally into RTN of $D\beta H^{+/+};;Vglut2^{fl/fl}$ mice; this procedure deleted *Vglut2* from ChR2-expressing neurons regardless of whether or not they were catecholaminergic. The ventilatory response elicited by phostimulation of $ChR2^{+}$ neurons was virtually absent in these mice. Resting ventilatory parameters were identical in the three groups of mice and their brains contained similar numbers of $ChR2^{+}$ catecholaminergic and non-catecholaminergic

neurons. From these results we conclude that RTN neurons increase breathing in conscious adult mice by releasing glutamate.

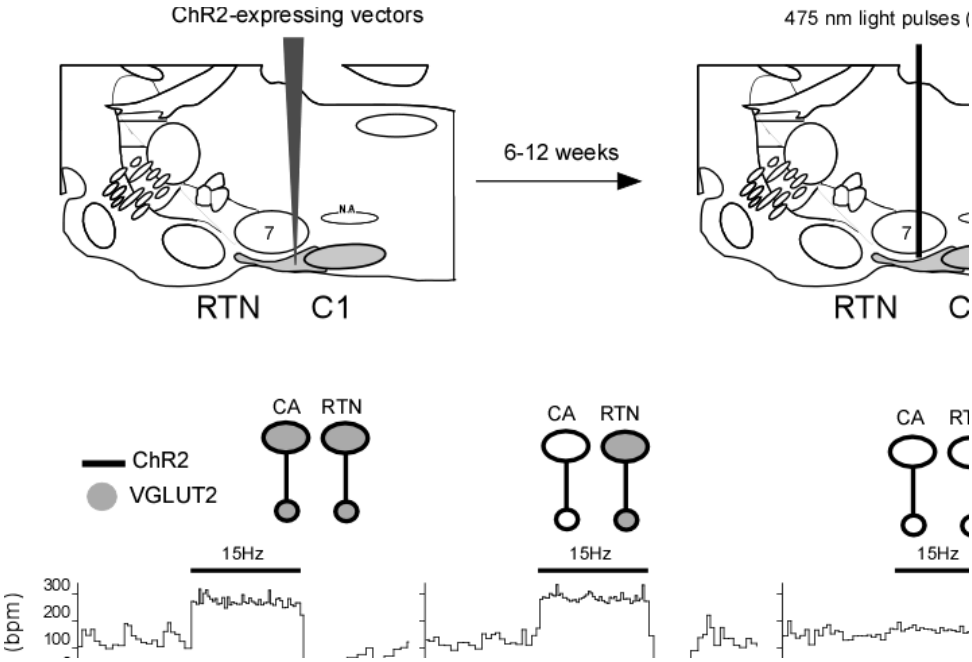

Summary of Abstract

Introduction

The retrotrapezoid nucleus (RTN) contributes to blood PCO_2 stability by regulating breathing frequency and amplitude in a feed-back manner [1-5]. Activation of these neurons by CO_2 *in vivo* is now attributed to their intrinsic pH-sensitivity, paracrine influences from surrounding pH-responsive astrocytes, and inputs from the carotid bodies and other CO_2-responsive CNS neurons [6-13].

RTN neurons may use glutamate as a transmitter because they contain *Vglut2* transcripts and their axonal varicosities are Vglut2-immunoreactive [3, 14]. However, the CNS is replete with Vglut2-expressing neurons in which transmitters other than glutamate seem to play the dominant role (e.g. orexinergic neurons, neuroendocrine cells in hypothalamus, dopaminergic neurons)[15-18]. Further, many RTN neurons also express galanin, a typically inhibitory peptide [14, 19, 20]. The present study seeks more definitive evidence that RTN neurons activate breathing by releasing glutamate in conscious adult mice.

Opto- and pharmacogenetic experiments have been instrumental in showing that RTN neurons activate breathing in rats [2, 4, 21]. In these experiments the actuator (opsin or allatostatin receptor) was introduced into RTN neurons using lentiviral vectors whose selectivity relies on a Phox2b-sensitive promoter, PRSx8 [22]. However, since Phox2b is expressed by both RTN and neighboring catecholaminergic (CA) neurons, such vectors cause transgene expression in both CA cells and the RTN [23].

Lower brainstem catecholaminergic cells, unlike RTN neurons, express dopamine-β-hydroxylase (DβH) and can be specifically targeted in $D\beta H^{Cre/0}$ mice [24].

ChR2-mediated stimulation of these lower brainstem catecholaminergic neurons increases breathing unless vesicular glutamate transporter-2 (*Vglut2, Slc17a6*) [25] is selectively knocked out of these cells [24]. Therefore these catecholaminergic neurons increase breathing by releasing glutamate [24].

To determine whether glutamate is the primary transmitter of RTN neurons *in vivo* we used ChR2-based optogenetics to activate RTN and catecholaminergic neurons in mice in which Vglut2 was expressed by both cell types or in mice in which *Vglut2* exon2 was selectively excised from the CA cells or excised from both CA and RTN neurons. *Vglut2* exon2 excision from both CA and RTN neurons was achieved by targeted injections of a Cre-expressing PRSx8 promoter-driven vector in $Vglut2^{(flox/flox)}$ mice [26, 27]. Selective *Vglut2* exon2 excision from the CA neurons was achieved by crossing $D\beta H^{Cre/0}$ mice with $Vglut2^{fl/fl}$ mice. In all mice, we photostimulated the ChR2-transduced neurons and measured their breathing responses using whole body plethysmography.

Materials and Methods

Animals

Animal use was in accordance with the NIH Guide for the Care and Use of Laboratory Animals and approved by the University of Virginia Animal Care and Use Committee. $D\beta H^{Cre/0}$ mice were obtained from the Mutant Mouse Regional Resource Center at the University of California, Davis, CA, USA [Tg(DβH-cre)KH212Gsat/Mmcd; stock # 032081-UCD] and maintained as hemizygous (Cre/0) on a C57BL/6J (C57) background. Homozygous $Vglut2^{flox/flox}$ mice (JAX Stock #012898; STOCK

Slc17a6$^{tm1Lowl/J}$)[27] were bred with *DβH*$^{Cre/0}$ mice to generate *DβH*$^{Cre/0}$*; Vglut2*$^{flox/0}$ mice and subsequently crossed with *Vglut2*$^{flox/flox}$ mice to generate *DβH*$^{Cre/0}$*; Vglut2*$^{flox/flox}$ and *DβH*$^{0/0}$*; Vglut2*$^{flox/flox}$ [28]. C57BL/6J(C57, JAX Stock#000664) mice were used in control experiments.

Experimental design

The experimental design is summarized in Table 1. The experiments are predicated on the following two assumptions that are supported by prior experiments in rats and mice and were verified here by a detailed histological analysis of every mouse that was used. First, the transgene of PRSx8 promoter-containing LVV (Cre or ChR2-eYFP) is selectively expressed in Phox2b-containing neurons [2, 5]. Second, at the ventral surface of the medulla oblongata, the Phox2b-containing neurons consist almost exclusively of catecholaminergic and RTN chemoreceptor neurons. The rostral ventrolateral medullary catecholaminergic neurons (C1 neurons) and RTN neurons contain *Vglut2* transcripts [23, 24]. Therefore when we injected PRSx8 Cre LVV together with a Cre-dependent ChR2 AAV in the rostral ventral medulla of C57 mice, we produced ChR2 expression in both catecholaminergic and RTN neurons and both cell types expressed Vglut2 (Group 1). To isolate the breathing effects resulting specifically from RTN stimulation, we injected PRSx8-ChR2 in *DβH*$^{Cre/0}$*;Vglut2*$^{fl/fl}$ mice, and therefore also produced expression of ChR2 in both cell types but Vglut2 was deleted in the CA neurons only (Group 2) [24]. Finally, in order to test whether glutamate is responsible for the breathing stimulation elicited by RTN neuron activation, we injected a mixture of PRSx8 Cre LVV and a Cre-dependent ChR2 AAV into the RTN region of *Vglut2*$^{fl/fl}$ mice.

In this case both CA and RTN were transduced with Cre and, the neurons that expressed ChR2 should no longer express Vglut2 because the recombinase should also have excised the *Slc17a6* exon2. In summary, if RTN stimulation drives breathing by releasing glutamate, the prediction is that photostimulation of ChR2-expressing neurons should produce robust breathing stimulation in groups 1 (C57) and 2 ($D\beta H^{Cre/0};Vglut2^{fl/fl}$) and little or no breathing stimulation in group 3 ($Vglut2^{fl/fl}$).

Unilateral viral vector injection and optical fiber implantation

The following viral vectors were used in these experiments: PRSx8-ChR2(H134R)-eYFP lentiviral vector (LVV, stock: $1.2x10^9$ viral particles/ml), PRSx8-Cre LVV (stock: $5.4x10^9$ viral particles /ml) and DIO-ChR2-eYFP AAV2; stock: $3.0x10^{12}$ viral particles/ml). PRSx8 is a Phox2b-activated promoter that restricts transgene expression to cells that express high levels of this transcription factor [22]. When PRSx8-containing LVV is injected accurately into RTN, transgene expression is restricted to Phox2b-immunoreactive neurons that reside at the ventral surface of the medulla oblongata [2, 4, 23]. Non-neuronal cells, including astrocytes, are not transduced [5]. The transduced neuronal population includes catecholaminergic neurons (C1 and A5 neurons) and non-catecholaminergic neurons, both of which contain *Vglut2* transcripts [29, 30]. Recordings performed in Phox2b-eGFP transgenic mice have shown that the vast majority of the non-catecholaminergic Phox2b+ population of neurons located below the facial motor nucleus (~95% in slices and ~80% after complete dissociation) are activated by acidification [6, 29]. In addition, the respiratory stimulation contributed by the same group of Phox2b+ neurons is strikingly dependent on blood pH in conscious

rats [5]. For these and other reasons [31], we refer to these Phox2b+ non-aminergic neurons as RTN chemoreceptors. Ten adult *DβH$^{Cre/0}$; Vglut2$^{flox/flox}$* mice (10-20 wks; 6 females, 4 males) received injections of PRSx8-ChR2-eYFP LVV (stock diluted 5 fold in sterile Dulbecco's phosphate buffered saline). A 1:15 (v/v) mixture of PRSx8-Cre LV stock and DIO-ChR2-eYFP AAV2 stock was injected into 8 C57 mice (7-11 wks; 1 female, 7 males) and in 9 *DβH$^{0/0}$; Vglut2$^{flox/flox}$* mice (7-11 wks; 5 females, 4 males).

Vector microinjection and implantation of optical fibers were performed under aseptic conditions in mice anesthetized with a mixture of ketamine (100 mg/kg) and dexmedetomidine (0.2 mg/kg; i.p.) as previously described [32]. Adequate anesthesia was judged by the absence of the corneal and hind-paw withdrawal reflex. Additional anesthetic was administered if necessary (20% of the original dose, i.p.). Anesthetized mice were placed into a modified stereotaxic device (Kopf) and maintained at 37ºC on a thermostatically controlled heating pad. Three 120 nl injections of PRSx8-ChR2-eYFP LVV or PRSx8-Cre LVV/DIO-ChR2-eYFP AAV2 mixture were aligned 0.2 mm apart in the rostrocaudal direction and located 1-4-1.5 mm lateral to the midline and 100 µm below the left facial motor nucleus. The lower boundary of this nucleus was identified electrophysiologically with antidromic field potentials as described previously [24].

Following microinjection of the viral vector(s), a 125 µm-diameter fiber optic, consisting of a stripped, glass-clad multimode optical fiber (105 µm-core, 0.22 numerical aperture; Thorlabs, Newton, NJ, USA) glued into a zirconia ferrule (1.25 mm O.D., 126 µm bore; Precision Fiber Products, Milpitas, CA, USA), was placed with its tip ~100 µm above the injection site. The fiber optic ferrule was secured to the skull with adhesive (Loctite 3092). Mice received post-operative boluses of atipamezole (α_2-adrenergic

antagonist, 2 mg/kg, s.c.), ampicillin (125 mg/kg, i.p.), and ketoprofen (4 mg/kg, s.c.). Ampicillin and ketoprofen were re-administered 24 hours post-operatively.

Combination optogenetics and whole-body plethysmography in conscious mice

Photostimulation of the ChR2-transduced neurons was performed as previously described [24]. Prior to implantation, the light output of each implanted optical fiber was measured with a light meter (Thorlabs) and the laser setting was adjusted to deliver ~9 mW. This setting was later used during the experiments. Photostimulation and plethysmography trials were carried out 6-12 wks after viral injections. Breathing parameters were measured in conscious mice using unrestrained whole-body plethysmography (EMKA Technologies, Falls Church, VA ,USA) as previously described [24]. The breathing parameters measured were breathing frequency (f_R in breaths/minute, bpm), tidal volume (V_T in µl/g) and minute volume (V_E in ml/(min x g). Before being placed in the plethysmography chamber, the mice were briefly anesthetized with isoflurane while the connection between the implanted optical fiber and the laser delivery system was established. Airflow signals were calibrated to air injected via a 1mL syringe. Tidal volume was determined by the area under the curve during inspiratory breaths divided by weight. The chamber was continuously flushed with dry, room-temperature air delivered at 0.5 liter/min. Chamber pressure signals were detected via a differential pressure transducer, amplified (x 500), band pass filtered (0.25Hz to 35Hz), and digitized at greater than 100 Hz with Spike 2 software (v7.10, Cambridge Electronic Design, Ltd., Cambridge, UK). Respiratory frequency (f_R; breaths/min) was analyzed exclusively during periods of behavioral quiescence. To evaluate the effects of photostimulation on

f_R, 10 s-long trains of 5 ms light pulses were delivered at three frequencies (5, 10 and 15 Hz). Behavioral quiescence was determined by direct observation or via an automated function using Spike2 software. For automated acquisition, laser stimulation was triggered at one of three frequencies (5 Hz, 10 Hz, 15 Hz), as determined by a random number generator, after an eleven second period of breathing in which max and min f_R were less than 200 bpm and greater than 90 bpm, no sighing occurred, mean f_R was between 130 and 170 bpm, and the preceding stimulation had occurred at a time greater than 60 s prior. All stimulation trials were visually inspected posthoc and only those trials that had occurred during behavioral quiescence were used for analysis. The reported changes in f_R reflect the average response of 5-10 trials per mouse at each stimulation frequency.

Histological procedures

At the end of experimental procedures in conscious mice, animals were anesthetized with an overdose of pentobarbital and perfused transcardially with 10-15 ml of phosphate buffered saline followed by 75-100 ml of 3% paraformaldehyde. Brains were extracted and post-fixed for 24-72 hours before sectioning on a vibrating microtome at room temperature. Thirty micron coronal sections throughout the medulla/pons were collected into cryoprotectant solution (30% ethylene glycol, 20% glycerol, 50% 100 mM sodium phosphate buffer, pH 7.4) and stored at -20°C until further processing.

One-in-three series of coronal sections were processed free floating for detection of Phox2b, eYFP and tyrosine hydroxylase (TH) by immunohistochemistry as previously

described [21]. Briefly, sections were incubated simultaneously in antibodies directed against Phox2b (rabbit; 1:8000, generously provided by J.F. Brunet (Institut de Biologie de l'Ecole normale supérieure, Paris, France), TH (sheep; 1:2000, EMD Millipore, Billerica, MA) and eYFP (chicken; 1:2000, AVES labs, Tigard, OR). The specificity of the Phox2b antibody has been established previously by demonstrating that *Phox2b* transcripts and Phox2b immunoreactivity are co-localized [33] and that immunoreactivity is absent in Phox2b knock-out mice [34]. After 24- 48 hours, sections were rinsed and incubated in secondary antibodies at 1:200 (anti-rabbit-biotin tagged IgG; anti-sheep IgG tagged with DyLight 647; anti-chicken IgY tagged with Alexa 488; all secondaries from Jackson ImmunoResearch, West Grove, PA) rinsed and incubated in streptavidin-HRP (1:200; Perkin-Elmer, Melville, NY). Rinsed and incubated in tyramide-Cy3 (1:200; Perkin-Elmer), then rinsed and mounted onto slides, dehydrated through alcohols and xylenes and covered with DPX mountant (Electron Microscopy Sciences, Hatfield, PA).

Sections were examined and cell distributions mapped with a computer-driven stage and Neurolucida software (v. 11, MBF Bioscience, Wiliston, VT) attached to a Zeiss Axioskop widefield fluorescence microscope (Carl Zeiss Microscopy, Thornwood, NY) using 20X (NA= 0.17) or 100x (oil, NA=1.4) objectives and images recorded with a Zeiss MRC rev. 3 CCD camera (1388x1040 pixels; Carl Zeiss Microscopy). Some images were rendered from maximum intensity projections of z-stacks captured at 0.3 micron intervals through 10-15 micron depth of tissue, then deconvolved through 7 iterations using the automatic 3D blind deconvolution in AutoQaunt X3 software (Media Cybernetics, Rockville, MD). Images were imported into Canvas software (v. 10, ACD

Systems, Seattle, WA), levels adjusted over the entire image to include all information containing pixels and assembled into figures.

Statistical analysis

Data were analyzed by one or two-way ANOVA with repeated measures with differences between groups determined using Sidak multiple comparisons using the PRISM software (GraphPad PRISM Version 6). Assumptions of the two-way ANOVA were tested with the Shapiro-Wilk test for normality on error residuals for both between and within subjects (R statistical software package version 3.2.0; R Core Team, 2013). Assumptions of the one-way ANOVA for normality were also confirmed with the Shapiro-Wilk test. Power was calculated using R software. The PRISM software tests for sphericity and generates a value for Geisser-Greenhouse epsilon if sphericity cannot be assumed. In such cases, the fractional df values used to compute a *P* value would be reported (this was not the case for any of our analyses). Test statistics where $P < 0.05$ were considered significant.

Results

Breathing responses elicited by ChR2 photostimulation

The light was delivered for 10 s at 5, 10 and 15 Hz in random order. This frequency range was selected because, in anesthetized rats, these neurons rarely discharge above 12 Hz when exposed to high levels of CO_2 [35]. In groups 1 and 2, in which RTN presumably expressed Vglut2, photostimulation produced a robust frequency-dependent rise in breathing rate (f_R) and tidal volume (V_T) (representative example in Fig. $1A_{1-4}$, B_{1-}

$_4$). By contrast, virtually no effect was observed in group 3, in which Vglut2 was deleted from both ChR2-expressing CA and RTN neurons (Fig. 1C$_{1-4}$). Of note, the breathing stimulation observed in groups 1 and 2 was instantaneous and its amplitude was also instantly maximal consistent with the release of a fast-acting transmitter.

Group data for f_R, V_T, and minute volume V_E are shown in Figures 2, 3 and 4, respectively. The groups were first analyzed for differences in baseline breathing using one-way ANOVA with baseline values averaged across all three stimulation frequencies. There was no significant main effect of group for baseline values of fR, V_T or V_E (see Table 2 for Shapiro-Wilk test of normality and Table 3 for *F* values). The power of this test was 0.93 for f_R, 0.99 for V_T and 0.99 for V_E (all with *P* set at 0.05). In short, there was no difference in baseline breathing variables between the three groups of mice.

Each mouse group was then analyzed separately with 2-way ANOVA with RM for both main effects of photostimulation and frequency of photostimulation (5, 10, 15 Hz) on f_R, V_T and V_E. In groups 1 and 2, in which RTN contained Vglut2, photostimulation produced a robust frequency-dependent increase in f_R, V_T and V_E (significant main effect of both photostimulation and stimulation frequency on f_R, V_T and V_E; see Shapiro-Wilk tests for normality in Table 2 and Table 3 for *F* values). By contrast, there was no effect of stimulation frequency in group 3 and only a small but statistically significant main effect of photostimulation (Tables 2 and 3).

To determine whether optogenetic stimulation had a different effect between the three groups of mice, we first tried a mixed factorial design two-way ANOVA for groups x stimulation frequency with RM on stimulation frequency, and we measured the change (delta) in breathing variables between baseline and stimulation. For V_E this analysis

revealed significant differences both between groups and between stimulation frequencies (Table 2 and 3; results of Tukey's multiple comparison tests shown in Fig. 4D). The assumptions of normality on error residuals were not met for f_R and V_T (see Table 2) so the factor of different stimulation frequencies was not examined and data were analyzed on all variables at the 15 Hz stimulation frequency by one-way ANOVA on groups. There was a significant effect of groups (see Tables 2, 3 for assumptions of normality and F stats). Post hoc Tukey's multiple comparison tests showed a highly significant difference for f_R, V_T and V_E between groups 1 and 3 and groups 2 and 3 but no difference between groups 1 and 2 (see Table 4). The statistically non-significant differences between groups 1 and 2 have 95% confidence intervals that span zero and are outside of the 95% confidence intervals for differences between groups 1 and 2 and group 3 for both f_R and V_E (although there was some overlap of the 95% confidence intervals for V_T). Thus, we conclude that the effect of stimulation on breathing was much greater in groups 1 and 2 than in group 3 and that, at least for f_R and V_E, there was no difference between groups 1 and 2.

The observed results are therefore consistent with the hypothesis that selective activation of RTN neurons produces breathing stimulation only if these neurons express Vglut2.

Histology

The first series of histological experiments was designed to verify that, in mice, injections of PRSx8-based lentiviral vectors (PRSX8-ChR2-eYFP LVV or mix of

PRSX8-Cre LVV and DIO-ChR2-eYFP AAV2) into the RTN region cause expression of ChR2 selectively in Phox2b-expressing neurons. In two *DβH*$^{Cre/0}$*;;Vglut2*$^{fl/fl}$ mice injected with PRSX8-ChR2-eYFP LVV, and three *Vglut2*$^{fl/fl}$ mice injected with mix of PRSX8-Cre LVV and DIO-ChR2-eYFP AAV2, 94.4 ± 1.7 % of transduced (eYFP-expressing) neurons had a Phox2b-immunoreactive nucleus (Fig. 5A-C). This population included 26.1 ± 5.5% TH-immunoreactive, i.e. catecholaminergic neurons (average for the five mice). Thus, in mice as in rats, LVVs with the PRSx8 promoter transduce Phox2b-immunoreactive neurons selectively when these vectors are targeted to the brain region of interest.

The second goal was to ascertain that the number and distribution of the ChR2-transduced neurons was comparable in the three groups of mice. The ChR2-eYFP transduced neurons were located superficially within the ventrolateral medulla from just caudal to the facial motor nucleus caudally to the level of the exit of the facial nerve. The rostrocaudal distribution of the transduced catecholaminergic or non-catecholaminergic (i.e. RTN) neurons was similar in all three groups (Fig. 5E,F). The total number of RTN neurons was estimated by multiplying the cell counts in a one in three series of sections by three and was not different between groups (C57, 195 ± 17.5; *DβH*$^{Cre/0}$*;;Vglut2*$^{fl/fl}$, 261 ± 50.8; *Vglut2*$^{fl/fl}$, 201 ± 16.7; one-way ANOVA, $F_{2,20} = 1.549$, $P = 0.237$; Shapiro-Wilk, $W = 0.9282$, $P = 0.09989$; power at α 0.05 = .9448; Fig. 5D). The total number of catecholamine cells transduced was comparable in each group, though group 1 contained fewer transduced CA neurons than did group 2 (C57, 98.1 ± 15.0; *DβH*$^{Cre/0}$*;;Vglut2*$^{fl/fl}$, 178 ± 10.3; *Vglut2*$^{fl/fl}$, 158.1 ± 30.3; $F_{2,20} = 4.575$, $P = 0.0231$; Shapiro-Wilk, $W = 0.9302$, $P = 0.1106$; power at α 0.05 = .999; Fig. 5D). Finally, the percentage of RTN neurons in total

transduced neurons was also similar (C57, 67 ± 4%; $D\beta H^{Cre/0};;Vglut2^{fl/fl}$, 57 ± 5%; group $Vglut2^{fl/fl}$, 58 ± 4%; one-way ANOVA, $F_{2,20} = 1.717$, $P = 0.205$; Shapiro-Wilk, $W = 0.95083$, $P = 0.3045$; power at α 0.05 = 0.9636).

RTN neurons innervate abundantly the ventral respiratory column, including the preBötzinger Complex, a subdivision of this column that is essential for breathing rate generation [14, 36, 37]. We therefore examined the eYFP-labeled nerve terminals located within this region of the medulla oblongata in groups 1 and 3 to verify that *Vglut2* was present in group 1 and had been effectively knocked out from the ChR2-transduced neurons in group 3. These projections are largely ipsilateral therefore only one side (the left) was examined. In group 1 (N = 3 mice) 89 ± 1% of eYFP-positive terminals counted (avg. 235 terminals counted per mouse) also contained detectable Vglut2-immunoreactivity whereas in group 3 (N = 3; avg. 246 terminals counted per mouse) only 9 ± 1.6% eYFP terminals were Vglut2-immunoreactive (Fig. 6A, RTN projections).

In order to confirm that Vglut2 was appropriately deleted from the RTN neurons in group 3, we used double-label immunohistochemistry and examined eYFP-labeled nerve terminals located in the ventral respiratory column (VRC). In contrast to terminals in VRC from group 1, terminals in this same area from group 3 lacked Vglut2 immunoreactivity (Fig. 6A). We used triple-label immunohistochemistry to determine that *Vglut2* was appropriately deleted from CA neurons in groups 2 and 3 but not in group 1. We examined the raphe pallidus, which receives projections from the CA neurons but not from RTN. Terminals were considered to originate from the CA neurons if they were eYFP+ and TH+ [24]. As illustrated in Figure 6B (CA projections), eYFP-positive terminals were TH-negative and Vglut2-positive in C57 mice (group 1) but these

terminals lacked Vglut2 immunoreactivity in both the *DβH*$^{Cre/0}$*;;Vglut2*$^{fl/fl}$ mice (group 2) and the *Vglut2*$^{fl/fl}$ mice injected with both PRSX8-Cre and ChR2-eYFP AAV2 (group 3).

Discussion

The presence of *Vglut2* transcripts in RTN neurons has been identified previously by *in situ* hybridization and by single cell PCR in rats and mice [3, 38]. Vglut2 immunoreactivity has also been detected in the axonal varicosities of these neurons [14]. Here, we show that Vglut2 expression by RTN neurons is required for these neurons to stimulate breathing in conscious adult mice. These results strongly suggest that glutamate is the main transmitter used by this particular group of chemoreceptors to increase breathing.

RTN neurons: definition and function

The retrotrapezoid nucleus has been variously defined over the years ([34, 39, 40] for reviews see [31, 41]. As in our previous publications, RTN neurons are defined here as a small collection (~800 in mice, ~2000 in rats) of Phox2b-positive non-catecholaminergic and non-cholinergic neurons located under the facial motor nucleus [23]. All of these neurons contain *Vglut2* transcripts, specific proton receptors [13] and lack markers of GABA or glycine neurotransmission [3, 29]. Half of them also express galanin [19, 29]. RTN neurons as defined above are probably identical to a cluster of similarly located *Vglut2*-expressing neurons that have been identified by genetic lineage studies as *Atoh1/egr-2/phox2b*-derived [34, 42, 43]. The vast majority of RTN neurons are activated by acid *in vitro* and by hypercapnia *in vivo* [3, 5, 38]. RTN neurons express

two proton detectors (TASK-2 and a G-protein coupled receptor, GPR4); genetic elimination of each protein separately attenuates the pH-sensitivity of RTN neurons and reduces the hypercapnic ventilatory reflex by 65% whereas genetic elimination of both proteins substantially eliminates both RTN neuron pH-sensitivity and the hypercapnic ventilatory reflex (>85% reduction) [7, 13, 44]. RTN neurons selectively innervate the pontomedullary regions that contain the respiratory rhythm and pattern generator and their selective activation increases breathing [2]. RTN neurons also receive input from various types of CNS neurons that contribute to the hypercapnic ventilatory reflex (serotonergic, noradrenergic and orexinergic)(reviewed in [31]). In short, RTN neurons are both central respiratory chemoreceptors and a nodal point for the chemoreflexes ([12, 45], for recent review: [31]).

Contribution of Vglut2 rostroventrolateral medullary CA neurons to breathing

We showed previously that the increased breathing elicited by stimulation of the C1 neurons (catecholaminergic neurons located in the rostral medulla) required expression of Vglut2 by these neurons [24]. Therefore, one could have expected more robust respiratory changes in control mice (group 1) than in group 2 in which the C1 cells lack Vglut2. However, this outcome was not found and breathing stimulation was identical in these two groups of mice at all stimulation frequencies. This outcome can be reasonably explained as follows. In our previous study the ChR2-expressing vector was administered more caudally in the ventrolateral medulla to deliberately target the largest possible number of C1 cells and, as a result, around 400 C1 cells expressed ChR2 [24]. In the present study, the ChR2-containing vector was delivered more rostrally to maximize

expression by RTN neurons and only around 100 C1 cells expressed ChR2. Accordingly, the contribution of the C1 cells to the respiratory stimulation must have been much smaller in the present study. Also, the C1 cells are functionally heterogeneous [46] and we do not know whether the most rostral ones are those that regulate breathing. Finally, the fiber optic was implanted caudal to the facial nucleus in the previous study (6.57±0.06 mm caudal to bregma) whereas, in the present study, fiber placement was within the coronal plane of the facial nucleus (6.13±0.03 mm caudal to bregma). This difference would also have favored the stimulation of RTN over the C1 cells given that effective stimulation requires that the tip of the optical fiber be located within 500 microns of the cell bodies. In sum, the similarities between the breathing response evoked in groups 1 and 2 likely reflect the fact that relatively few C1 cells were photoactivated in either group.

Baseline ventilation parameters after Vglut2 deletion from C1 and RTN neurons

The resting ventilatory parameters were identical in the three groups of mice. This result conforms to expectations. Resting ventilatory parameters of C57 and $D\beta H^{Cre/0}$; $Vglut2^{flox/flox}$ mice are identical [24]. The total population of RTN neurons in mice is about 800 [29] and *Vglut2* was knocked out of fewer than half in group 3, and only on one side. Significant loss of function (chemoreflex) requires elimination of over 75 % of the RTN neurons [42, 47].

RTN signals by releasing glutamate

Selective activation of the C1 cells no longer causes breathing stimulation when Vglut2 is deleted from these neurons [24]. We show here that, after Vglut2 has been deleted selectively from the rostral CA cells, photoactivation of a mixture of catecholaminergic and RTN neurons still produced a robust activation of breathing (group 2). This response must therefore have resulted from the activation of ChR2-transduced RTN neurons. RTN-derived breathing stimulation was instantly maximal, consistent with the hypothesis that these cells signal with glutamate. This fast response is in sharp contrast with the slow and gradual breathing recruitment elicited, also in mice, by activating serotonergic neurons using a similar optogenetic method [48].

The breathing stimulation elicited by combined stimulation of RTN and neighboring catecholaminergic neurons was drastically reduced when Vglut2 was deleted from both neuronal types (group 3). The number of transduced RTN neurons was on average the same as in the other two groups of mice. Furthermore, the level of expression of ChR2 should have been very similar in groups 1 (Vglut2 present in both C1 and RTN neurons) and 3 (Vglut2 absent from both neuronal types) because these mice received the same combination of vectors. Accordingly, the most plausible interpretation is that glutamate release mediates the breathing stimulation elicited by RTN. This interpretation is consistent with the presence of *Vglut2* transcripts in RTN cell bodies and Vglut2 immunoreactivity in their terminals [3, 14, 38]. In addition, within the ventral respiratory column, RTN neurons form asymmetric synapses with their target neurons, characteristic of excitatory glutamatergic transmission [14].

An alternative interpretation of the present results deserves mention though it seems much less plausible. *Vglut2* deletion from RTN neurons could potentially cause the

retraction of synapses between the affected RTN neurons and their targets within the respiratory pattern generator (plasticity hypothesis). For example, *Vglut2* deletion from dopaminergic neurons does interfere with their proper connectivity [49-51]. However, these changes are the consequence of deleting *Vglut2* early during development, and are therefore likely a consequence of altered development of these synapses rather than the retraction of properly formed synapses. In the present case we excised *Vglut2* from neurons that had already established their adult connections.

The small residual breathing stimulation that remained in group 3 could have resulted from the release of a transmitter other than glutamate from either RTN or a subset of catecholaminergic neurons. An equally likely explanation is the incomplete excision of *Vglut2* exon2 in the neurons that expressed the Cre recombinase because Vglut2 immunoreactivity could still be detected in approximately 9% of eYFP-positive terminals in group 3.

Finally, while the present study was being submitted, inactivation of glutamatergic synaptic transmission in a population of RTN neurons defined by intersection genetics (co-expression of Atoh1 and Phox2b) was shown to abrogate CO_2 chemosensitivity in neonatal mice [43]. These Phox2b^{on}/Atoh1^{on} neurons are very likely either the same as (or a large subset of) the Phox2b-immunoreactive neurons targeted in our study. These two studies therefore provide congruent evidence that glutamate release is necessary for RTN neurons to **activate** breathing in conscious mice in both pups [43] and adults (present study). This observation does not exclude the possibility that RTN might release additional transmitters whose effect might be to amplify or otherwise modulate the effect of glutamate.

Acknowledgments

This work was supported by grants from the National Institutes of Health (HL 074011 and HL028785 to PGG). We thank Chase Ford, Statistical Research Consultant for Research Data Services at the University of Virginia Library for his help with the statistics.

Works Cited

1. Guyenet, P.G., R.L. Stornetta, and D.A. Bayliss, *Central respiratory chemoreception.* J. Comp. Neurol., 2010. **518**(19): p. 3883-3906.
2. Abbott, S.B., et al., *Photostimulation of retrotrapezoid nucleus phox2b-expressing neurons in vivo produces long-lasting activation of breathing in rats.* J. Neurosci., 2009. **29**(18): p. 5806-5819.
3. Mulkey, D.K., et al., *Respiratory control by ventral surface chemoreceptor neurons in rats.* Nat. Neurosci., 2004. **7**(12): p. 1360-1369.
4. Marina, N., et al., *Essential role of Phox2b-expressing ventrolateral brainstem neurons in the chemosensory control of inspiration and expiration.* J Neurosci, 2010. **30**(37): p. 12466-73.
5. Basting, T.M., et al., *Hypoxia Silences Retrotrapezoid Nucleus Respiratory Chemoreceptors via Alkalosis.* J Neurosci, 2015. **35**(2): p. 527-43.
6. Wang, S., et al., *Phox2b-expressing retrotrapezoid neurons are intrinsically responsive to acidification and CO_2.* Journal of Neuroscience, 2013. **33**: p. 7756-7761.
7. Wang, S., et al., *TASK-2 channels contribute to pH sensitivity of retrotrapezoid nucleus chemoreceptor neurons.* J. Neurosci., 2013. **33**(41): p. 16033-16044.
8. Gourine, A.V., et al., *Astrocytes control breathing through pH-dependent release of ATP.* Science, 2010. **329**(5991): p. 571-575.
9. Huckstepp, R.T., et al., *Connexin hemichannel-mediated CO2-dependent release of ATP in the medulla oblongata contributes to central respiratory chemosensitivity.* J. Physiol., 2010. **588**: p. 3901-3920.

10. Nattie, E. and A. Li, *Central chemoreception in wakefulness and sleep: evidence for a distributed network and a role for orexin.* J. Appl. Physiol., 2010. **108**(5): p. 1417-1424.

11. Hawryluk, J.M., et al., *KCNQ channels determine serotonergic modulation of ventral surface chemoreceptors and respiratory drive.* J.Neurosci., 2012. **32**(47): p. 16943-16952.

12. Hodges, M.R. and G.B. Richerson, *Medullary serotonin neurons and their roles in central respiratory chemoreception.* Respir. Physiol. Neurobiol., 2010.

13. Kumar, N.N., et al., *Regulation of breathing by CO2 requires the proton-activated receptor GPR4 in retrotrapezoid nucleus neurons.* Science 2015. **In press**.

14. Bochorishvili, G., et al., *Pre-Botzinger complex receives glutamatergic innervation from galaninergic and other retrotrapezoid nucleus neurons.* J. Comp. Neurol., 2012. **520**(5): p. 1047-1061.

15. Rosin, D.L., et al., *Hypothalamic orexin (hypocretin) neurons express vesicular glutamate transporters VGLUT1 or VGLUT2.* Journal of Comparative Neurology, 2003. **465**(4): p. 593-603.

16. Van den Pol, A.N., *Neuropeptide transmission in brain circuits.* Neuron, 2012. **76**(1): p. 98-115.

17. Stuber, G.D., et al., *Dopaminergic terminals in the nucleus accumbens but not the dorsal striatum corelease glutamate.* J.Neurosci., 2010. **30**(24): p. 8229-8233.

18. Lin, W., et al., *Distribution of vesicular glutamate transporter-2 messenger ribonucleic Acid and protein in the septum-hypothalamus of the rat.* Endocrinology, 2003. **144**(2): p. 662-670.

19. Stornetta, R.L., et al., *Galanin is a selective marker of the retrotrapezoid nucleus in rats.* J Comp Neurol, 2009. **512**(3): p. 373-383.

20. Pieribone, V.A., et al., *Electrophysiologic effects of galanin on neurons of the central nervous system.* Ann.N.Y.Acad.Sci., 1998. **863**: p. 264-273.

21. Abbott, S.B., et al., *Phox2b-expressing neurons of the parafacial region regulate breathing rate, inspiration, and expiration in conscious rats.* J. Neurosci., 2011. **31**(45): p. 16410-16422.

22. Hwang, D.Y., et al., *A high-efficiency synthetic promoter that drives transgene expression selectively in noradrenergic neurons.* Human Gene Therapy, 2001. **12**(14): p. 1731-1740.

23. Stornetta, R.L., et al., *Expression of Phox2b by brainstem neurons involved in chemosensory integration in the adult rat.* J. Neurosci., 2006. **26**(40): p. 10305-10314.

24. Abbott, S.B., et al., *Vesicular glutamate transporter 2 is required for the respiratory and parasympathetic activation produced by optogenetic stimulation of catecholaminergic neurons in the rostral ventrolateral medulla of mice in vivo.* European Journal of Neuroscience, 2014. **39**(1): p. 98-106.

25. Takamori, S., et al., *Identification of a vesicular glutamate transporter that defines a glutamatergic phenotype in neurons.* Nature, 2000. **407**(6801): p. 189-194.

26. Kaur, S., et al., *Glutamatergic signaling from the parabrachial nucleus plays a critical role in hypercapnic arousal.* J Neurosci, 2013. **33**(18): p. 7627-40.

27. Tong, Q., et al., *Synaptic glutamate release by ventromedial hypothalamic neurons is part of the neurocircuitry that prevents hypoglycemia.* Cell Metab., 2007. **5**(5): p. 383-393.

28. Depuy, S.D., et al., *Glutamatergic neurotransmission between the C1 neurons and the parasympathetic preganglionic neurons of the dorsal motor nucleus of the vagus.* Journal of Neuroscience, 2013. **33**(4): p. 1486-1497.

29. Lazarenko, R.M., et al., *Acid sensitivity and ultrastructure of the retrotrapezoid nucleus in Phox2b-EGFP transgenic mice.* J. Comp. Neurol., 2009. **517**(1): p. 69-86.

30. Stornetta, R.L., et al., *Vesicular glutamate transporter DNPI/GLUT2 is expressed by both C1 adrenergic and nonaminergic presympathetic vasomotor neurons of the rat medulla.* Journal of Comparative Neurology, 2002. **444**(3): p. 207-220.

31. Guyenet, P.G., *Regulation of breathing and autonomic outflows by chemoreceptors.* Compr. Physiol., 2014. **4**(4): p. 1511-62.

32. Abbott, S.B., et al., *Selective optogenetic activation of rostral ventrolateral medullary catecholaminergic neurons produces cardiorespiratory stimulation in conscious mice.* Journal of Neuroscience, 2013. **33**: p. 3164-3177.

33. Pattyn, A., et al., *Expression and interactions of the two closely related homeobox genes Phox2a and Phox2b during neurogenesis.* Development, 1997. **124**(20): p. 4065-4075.

34. Dubreuil, V., et al., *Defective respiratory rhythmogenesis and loss of central chemosensitivity in phox2b mutants targeting retrotrapezoid nucleus neurons.* J.Neurosci., 2009. **29**(47): p. 14836-14846.

35. Guyenet, P.G., et al., *Regulation of ventral surface chemoreceptors by the central respiratory pattern generator.* J. Neurosci., 2005. **25**(39): p. 8938-8947.

36. Kam, K., et al., *Emergence of population bursts from simultaneous activation of small subsets of preBotzinger complex inspiratory neurons.* J. Neurosci., 2013. **33**(8): p. 3332-3338.

37. Feldman, J.L., C.A. Del Negro, and P.A. Gray, *Understanding the rhythm of breathing: so near, yet so far.* Annu Rev Physiol, 2013. **75**: p. 423-52.

38. Lazarenko, R.M., et al., *Anesthetic activation of central respiratory chemoreceptor neurons involves inhibition of a THIK-1-like background K(+) current.* J. Neurosci., 2010. **30**(27): p. 9324-9334.

39. Smith, J.C., et al., *Brainstem projections to the major respiratory neuron populations in the medulla of the cat.* J.Comp.Neurol., 1989. **281**(1): p. 69-96.

40. Onimaru, H. and I. Homma, *A novel functional neuron group for respiratory rhythm generation in the ventral medulla.* J.Neurosci., 2003. **23**(4): p. 1478-1486.

41. Guyenet, P.G., et al., *The retrotrapezoid nucleus and breathing.* Adv. Exp. Med. Biol., 2012. **758**: p. 115-122.

42. Ramanantsoa, N., et al., *Breathing without CO2 chemosensitivity in conditional Phox2b mutants.* J. Neurosci., 2011. **31**(36): p. 12880-12888.

43. Ruffault, P.L., et al., *The retrotrapezoid nucleus neurons expressing Phox2b and Atoh-1 are essential for the respiratory response to CO2.* Elife, 2015. **4**: p. doi: 10.7554/eLife.07051.

44. Gestreau, C., et al., *Task2 potassium channels set central respiratory CO2 and O2 sensitivity.* Proc. Natl. Acad. Sci. U.S.A, 2010. **107**(5): p. 2325-2330.

45. Li, A. and E. Nattie, *Antagonism of rat orexin receptors by almorexant attenuates central chemoreception in wakefulness in the active period of the diurnal cycle.* J. Physiol., 2010. **588**(Pt 15): p. 2935-2944.

46. Guyenet, P.G., et al., *C1 neurons: the body's EMTs.* Am J Physiol Regul Integr Comp Physiol, 2013. **305**(3): p. R187-204.

47. Takakura, A.C., et al., *Selective lesion of retrotrapezoid Phox2b-expressing neurons raises the apnoeic threshold in rats.* Journal of Physiology, 2008. **586**(Pt 12): p. 2975-2991.

48. Depuy, S.D., et al., *Control of breathing by raphe obscurus serotonergic neurons in mice.* J.Neurosci., 2011. **31**(6): p. 1981-1990.

49. Hnasko, T.S., et al., *Vesicular glutamate transport promotes dopamine storage and glutamate corelease in vivo.* Neuron, 2010. **65**(5): p. 643-656.

50. Berube-Carriere, N., et al., *Ultrastructural characterization of the mesostriatal dopamine innervation in mice, including two mouse lines of conditional VGLUT2 knockout in dopamine neurons.* Eur. J. Neurosci., 2012. **35**(4): p. 527-538.

51. Fortin, G.M., et al., *Glutamate corelease promotes growth and survival of midbrain dopamine neurons.* J.Neurosci., 2012. **32**(48): p. 17477-17491.

52. Abbott, S.B., et al., *Vesicular glutamate transporter 2 is required for the respiratory and parasympathetic activation produced by optogenetic stimulation of catecholaminergic neurons in the rostral ventrolateral medulla of mice in vivo.* Eur J Neurosci, 2014. **39**(1): p. 98-106.

53. Holloway, B.B., et al., *Monosynaptic glutamatergic activation of locus coeruleus and other lower brainstem noradrenergic neurons by the C1 cells in mice.* J Neurosci, 2013. **33**(48): p. 18792-805.

54. Abbott, S.B., et al., *Selective optogenetic activation of rostral ventrolateral medullary catecholaminergic neurons produces cardiorespiratory stimulation in conscious mice.* J Neurosci, 2013. **33**(7): p. 3164-77.

Table 1: Experimental design

Group	Mouse	Vector(s)	C1 cells	RTN cells	Breathing stimulation
1	*DβH*$^{+/+}$*;;Vglut2*$^{+/+}$ *(*C57*)*	PRSx8-Cre LV + DIO-ChR2-eYFP AAV	ChR2+/Vglut2+	ChR2+/Vglut2+	Yes^{+}
2	*DβH*$^{Cre/0}$*;;Vglut2*$^{fl/fl}$	PRSx8-ChR2-eYFP LV	ChR2+/Vglut2-	ChR2+/Vglut2+	Yes^{+}
3	*DβH*$^{+/+}$*;;Vglut2*$^{fl/fl}$	PRSx8-Cre LV + DIO-ChR2-eYFP AAV	ChR2+/Vglut2-	ChR2+/Vglut2-	No^{+}

Table 1: Groups 1-3: new experiments performed in the present study. $^{+}$ expected result if selective stimulation of RTN neurons increases breathing by releasing glutamate.

Table 2: Shapiro-Wilk Statistics

Shapiro Wilk test statistics on residuals for 2 WAY RM ANOVA						
	f_R within	f_R between	V_T within	V_T between	V_E within	V_E between
Group 1 effect of stim freq x before/during stim N = 8	W = 0.9514 *P* = 0.742	W = 0.9460 *P* = 0.4292	W = .9235 *P*= 0.4973	W = 0.9352 *P* = 0.2941	W =0.8276 *P* = 0.0760	W = 0.9322 *P* = 0.2644
Group 2 effect of stim freq x before/during stim N = 9	W = 0.9142 *P* = 0.3849	W = 0.9725 *P* = 0.8436	W =0.9795 *P* = 0.9604	W = 0.9462 *P* = 0.3683	W =0.9420 *P* = 0.6305	W = 0.9812 *P* = 0.9612
Group 3 effect of stim freq x before/during stim N= 6	W = 0.9682 *P* = 0.8638	W = 0.9825 *P*= 0.9918	W = .8450 *P* = 0.1793	W = 0.9587 *P* = 0.7657	W = .7763 *P* = .05119	W = 0.8737 *P* = 0.0728
delta stim w groups x freq of stim	W = 0.9483 *P* = 0.0404*	W = 0.9635 *P* = 0.5642	W =0.9936, *P* = 0.9964	W = 0.8723 *P* = 0.008*	W = 0.9738 *P* = 0.3792	W = 0.9593 *P* = 0.4758
Shapiro-Wilk test statistic on residuals for One-Way ANOVA for all groups at baseline						
	f_R		V_T		V_E	
Baseline on groups	W = 0.93006 *P* = 0.1097		W = 0.97722 *P* = 0.8538		W = 0.97501 *P* = 0.8065	
Shapiro-Wilk test statistic on residuals for One-Way ANOVA for all groups at 15 Hz stimulation						
delta stim @ 15 hz on 3 groups	W = 0.9810 *P*= 0.9206		W = 0.9748 *P*= 0.8011		W = 0.94447 *P* = 0.2239	

Table 3: *F* statistics

F-test statistics for Two-Way ANOVAs						
test/ group	main effect of stim (before/during)	main effect of stim frequency	main effect of stim (before/during)	main effect of stim frequency	main effect of stim (before/during)	main effect of stim frequency
	f_R		V_T		V_E	
Group 1 N=8 RM on both before/during and freq of stim	$F_{1,7} = 87.77$ $P < 0.0001$	$F_{2,14} = 26.19$ $P < 0.0001$	$F_{1,7} = 20.92$ $P = 0.0026$	$F_{2,14} = 7.664$ $P = 0.0056$	$F_{1,7} = 57.31$ $P = 0.0001$	$F_{2,14} = 23.97$ $P < 0.0001$
Group 2 N=9 RM on both before/during and freq of stim	$F_{1,8} = 133.4$ $P < 0.0001$	$F_{2,16} = 91.76$ $P < 0.0001$	$F_{1,8} = 30.65$ $P = 0.0005$	$F_{2,16} = 12.97$ $P = 0.0004$	$F_{1,8} = 65.28$ $P < 0.0001$	$F_{2,16} = 41.05$ $P < 0.0001$
Group 3 N=6 RM on both before/during and freq of stim	$F_{1,5} = 34.71$ $P = 0.0020$	$F_{2,10} = 2.027$ $P = 0.1824$	$F_{1,5} = 11.72$ $P = 0.0188$	$F_{2,10} = 2.395$ $P = 0.1413$	$F_{1,5} = 114.4,$ $P = 0.0001$	$F_{2,10} = 1.858$ $P = 0.206$
	main effect of group for V_E		main effect of stim frequency for V_E			
delta stim w groups x freq (RM on freq)	$F_{2,20} = 17.48,$ $P = 4.07e\text{-}05$		$F_{2,40} = 84.22,$ $P = 4.59e\text{-}15$			
F test statistics for One-Way ANOVA for all groups at baseline						
	f_R		V_T		V_E	
Baseline breathing	$F_{2,20} = 1.452$ $P = 0.258$		$F_{2,20} = 3.05$ $P = 0.0698$		$F_{2,20} = 3.489$ $P = 0.0501$	

on groups			
F test statistics for One-Way ANOVA for all groups at 15 hz stimulation			
	f_R	V_T	V_E
delt a stim @ 15 hz on groups	$F_{2,20} = 34.3$ $P = 3.43e-07$	$F_{2,20} = 7.826$ $P = 0.00309$	$F_{2,20} = 18.42$ $P = 2.91e-05$

Table 4: Tukey's multiple comparison test statistics for all group differences at 15 Hz stimulation.

	f_R		V_T	V_E		
	q and P	95% confidence interval	q and P	95% confidence interval	q and P	95% confidence interval
Group 1vs. Group 2	q_{20} = 3.351 P = 0.0690	-68.35 to 2.242	q_{20} = 0.6241 P = 0.8987	-0.7192 to 1.023	q_{20} = 0.6947 P = 0.8763	-0.4797 to 0.3237
Group 1 vs. Group 3	q_{20} = 8.273 P < 0.0001	51.47 to 129.9	q_{20} = 5.186 P = 0.0042	0.4351 to 2.372	q_{20} = 7.191 P = 0.0002	0.4509 to 1.344
Group 2 vs. Group 3	q_{20} = 11.57 P < 0.0001	85.47 to 162.0	q_{20} = 4.739 P = 0.0085	0.3065 to 2.196	q_{20} = 8.009 P < 0.0001	0.5397 to 1.411

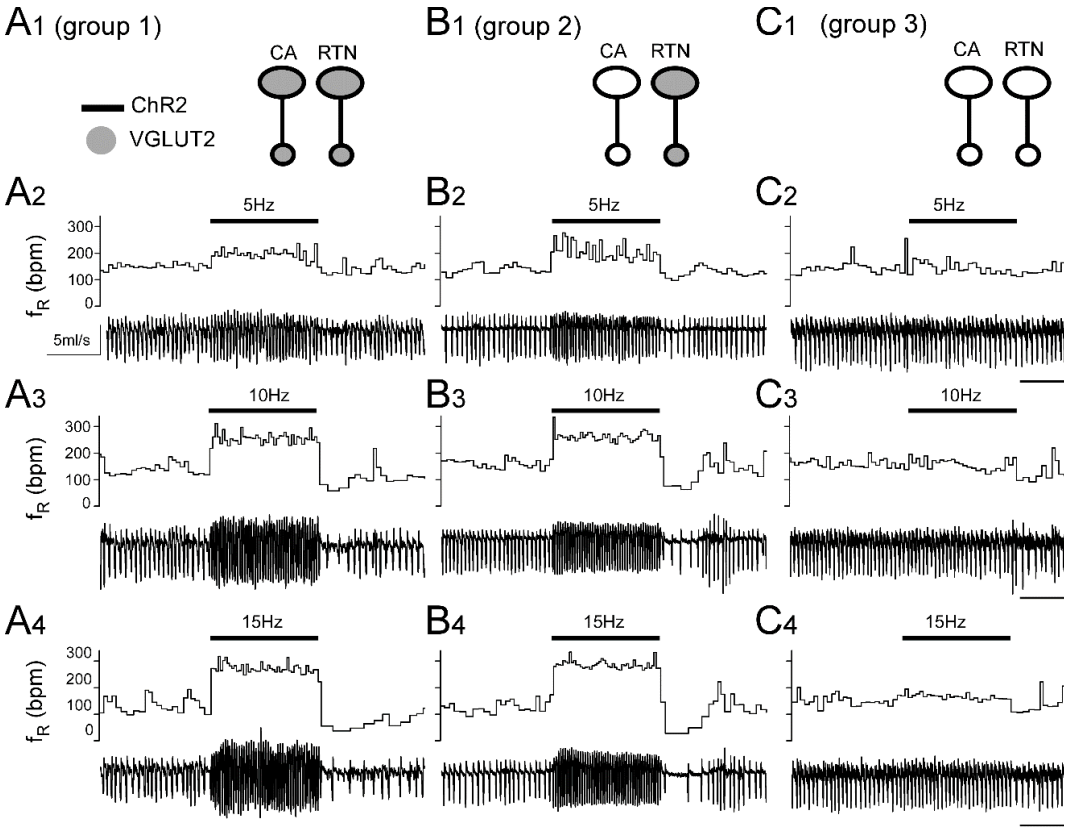
A1 (group 1)
B1 (group 2)
C1 (group 3)
CA
RTN
ChR2
VGLUT2
A2
B2
C2
5Hz
A3
B3
C3
10Hz
A4
B4
C4
15Hz
fR (bpm)
300
200
100
0
5ml/s

Figure 1. **Breathing stimulation elicited by combined optogenetic activation of RTN and C1 neurons in mice in which *Vglut2* was deleted from the C1 neurons or from both RTN and C1 neurons.**

A1-A4: photostimulation of a mix of ChR2-transduced RTN and C1 neurons in control mice (C57). Unilateral stimulation was done in conscious mice using trains of 5 ms-long light pulses delivered at 5, 10 or 15 Hz. In each panel, the bottom trace is the raw plethysmography signal (airflow with inspiration downward) and the top trace is the breathing frequency. Note the immediate and sustained increase in breathing frequency. The apnea that follows the stimulation period is likely caused by the reduction in blood PCO_2 consecutive to the hyperventilation. B1-B4: same experiment in a group 2 mouse in which ChR2-transduced C1 neurons no longer express Vglut2 but RTN neurons still express this vesicular transporter. C1-C4: same experiment in a group 3 mouse in which few or none of the ChR2-transduced neurons express Vglut2. Note the almost complete loss of the breathing response.

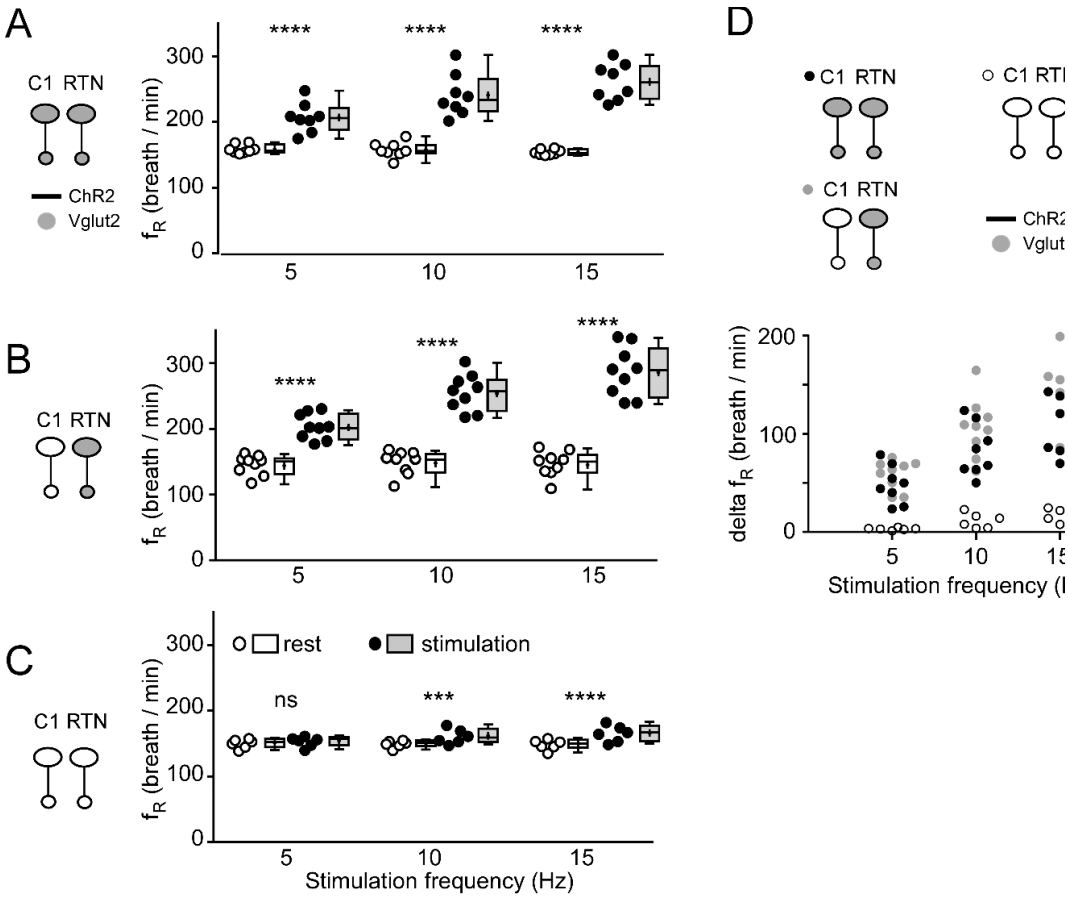
A
C1 RTN
ChR2
Vglut2
****
****
****
300
200
100
0
f_R (breath / min)
5
10
15
B
C1 RTN
****
****
****
300
200
100
0
f_R (breath / min)
5
10
15
C
C1 RTN
rest
stimulation
ns
***
****
300
200
100
0
f_R (breath / min)
5
10
15
Stimulation frequency (Hz)
D
C1 RTN
C1 RTN
C1 RTN
ChR2
Vglut
200
100
0
delta f_R (breath / min)
5
10
Stimulation frequency (

Figure 2. **Optogenetic activation of RTN and C1 neurons: effect on breathing frequency**

A. Breathing frequency (f_R) at rest (open circles represent individual data points and box and whisker plots summarize each data set with means indicated by crosses) and during photostimulation (black circles and gray boxes) in control mice. In these mice Vglut2 is expressed by both types of ChR2-tranasduced neurons (C1 and RTN). B. Breathing frequency (f_R) at rest (open circles and boxes) and during photostimulation (black circles and gray boxes) in mice in which ChR2-transduced RTN express Vglut2 but ChR2-transduced C1 cells do not express Vglut2. C. Breathing frequency (f_R) at rest (open circles and boxes) and during photostimulation (black circles and gray boxes) of neurons in mice in which neither C1 nor RTN ChR2-transduced neurons express Vglut2. D. change in breathing frequency produced by photostimulating ChR2-transduced neurons in the three mice groups.

In A-C *** $P = 0.0003$ and **** $P < 0.0001$ (post hoc Sidak multiple comparison between rest and stimulation). In D, **** $P < 0.0001$ (between group 3 and groups 1 or 2 at 15 Hz by Tukey's post hoc multiple comparison test between groups, see Table 4 for q and P values).

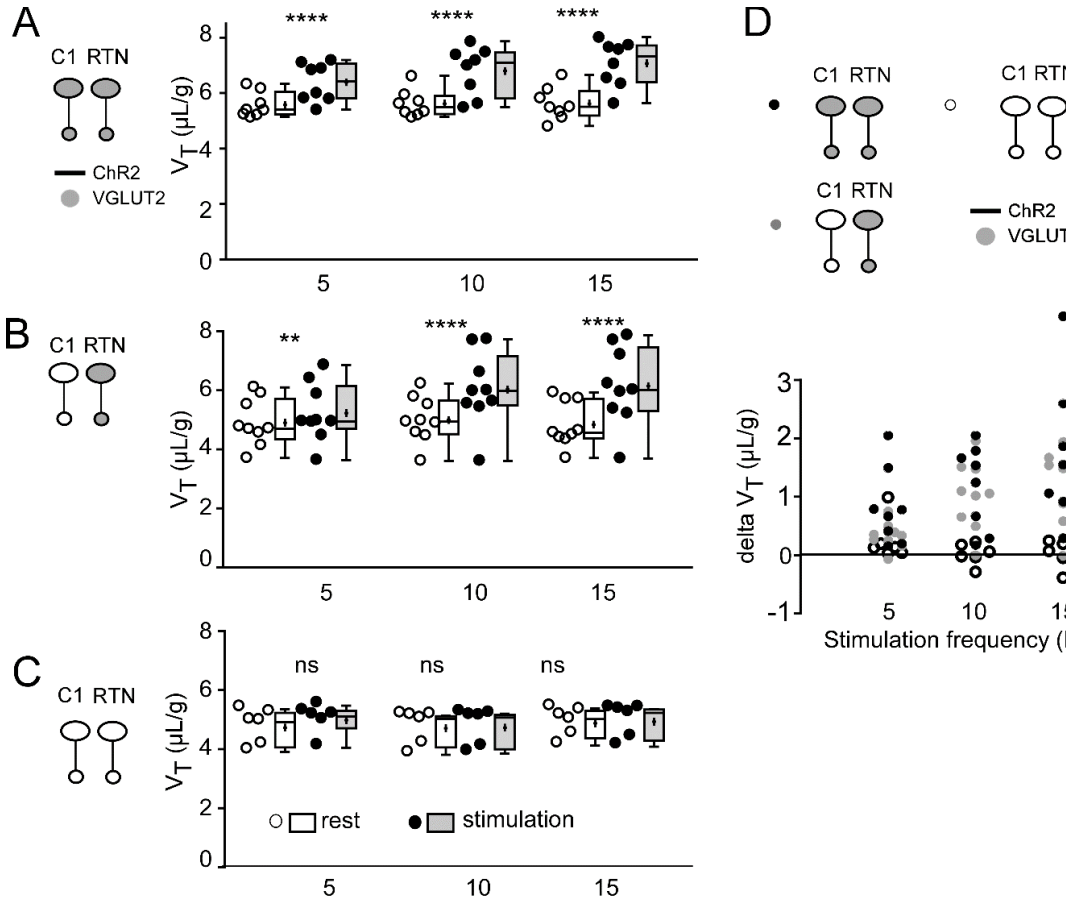
A
C1 RTN
ChR2
VGLUT2
V_T (µL/g)
****
****
****
5
10
15
B
C1 RTN
**
****
****
C
C1 RTN
ns
ns
ns
rest
stimulation
D
C1 RTN
C1 RTN
ChR2
delta V_T (µL/g)
Stimulation frequency

Figure 3. **Optogenetic activation of RTN and C1 neurons: effect on tidal volume (V_T)**

The data is presented as in Figure 2. A-C. V_T at rest (open circles represent individual data points and box and whisker plots summarize each data set with means indicated by crosses) and during photostimulation (black circles and gray boxes) in control mice (A, group 1), in mice in which ChR2-transduced RTN express Vglut2 but ChR2-transduced C1 cells do not express Vglut2 (B, group 2) and in mice in which neither C1 nor RTN ChR2-transduced neurons express Vglut2 (C, group 3). D. changes in V_T produced by photostimulating ChR2-transduced neurons in the three mice groups.

In A-C ** $P = 0.0097$ and **** $P < 0.0001$ (post hoc Sidak multiple comparison tests between rest and stimulation). In D, ** $P < 0.01$ (between group 3 and groups 1 or 2 at 15 Hz by Tukey's post hoc multiple comparison test between groups, see Table 4 for q and exact P values).

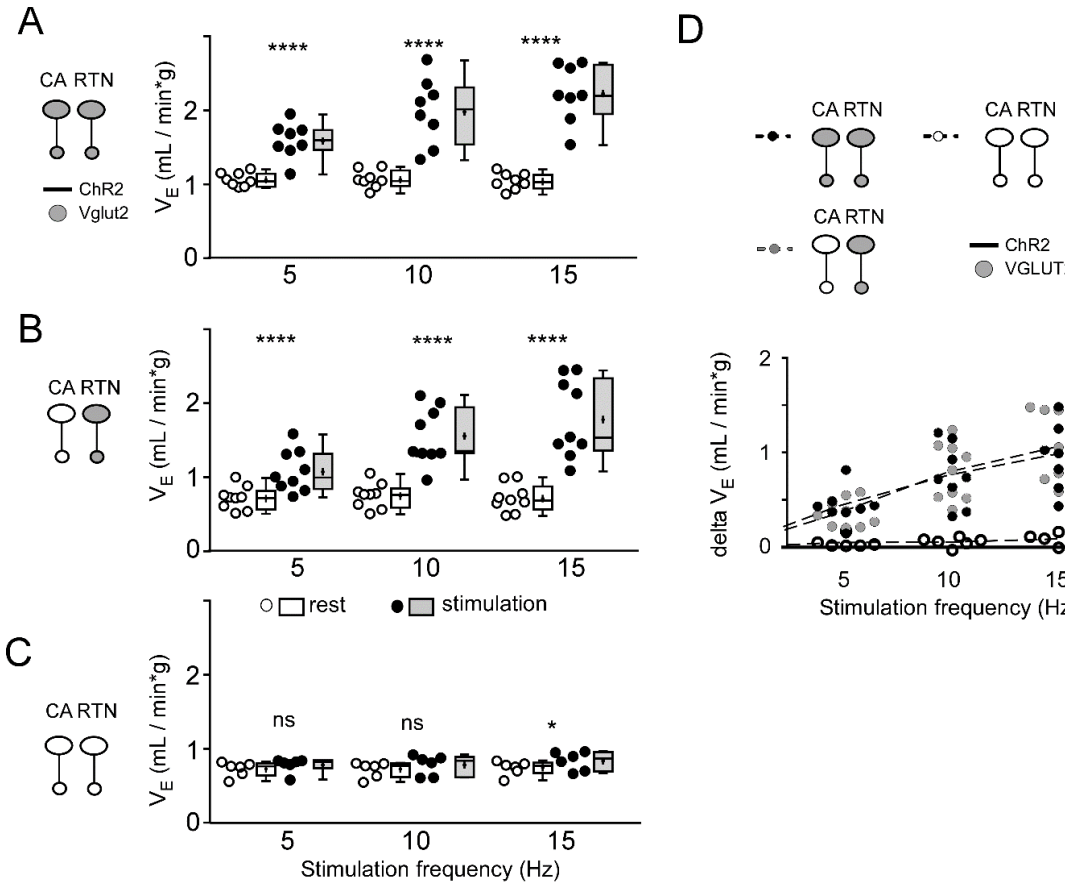
A
CA RTN
ChR2
Vglut2
V_E (mL / min*g)
****
****
****
5
10
15
B
CA RTN
rest
stimulation
C
CA RTN
ns
ns
*
Stimulation frequency (Hz)
D
CA RTN
CA RTN
CA RTN
ChR2
VGLUT
delta V_E (mL / min*g)
Stimulation frequency (Hz)

Figure 4. **Optogenetic activation of RTN and CA neurons: effect on minute volume (V_E)**

The data is presented as in Figure 2. A-C. Minute volume ($V_E = f_R \times V_T$) at rest (open circles and boxes) and during photostimulation (black circles and gray boxes) in control mice (A, group 1), in mice in which ChR2-transduced RTN express Vglut2 but ChR2-transduced C1 cells do not express Vglut2 (B, group 2) and in mice in which neither CA nor RTN ChR2-transduced neurons express Vglut2 (C, group 3). D. changes in V_E produced by photostimulating ChR2-transduced neurons in the three mice groups.

In A-C * $P = 0.0161$ and **** $P < 0.0001$ (Sidak post hoc multiple comparisons). In D, *** $P = 0.0002$ and **** $P < 0.0001$ (between group 3 and groups 1 or 2 at 15 Hz by Tukey's post hoc multiple comparison test between groups, see Table 4 for *q* and P values).

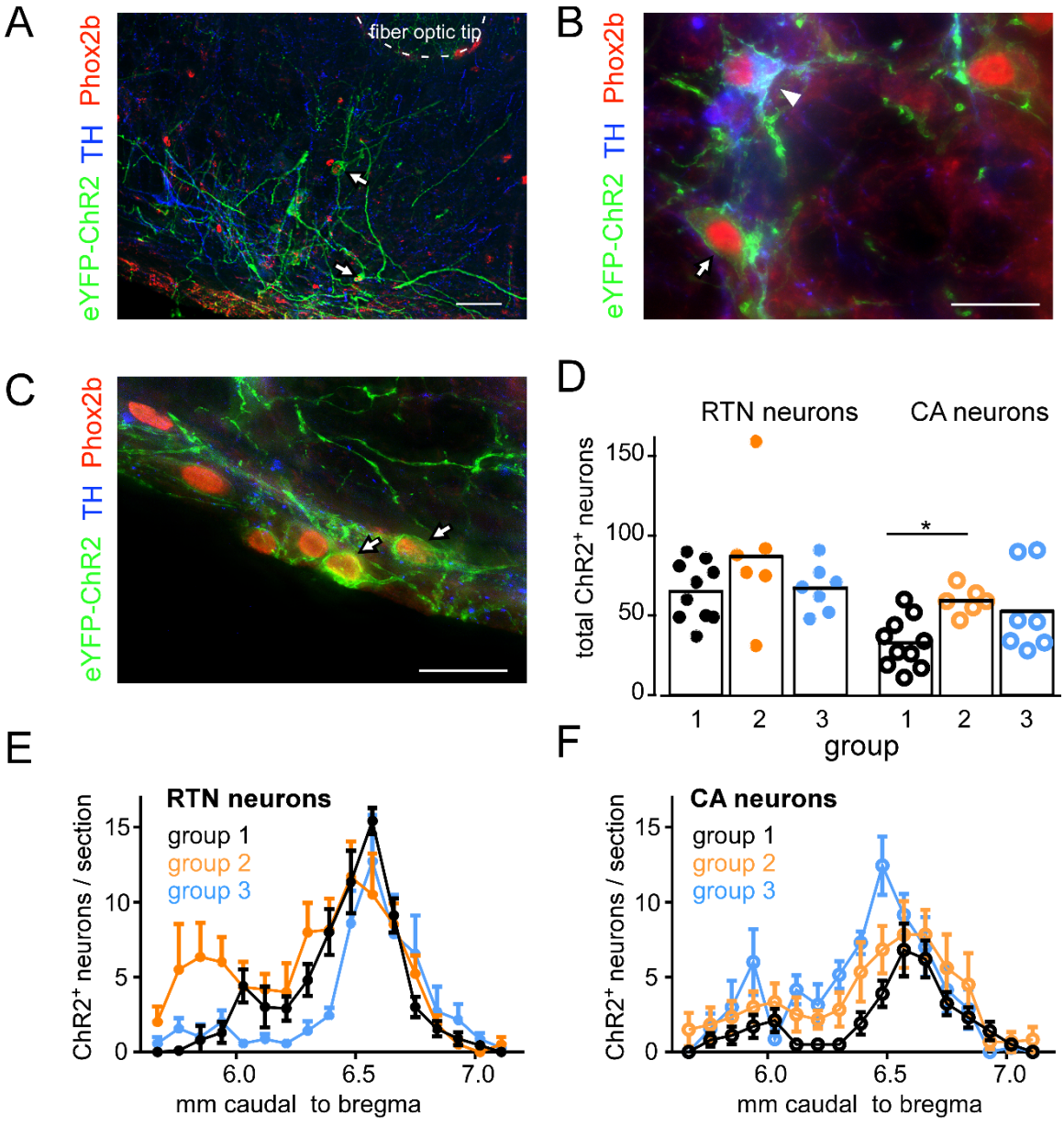
A
eYFP-ChR2 TH Phox2b
fiber optic tip
B
eYFP-ChR2 TH Phox2b
C
eYFP-ChR2 TH Phox2b
D
RTN neurons
CA neurons
total ChR2+ neurons
150
100
50
0
*
1 2 3 1 2 3
group
E
RTN neurons
group 1
group 2
group 3
ChR2+ neurons / section
15
10
5
0
6.0 6.5 7.0
mm caudal to bregma
F
CA neurons
group 1
group 2
group 3
ChR2+ neurons / section
15
10
5
0
6.0 6.5 7.0
mm caudal to bregma

Figure 5

Figure 5. PRSx8-ChR2-eYFP LVV selectively transduces Phox2b-expressing neurons

A. Transverse section through the rostral ventrolateral medulla at the level of the posterior edge of the facial motor nucleus (FN). The ventral surface of the medulla is showing at the lower left corner. All the ChR2-eYFP transduced neurons (black-rimmed white arrows) have Phox2b-immunoreactive nuclei. The section also shows the location of the tip of the optical fiber that was implanted to photoactivate the ChR2-expressing neurons. B. Side by side example of a ChR2-transduced catecholaminergic neuron (TH-immunoreactive; white arrowhead) and a ChR2-transduced RTN neuron (TH-negative; black-rimmed white arrow). Both neurons contain plasma membrane-associated eYFP and a Phox2b-immunoreactive nucleus. The catecholaminergic neurons also contains TH. C. Typical example of

RTN neurons (positive for Phox2b-and ChR2-eYFP but TH-negative) lining the ventral surface of the brainstem ventral to the facial motor nucleus. D-F. Rostro-caudal distribution of ChR2-transduced RTN and catecholaminergic neurons in the three experimental groups. More RTN than CA neurons were transduced with ChR2-eYFP although all experimental groups were transduced with similar populations of these neurons. Scale bar in A, 50 μm; in B and C, 20 μm.

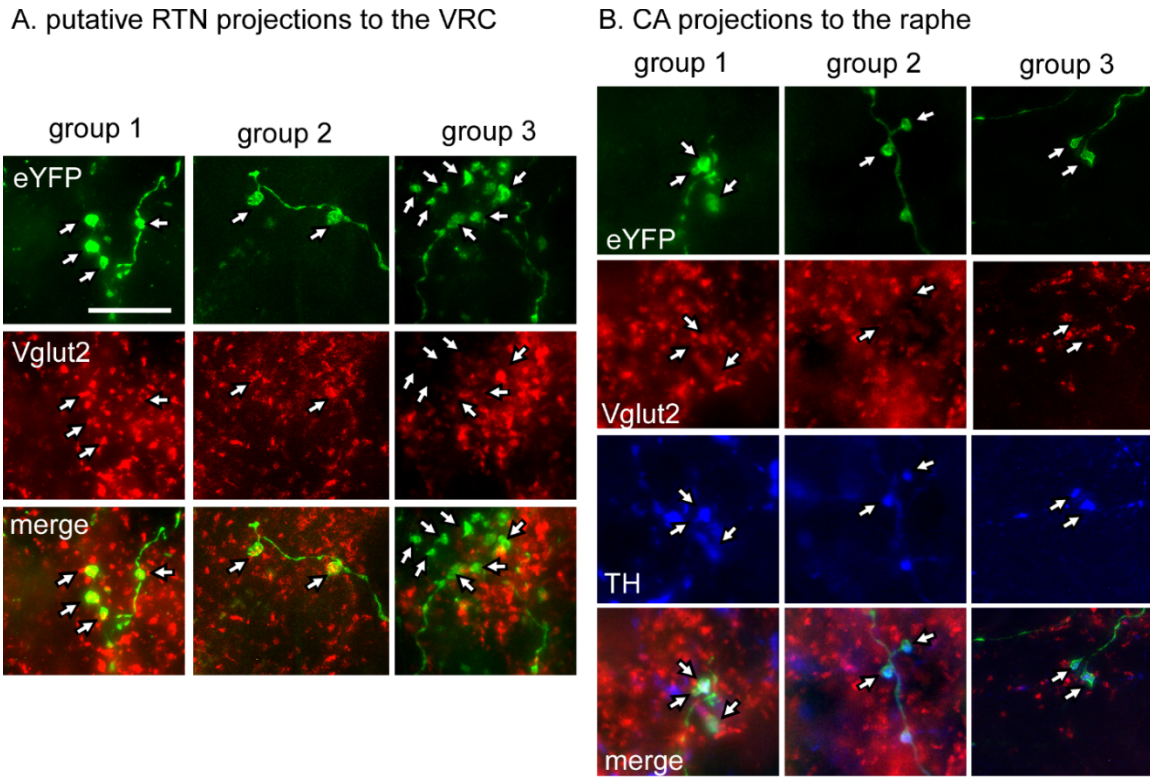
A. putative RTN projections to the VRC
group 1
group 2
group 3
eYFP
Vglut2
merge
B. CA projections to the raphe
group 1
group 2
group 3
eYFP
Vglut2
TH
merge

Figure 6

Figure 6. **Appropriate deletion of Vglut2 from RTN and CA terminals**

A. eYFP-positive terminals from RTN injections seen in the ventral respiratory column (vrc) are Vglut2 positive in groups 1 and 2 but lack Vglut2 immunoreactivity in group 3.

B. eYFP-positive terminals in raphe pallidus from catecholaminergic neurons (CA, defined by their tyrosine hydroxylase (TH) immunoreactivity) contain Vglut2 in group 1 but lack Vglut2 in groups 2 and 3. Scale bar = 10 ⌣m.

Chapter 4: Summary and implications of major findings

4.1 The RVLM and blood pressure regulation

The rostral ventrolateral medulla oblongata (RVLM) plays an important role in regulating cardiovascular and respiratory systems. In the first project of my dissertation research, I investigated whether a population in the RVLM other than C1 neurons was capable of increasing blood pressure in conscious animals. There is much evidence in indicating that sympathetic tone sets resting blood pressure conscious mammals, and—extrapolating from anesthetized studies—that sympathetic tone is dependent on both supraspinal input and the integrity of the RVLM. The neurons within the RVLM that are necessary for this maintenance are unknown, and recent studies have cast doubt on the most promising candidates—the catecholaminergic C1 neurons. It is critical to identify the neural mechanisms which drive sympathetic tone and set resting blood pressure, as these are likely to be involved in the generation and maintenance of hypertension. Therefore, I explored whether stimulation of neurons within RVLM after lesion of C1 neurons could increase blood pressure in conscious mice. I discovered that stimulation of non-catecholaminergic RVLM raised blood pressure independent of C1 lesion, and I then demonstrated that this increase could also be produced by stimulation of only the spinally-projecting RVLM neurons. These results are consistent with the emerging theory of the RVLM: C1 neurons are not critical in maintenance of blood pressure, but sympathetic tone and blood pressure are maintained by non-catecholaminergic neurons within the RVLM. These data are also consistent with model of a direct projection from the RVLM to preganglionc sympathetic neurons setting resting blood pressure, though these two theories are not mutually exclusive, i.e. RVLM may be critical for blood

pressure maintenance through indirect circuits, and stimulation of spinally-projecting RVLM may increase blood pressure but have nothing to do with setting resting blood pressure. Nonetheless, these results open up exciting new lines of research that may finally identify the critical supraspinal neurons in the medulla that maintain sympathetic tone and blood pressure—a question asked but unanswered since the seminal studies from Owsjannikow, Dittmar, and Carl Ludwig in the early 1870s.

4.2 C1 neurons as mediators of acute stress

In my second research project, I explored the role of C1 neurons as vanguards of the acute stress response (fight-or-flight response). One of the defining aspects of the acute stress response is catecholamine release, both peripherally and within the brain. C1 neurons are activated by both physiological and psychological acute stress, and previous work has demonstrated that C1 neurons are capable of increasing sympathetic nerve activity—which promotes release of peripheral catecholamines. During the acute stress response, peripheral catecholamine release decreases blood flow to the digestive system and increases cardiac output and blood flow to skeletal muscle—all important physiological responses for surviving acute stress. However, the effects of catecholamine release in the brain are as equally important as the peripheral consequences of catecholamine release for survival of acute stress. Release of catecholamines from the catecholaminergic neurons within the brain promote arousal, and increase attention and vigilance. Neuroanatomical data indicates that C1 axons form close appositions with many of the brain's catecholaminergic neurons, and stimulation of C1 in anesthetized rats increases activity of locus coeruleus neurons—the largest catecholaminergic population

in the brain. Therefore, I investigated whether C1 neurons directly project to the brain's catecholaminergic system. I discovered that excitation of C1 axons excited three populations of catecholaminergic neurons—A1, A2, and locus coeruleus. I then demonstrated that this excitation was due to monosynaptic release of glutamate, establishing that C1 neurons directly control the brain's catecholaminergic system. These data are consistent with the emerging role of C1 neurons as mediators of the acute stress response, and may help direct future studies to explore physiological and physiological stress circuits, the relationship between chronic stress and hypertension, and the consequences of long-term activation of the acute stress response—important for understanding and treating psychological stress disorders.

4.3 The regulation of breathing via the RVLM

Neurons within the RVLM—the retrotrapezoid nucleus neurons—adjust breathing to maintain blood gases despite varying degrees of metabolic activity. RTN are chemosensitive and adjust breathing in a CO_2-dependent manner. Much is known about the intrinsic chemosensitive nature of RTN neurons, however much of the upstream and downstream circuits in which RTN is involved remain speculative. Currently, there is no technique that allows the exclusive targeting of RTN, severely limiting the potential research avenues available to neurons which can be directly targeted. Studies of RTN at the cellular level have side-stepped this issue by either demonstrating intrinsic chemosensitivity—the hallmark of RTN—or identifying the RNA or protein fingerprints of RTN neurons post-hoc. The most specific technique developed for targeting RTN neurons is the use of the artificial promoter PRSx8—a multimer of the Phox2a/b-

recognition site. Within the RVLM, PRSx8 causes expression viral payloads in RTN and C1 neurons. For conscious studies, however, there is no transgenic or promoter-based technique to specifically target RTN versus C1, and no approach to overcome the limitations of the PRSx8 labelling of C1 neurons has been developed. Therefore, in my third study I attempted to design an approach to specifically stimulate RTN in conscious mice.

The approach I designed was based on the selectivity of PRSx8 for C1 and RTN in the RVLM, and the DβH-Cre$^{+/0}$ mouse. DβH-Cre mice express the Cre protein in noradrenergic neurons, and as C1 are the only noradrenergic neurons in the RVLM local injections of viral vectors can be used to target C1 exclusively. We first demonstrated that the changes in breathing and vagal nerve activity due to stimulation of C1 is dependent on Vglut2 expression in C1 neurons [52]. Further, two prior studies identified glutamate as the principal neurotransmitter for postsynaptic excitation by C1 onto noradrenergic neurons or dorsal motor vagal neurons [53] [54]. Thus, optogenetic stimulation of C1 in DβH-Cre_Vglut2$^{flox/flox}$ mice—which lack Vglut2 protein in noradrenergic neurons, namely C1—produces no detectable change in breathing [52]. Based on these results, I injected PRSx8-ChR2 into DβH-Cre_Vglut2$^{flox/flox}$ mice to identify the physiological consequences of stimulating RTN without those produced by stimulation of C1. Stimulation of RTN in DβH-Cre_Vglut2$^{flox/flox}$ mice resulted in a robust increase in breathing, despite the fact that C1 neurons were incapable of producing this effect, indicating RTN alone is driving this increase.

It is likely that a transgenic mouse or new promoter will be developed to specifically target RTN neurons. Until this time, however, my strategy uses available

methods to specifically target RTN, opening up new lines of research on RTN at physiological and circuitry levels. Using this strategy, any circuit-level investigation which produces monosynaptic glutamatergic excitation can safely be attributed to RTN as opposed to RTN/C1. At the physiological level, the consequences of RTN perturbation can be characterized distinct from C1 as discussed above.

A second approach I designed for this study has a more general application for testing the consequences of optogenetic stimulation after genetic modification of specific group of neurons. This technique can be applied to any mouse strain which contains a floxed gene. As an example, I tested the necessity of Vglut2 in the increase in breathing due to RTN stimulation. I injected a PRSx8-Cre/flex-ChR2 viral cocktail into WT and Vglut2$^{flox/flox}$ mice. In WT mice this lead to expression of ChR2 in both RTN and C1 neurons, and optogenetic stimulation robustly increased breathing in conscious mice. InVglu2$^{flox/flox}$ mice, however, a critical segment of the Vgut2 gene is excised and Vglut2 expression is prevented in C1 and RTN neurons which express Cre. In these mice, ChR2 expression is also dependent on Cre expression, thus only those C1 and RTN neurons that express Cre—and therefore lack Vglut2—will be optogenetically stimulated. In these mice, optogenetic stimulation of C1/RTN lacking Vglut2 produced no change in breathing, demonstrating that Vglut2 expression in RTN is necessary for the RTN-evoked activation of breathing.